

Annual Report of Naka Fusion Research Establishment
from April 1, 2004 to March 31, 2005

Naka Fusion Research Establishment

Japan Atomic Energy Research Institute
Naka-shi, Ibaraki-ken

(Received August 12, 2005)

This annual report provides an overview of research and development (R&D) activities at Naka Fusion Research Establishment during the period from 1 April, 2004 to 31 March, 2005, including those performed in collaboration with other research establishments of JAERI, research institutes, and universities.

In the JT-60 research program, the pulse length of the tokamak discharge was extended successfully up to 65 s in FY 2003. In FY 2004, following the successful results, optimization of long pulse discharges was continued in order to explore the boundaries of facility capabilities for the long pulse operation. The pulse length of the negative-ion based neutral beam injection system has reached up to 25 s with an injection power of 1MW. In electron cyclotron wave system, the pulse length has also extended up to 45 s with an RF power of 0.35 MW by using four gyrotrons in a series operation. Sustainment of higher normalized β of $\beta_N > 2.3$ for 22.3 s, or $\beta_N > 2.5$ for 15.5 s has been achieved by exploiting available plasma heating systems. This discharge exhibits not only the high β_N , but also high confinement improvement with the H factor of $H_{89p} = 1.9-2.3$ and high normalized fusion performance of $G = H_{89p} \beta_N / q_{95}^2 = 0.4-0.5$ during the sustainment, where q_{95} is a safety factor at the edge. $G \sim 0.4$ corresponds to the fusion energy gain of $Q = 10$ for the ITER standard scenario. The H-mode plasma with $H_{89p} \sim 1.4$ has been maintained for about 30 s, although degradation of the performance was observed at the later half of the discharge. In the reversed shear plasmas, the operation regime was successfully extended to the density higher than Greenwald density limit, while maintaining high confinement and high radiation loss fraction by tailoring the internal transport barriers of the density and temperature. Demonstration of neoclassical tearing mode stabilization and improvement of plasma performance in the high beta region ($\beta_N \sim 3$) has been performed using local current drive by the second harmonic electron cyclotron waves. In addition, a real-time control system of safety factor profile has been developed. This system enables spatial control of driven current by adjusting the parallel refractive index of lower-hybrid waves through the change of phase difference between multi-junction launcher modules.

The design of National Centralized Tokamak (NCT), which is the superconducting modification of JT-60, progressed both in physics and engineering. Machine has been designed to have a wide-range capability of operation in aspect ratio and plasma shape. Engineering design of the main components of superconducting toroidal and poloidal magnetic field coils, vacuum vessel, in-vessel components, and cryostat has been performed to investigate the structure optimization from viewpoints of manufacturing processes, operation and maintenance feasibility.

A series of the experimental programs on the JFT-2M were completed in FY 2003. In FY 2004, experimental data on the Advanced Material Tokamak Experiment (AMTEX) using the reduced

activation ferritic steel (F82H), high performance experiment, characteristics of SOL and divertor plasma and compact toroid injection for fueling have been analyzed and evaluated. Concerning the AMTEX, analysis of high- β experiments with the Ferritic Inside Wall (FIW) facing close to the plasma have shown a wall stabilization effect. By using an MHD equilibrium code, it has been confirmed that the plasma with $\beta_N \sim 3.5$ is compatible with FIW.

In the theoretical and analytical researches, significant progress was made in the studies of transport simulation of current hole plasma, role of low order rational q-values in the ITB events, the theory of Alfvén eigenmodes in tokamaks, current spike behavior of disruptive plasma, and stability of external MHD modes. In the project of numerical experiment of tokamak (NEXT), the studies of the structure formations in toroidal electron temperature gradient driven turbulence, control of the zonal flow, and formation of current hole also progressed.

R&Ds of fusion reactor technologies have been carried out both to further improve technologies necessary for ITER construction, and to accumulate technological database to assure the design of fusion DEMO plants. For the design optimization of ITER superconducting magnets, degradation of critical current performances of the Nb₃Sn conductors has been experimentally and numerically examined and a new simulation model has been developed to predict degradation behavior in a large current superconductor. For ITER Neutral Beam Injector, MeV-range accelerator R&D is being in progress and the current density has been extended to 100 A/m². For the further pulse extension and power increase of 170 GHz gyrotron, a built-in radiator at the mode converter has been optimized to improve the efficiency of gyrotron output power and to reduce stray radiation, and pre-program controls of a cathode heater power has been employed to stabilize the beam current and the output power. In the R&Ds on Plasma Facing Components, a screw tube has been developed as a possible option for the ITER divertor. For the design of ITER Test Blanket Module (TBM), two candidates, namely Water Cooled Solid Breeder TBM and Helium Cooled Solid Breeder TBM have been proposed, and elementary technology R&Ds have been progressed for fabrication of the TBM, thermo-mechanical properties of the packed bed, and irradiation technologies. An outline design of an electrochemical hydrogen pump has been carried out as a candidate of the advanced Blanket Tritium Recovery system. Using DT neutrons, neutronics integral experiments have been performed with a blanket mockup at FNS facility to predict the tritium breeding ratio with an error less than 5%. As one of the most promising structural materials for the ITER TBM and DEMO blankets, F82H has been investigated with its neutron irradiation effects using HFIR, JMTR, and so on. In the IFMIF program, transitional activities have been continued.

In the ITER Program, along the work plan approved on June 2004 under the framework of the ITER Transitional Arrangements, the Design and R&D Tasks have been carried out by the Participant Teams. In FY 2004 JAERI has been in charge of fifty-five Design Tasks that make the implementation of preparing the procurement documents for facilities and equipments that are scheduled to be ordered at an early stage of ITER construction. The site issues have been continuously discussed among the delegations of six parties/area and through the bilateral negotiation between Japan and the EU based on a viewpoint of “a broader approach” concept.

Finally, in the fusion reactor design studies, the conceptual design of the fusion DEMO plant which is placed beyond ITER has progressed. Three options with different capabilities of center solenoid (CS) coil are studied. Researches on the physics related to the ramp up CS-less reactor, and waste management have progressed.

Keywords; JAERI, Fusion Research, JT-60, JFT-2M, Fusion Technology, ITER, Fusion Power Demonstration Plants, Fusion Reactor

Contents

- I. JT-60 Program
 1. Experimental Results and Analyses
 - 1.1 Long Pulse Operation and Extended Plasma Regimes
 - 1.2 Enhanced Performance and Steady State Research
 - 1.3 MHD Instabilities and Control
 - 1.4 H-Mode and Pedestal Research
 - 1.5 Current Drive Research
 - 1.6 Divertor/SOL Plasmas and Plasma-wall Interaction
 2. Operation and Machine Improvements
 - 2.1 Tokamak Machine
 - 2.2 Control System
 - 2.3 Power Supply System
 - 2.4 Neutral Beam Injection System
 - 2.5 Radio-frequency Heating System
 - 2.6 Diagnostic System
 3. Design Progress of the National Centralized Tokamak Facility
 - 3.1 Physics Design
 - 3.2 Engineering Design
- II. JFT-2M Program
 1. Advanced Material Tokamak Experiment (AMTEX) Program
 2. High Performance Experiments
 - 2.1 Study of H-Mode Physics
 - 2.2 High Recycling Steady H-Mode
 - 2.3 Study on Divertor and Scrape-off Plasma
 - 2.4 Compact Toroid Injection
- III. Theory and Analysis
 1. Confinement and Transport
 - 1.1 Transport Simulation of Current Hole Plasma in JT-60U
 - 1.2 Role of Rational q-values in the ITB Events in Reverse Shear Plasmas
 2. MHD Stability
 - 2.1 Development of the Theory of Alfvén Eigenmodes in Tokamaks
 - 2.2 TSC Simulation on Current Spike Behavior of JT-60U Disruptive Plasmas
 - 2.3 Critical β Analyses with Ferromagnetic and Wall Geometry Effects
 - 2.4 Stability Analysis of External MHD Modes by the 2-D Newcomb Equation
 - 2.5 Rotational Stabilization of High-n Ballooning Modes

3. Numerical Experiment of Tokamak (NEXT)
 - 3.1 Structure Formations in Toroidal ETG Turbulence
 - 3.2 Confinement Improvement by Control of Zonal Flow Behavior
 - 3.3 Formation of Current Hole by Pair Vortex Motion

IV. Fusion Reactor Design Study

1. Reactor Design Study
 - 1.1 Conceptual Design of Fusion DEMO Plant
 - 1.2 Current Ramp Simulation for CS-less Tokamak Reactor
2. Waste Management Study
 - 2.1 Nitrogen Concentration of F82H for Shallow Land Burial
 - 2.2 Waste Assessment for D-³He Reactor

Appendix

- A.1 Publication List (April 2004 – March 2005)
- A.2 Personnel

I. JT-60 PROGRAM

Objectives of the JT-60 project are to contribute to physics R&D of the International Thermonuclear Experimental Reactor (ITER), and to establish the physics basis for the steady state tokamak fusion reactor.

In the fiscal year of 2004, the reactor-relevant performance progressed much with the collaboration with the universities and institutes.

This part is divided into the three chapters; Experimental Results and Analyses (Chap.1), Operation and Machine Improvements (Chap.2) and Design Progress of the National Centralized Tokamak Facility (Chap.3).

1. Experimental Results and Analyses

1.1 Long Pulse Operation and Extended Plasma Regimes

Following the successful results in the long pulse experiments in FY2003, in order to explore the boundaries in the long pulse operation capabilities of the facility, optimization of long pulse discharges was continued. Extension of the heating and current drive pulses has contributed to the long pulse experiments. The pulse length of N-NB has reached up to 25 s with injection power of 1 MW. The ECRF pulse has reached 44.6 s. The input energy reached 15 MJ using four Gyrotrons in series (44.6 s) or three Gyrotrons in parallel (14.8 s). A grill mouth made of carbon was newly placed at the LHRF launcher. Conditioning was

undergoing, with the maximum injection power 1.3 MW (about 60% of the previous value) and the input energy of 16.3 MJ (before carbon mouth placed it was 10.9 MJ).

1.1.1 Sustainment of High Normalized Beta Value β_N

For economical fusion reactors, steady sustainment of high β_N is required, since fusion power density is proportional to the square of β_N . We reported, in FY2003, that $\beta_N > 1.9$ was sustained for 24s and that the current profile reached in steady state. In 2004, we have achieved sustainment of much higher $\beta_N > 2.3$ for 22.3s, or $\beta_N > 2.5$ for 15.5s [1.1-1], exploiting available P-NB, N-NB, and ECRF systems. Figure I.1.1-1 shows waveforms of a high β_p ELMy H-mode discharge (E043903) at $I_p = 0.9\text{MA}$ and $B_t = 1.7\text{T}$ ($q_{95} = 3.4$) where $\beta_N = 2.5$ was sustained for 15.5s. This discharge exhibits not only the high β_N , but also high confinement improvement $H_{89P} = 1.9\text{-}2.3$ and high value of $G = H_{89P}\beta_N/q_{95}^2 = 0.4\text{-}0.5$ during the sustainment. The index G is a measure of the fusion gain [1.1-2]; $G \sim 0.4$ corresponds to ITER standard scenario of $Q = 10$. Current and pressure profiles at initial phase were optimized, adjusting NB deposition profile, in order to avoid a neo-classical tearing mode (NTM) that limits attainable β_N . There was no significant electromagnetic instability ($n = 0\text{-}3$) observed by saddle loops. The current density profile reached a steady state (Fig. I.1.1-1). In the discharge, the resistive diffusion time, defined by $\tau_R = (1/12)\mu_0 \langle \sigma_{NC} \rangle a^2$, was 1.6s, therefore the sustained period (15.5s) corresponds to $9.5\tau_R$. Here, we used a formulation of τ_R by Mikkelsen [1.1-3]. In

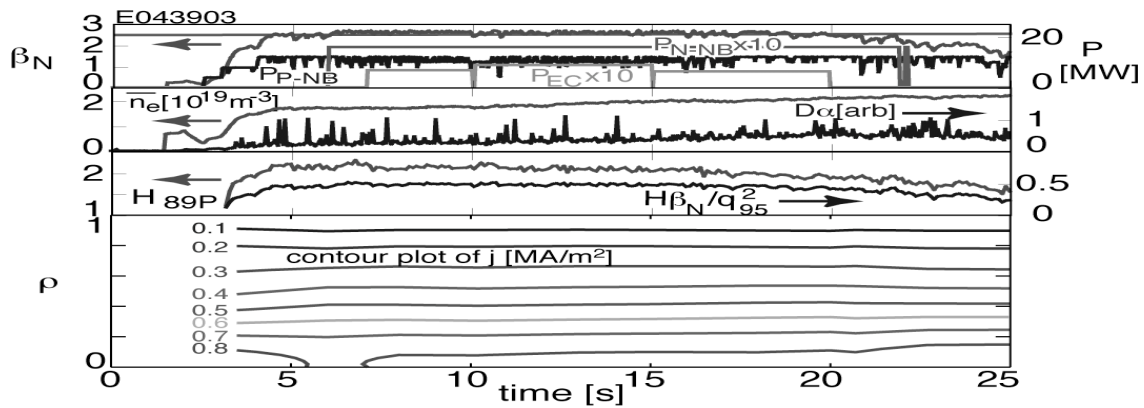


Fig. I.1.1-1. Temporal evolutions of β_N , injection power (P-NB, N-NB, EC), line averaged electron density, D_α intensity, H-factor, and $H\beta_N/q_{95}^2$. Sustained duration of $\beta_N = 2.5$ reached 15.5s, during which H_{89P} and $H_{89P}\beta_N/q_{95}^2$ were 1.9-2.3 and 0.4-0.5, respectively. Contour plot of current density profile (each 0.1MA/m^2 interval) evaluated using equilibrium reconstructions with MSE is shown in the bottom, showing the current profile reached steady state.

the above equation, a is averaged minor radius and σ_{NC} is the neoclassical conductivity. Although we intended to increase particle exhaust rate by adjusting strike points near the pumping slot at the divertor, the intensity of the D_α emission continuously increased (Fig. I.1.1-1) even without gas-puffing. The increased recycling raised line averaged electron density continuously from $1.6 \times 10^{19} \text{m}^{-3}$ to $2.1 \times 10^{19} \text{m}^{-3}$, corresponding to Greenwald density fraction of 46% and 58%, respectively. During $t=7-20\text{s}$, the electron density increased by 22% and H_{89PL} degraded by 15%.

1.1.2 Long Pulse High Recycling H-mode

Research in JT-60U has been expanded to never-explored-regime towards the steady-state operation owing to extension of the pulse length to 65 s and NB heating pulse length to 30 s [1.1-4]. In 30s-ELMy-Hmode discharges, wall saturation, which is defined as zero wall-pumping rate, or constant wall inventory, was observed by particle balance analysis [1.1-5].

Figure I.1.1-2 shows waveforms of the 30s-ELMy H-mode discharge in which the wall saturation was observed. At a toroidal magnetic field of 2.6 T, the flat-top of a plasma current (1.0 MA) was maintained for 34 s and the divertor configuration was kept for 36 s. The positive ion source based neutral beam (P-NB) was injected for 30 s with a heating power of 7-12 MW and the negative one for 25 s with 0.6 - 1.5 MW. The line-averaged electron density was controlled at 66% of the Greenwald density by the feedback control system of a gas-puffing rate. As Figure I.1.1-2(d) shows, the wall inventory, invoked from the following particle balance equation,

$$\int_0^t \{ \Gamma_{NB}(t) + \Gamma_{gas}(t) \} dt = N_{plasma}(t) + \int_0^t \{ \Gamma_{pump}(t) + \Gamma_{wall}(t) \} dt$$

increases until $t = 19$ s. This increase means that the wall-pumping was effective because particles continued to be retained in the wall during the increase. After $t = 19$ s, on the contrary, the wall inventory is constant. Since the local particle-releasing and wall-pumping cannot be investigated from the above particle balance equation, this constant wall inventory does not directly indicate that the inventory of all the tiles is saturated but indicates that the wall neither pumps nor releases particles on balance. The outer divertor tiles are considered to release particles because of the increase in the surface temperature as shown in Fig.

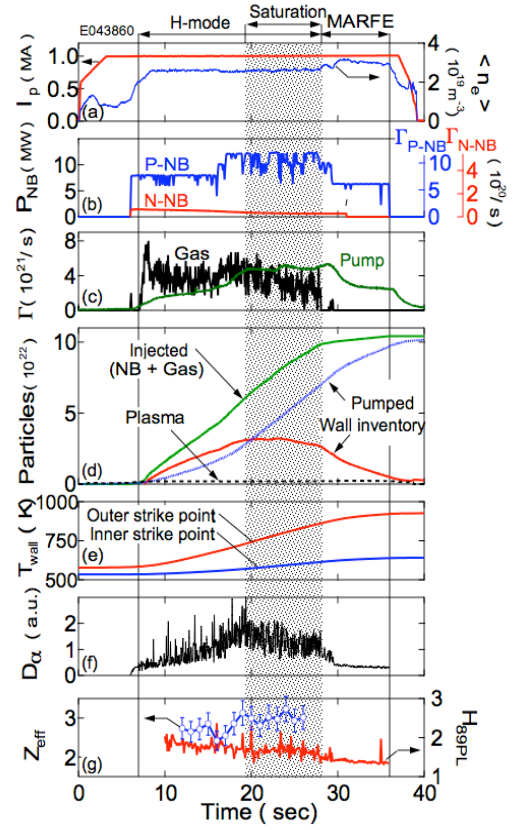


Fig. I.1.1-2 Waveforms of a long pulse, ELMy H-mode plasma. (a) the plasma current (I_p), the line-averaged electron density ($\langle n_e \rangle$), (b) the positive and the negative ion source based neutral beam heating power (P_{NB}) as well as the particle-fueling rate, (Γ_{P-NB} and Γ_{N-NB} , respectively), (c) the gas-puffing rate (Γ_{gas}), the divertor-pumping rate (Γ_{pump}), (d) the numbers of injected particles, plasma particles, pumped particles and retained in the surface materials, (e) the temperature around the outer and the inner strike point measured by thermocouples, (f) D_α emission intensity from the divertor plasma, (g) plasma effective charge (Z_{eff}), and H-factor (H_{89PL}). The periods of H-mode, the wall saturation and MARFE are shown at the top of this figure. The shaded area indicates the H-mode period under the condition of the wall saturation.

I.1.1-2(e) while other tiles with the surface temperature still low are considered to continue pumping particles. Hence, this situation is interpreted as net wall saturation. This wall saturation was sustained until $t = 28$ s. Even under the condition of the wall saturation, the ELMy H-mode plasma, indicated by the ELM activity of D_α shown in Fig. I.1.1-2(f), with a constant plasma effective charge ($Z_{eff} \sim 3$) and a constant H-factor ($H_{89PL} \sim 1.7$) was sustained as shown in Fig. I.1.1-2(g).

At $t = 28$ s, the outer divertor plasma detached, resulting in an X-point MARFE. At this detachment, the particle flux to the outer divertor tiles decreased, and the wall inventory started to decrease as shown in Fig. I.1.1-2 (d). From this observation, this decrease of

the particle flux to the outer divertor tiles is considered to result in the particle release (probably from the outer divertor tiles), or the decrease in the wall inventory. This situation is similar to the dynamic retention process: particles that retained in the wall during a plasma exposure are released when the plasma exposure is ended.

1.1.3 Extension of JT-60U Pulse Length

The 30 s H-mode plasma has been optimized up to $I_p = 1.4$ MA as shown in Fig.I.1.1-3 [1.1-4]. Although, H-mode was maintained throughout the heating period (~30 s), the performance was reduced at the later half of the discharge, due to some beam faults including N-NB. However, $H_{89p} \sim 1.4$ was maintained for about 30 s. It should be noted that similar to the other long pulse discharges, the wall recycling increased in the later half of the discharge and might affected the performance. Before the beam faults, $H_{89p} \sim 1.8$ was maintained for about 14-15 s. Following the results in the last year, these new results have shown progress towards standard H-mode operation in ITER.

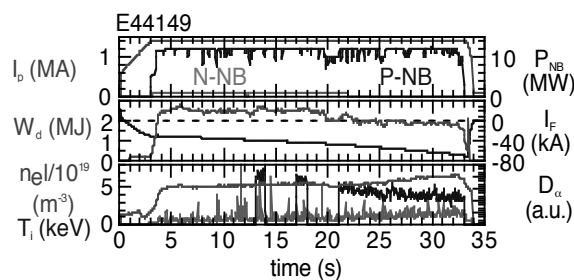


Fig.I.1.1-3, Typical waveforms of a 1.4 MA 30 s ELMy H-mode discharge.

References

- 1.1-1 Suzuki, T., et al., in *Fusion Energy 2004 (Proc. 20th Int. conf. Vilamoura, 2004)* IAEA-CN-116/EX/1-3, submitted to Nuclear Fusion.
- 1.1-2 Luce, T. et al., *Phys. Plasmas* **11**, 2627 (2004).
- 1.1-3 Mikkelsen, D. R., *Phys. Fluids* **B1**, 333 (1989).
- 1.1-4 Ide, S and the JT-60 Team, "Overview of JT-60U Progress towards Steady-state Advanced Tokamak", *Proceedings of 20th IAEA Fusion Energy Conference, Nov. 1-6, 2004 Vilamoura, Portugal*, IAEA-CN-116/OV/1-1 subitted to Nucl. Fusion.
- 1.1-5 Nakano, T., Asakura, N., et al., "Impact of nearly-saturated divertor plates on particle control in long and high-power-heated discharges in JT-60U", submitted to Nucl. Fusion.

1.2 Enhanced Performance and Steady State Research

1.2.1 Sustainment of weak shear plasma in nearly full CD [1.2-1]

The high β_p H-mode plasmas in JT-60U are characterized by a monotonic safety factor (q) profile with weak magnetic shear owing to the bootstrap current based on the internal transport barrier formation. Such a weak shear configuration is compatible with the ITER steady-state operation with $Q > 5$. The high β_p H-mode plasmas were optimized towards ITER steady-state operation scenario [1.2-2]. One of the key issues for obtaining a high-performance high β_p H-mode plasma is suppression of NTMs. Since the NTMs are destabilized at rational surfaces, the scenario for the avoidance of 3/2 NTM is considered that the $q=1.5$ surface is removed from whole plasma region.

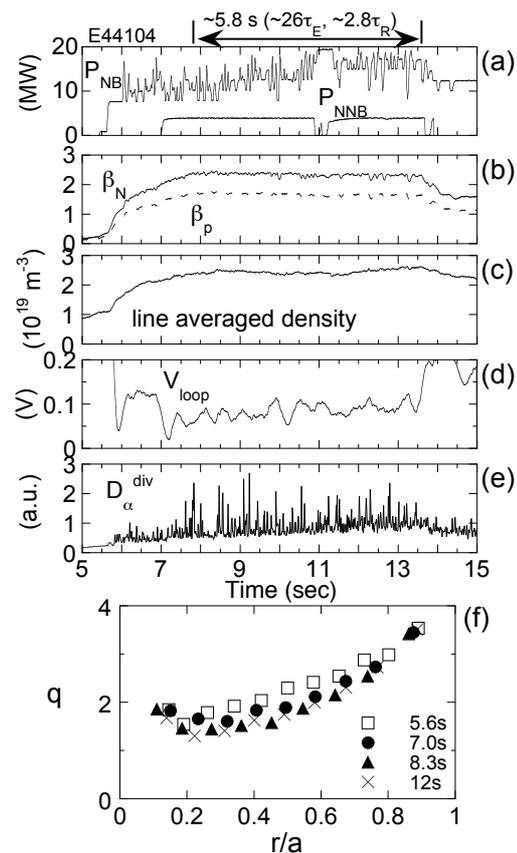


Fig.I.1.2-1 Typical waveforms of weak shear plasma with $q_{min} \sim 1.5$: (a) injection power of P-NB and N-NB, (b) normalized beta (β_N : solid curve) and poloidal beta (β_p : dotted curve), (c) line averaged electron density, (d) loop voltage, (e) deuterium recycling emission at the divertor. (f) Time evolution of q profile.

Typical waveforms of such a scenario are shown in Fig.I.1.2-1, where $I_p=1$ MA, $B_T=2.4$ T, $R=3.35$ m, $a=0.8$ m, $\kappa=1.44$, $\delta=0.5$, $q_{95}=4.5$. In this plasma, $\beta_N \sim 2.4$ ($\beta_p \sim 1.7$) has been sustained for 5.8s. This duration corresponds to $\sim 26\tau_E$ and $\sim 2.8\tau_R$, which was limited by the pulse length of N-NB (~ 4 MW, ~ 6.5 s). The $H_{89} \sim 2.2$ and $HH_{98y2} \sim 1.0$ were obtained at $t=8.3$ s. The electron density was almost kept constant at 54% of the Greenwald density. Loop voltage was reduced to near zero (~ 0.075 V), which indicates the nearly full non-inductive current drive condition. It should be emphasized that no NTM was observed in this discharge by the optimization of q profile. For avoidance of NTM, the alignment of the local pressure gradient and rational surfaces (such as $q=1.5, 2$) is important. The temporal evolution of q profile is shown in Fig.I.1.2-1(f). Pressure and q profiles were optimized as follows by feedback control of the stored energy and the injection timing of NBs. P-NB was injected at $t \sim 5.6$ s before the full penetration of inductive current when the shape of q profile is monotonic and $q > 1.5$ in the whole plasma region. During the initial phase of P-NB heating ($t = 5.6-7.0$ s), β_N was gradually raised to ~ 2.0 by feedback control of stored energy in order to expand the location of $q=2$ surface by the evolution of bootstrap current. At $t=7.0$ s, the shape of q profile was flattened and $q=2$ surface moved outward and $q > 1.5$ in the whole plasma region due to the evolution of bootstrap current around off-axis region, where the q profile in the core region becomes slightly reversed. After the flattening of q profile, N-NB was injected to enhance the non-inductive current drive and to increase β_N from ~ 2.0 to ~ 2.4 . At the later phase of the discharge, q profile was similar to that at $t=7.0$ s, but slightly decreased. The minimum value of q was kept $> \sim 1.5$ and $q=2$ surface located at small temperature gradient region, then no NTM was observed. The change in the shape of q profile is small by N-NB injection, which indicates that the inductive current before N-NB injection could be replaced with the beam driven current by N-NB. The analysis of non-inductive current drive indicates that $f_{BS} \sim 50-43\%$ and $f_{BD} \sim 52-47\%$ were obtained, which indicates nearly full non-inductive current drive condition. The values of β_N , f_{BS} and q_{95} are close to requirements for the ITER steady-state operation scenario.

1.2.2 Compatibility of an Advanced Tokamak Plasma with High Density and High Radiation Loss Operation [1.2-3]

Advanced tokamak plasmas with an internal transport barrier (ITB) have advantages of compatibility with high bootstrap current fraction and high confinement, which are essential for the steady-state operation. In order to apply these plasmas to fusion reactors, compatibility with high density and high radiation loss is also required for attaining high fusion power and reducing heat load localized onto the divertor plates. In a fusion reactor, high density operation above the Greenwald density (n_{GW}) is preferable and the radiation loss fraction of about 0.9 is necessary to reduce the heat load onto the divertor plates sufficiently.

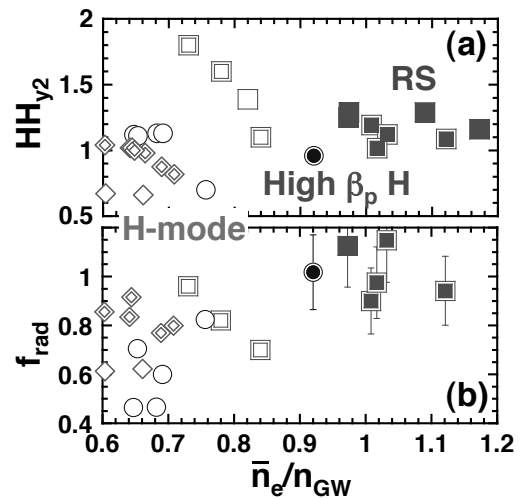


Fig. I.1.2-2 (a) HH_{y2} and (b) radiation loss fraction as a function of \bar{n}_e/n_{GW} . Squares : RS plasma. Circles : high β_p H-mode plasma. Diamonds : ELMY H-mode plasma. Closed and open symbols show new (during 2003-2004) and old (before 2002) data. Double lines show the data with impurity seeding.

In the reversed shear (RS) plasmas, the operation regime was successfully extended to high density above n_{GW} with high confinement ($HH_{y2} > 1$) and high radiation loss fraction ($f_{rad} > 0.9$) by tailoring the density and temperature ITBs as shown in Fig. I.1.2-2. In these plasmas, a large volume configuration ($V_p = 75-80$ m³) with a small outer gap ($\Delta = 0.08-0.16$ m) between the plasma and the outside wall was used with the plasma current of $I_p = 1.0$ MA, the toroidal magnetic field of $B_T = 2.5-2.9$ T and the safety factor at the 95% flux surface of $q_{95} = 5.8-6.5$. The high confinement of $HH_{y2} = 1.3$ was obtained in the high density region above n_{GW} with NB fuelling only. In this plasma, the

high \bar{n}_e/n_{GW} was obtained owing to the peaked density profile inside the ITB, although the pedestal density was smaller than $0.4n_{GW}$. With Ne seeding, the total radiation loss was enhanced to a level greater than 90% of the net heating power with high confinement of $HH_{y2}=1.1$ at $\bar{n}_e/n_{GW}=1.1$. Without Ne seeding, high radiation loss fraction was also obtained. However, in these discharges, the radiation from the main plasma was enhanced.

In the large volume RS plasmas, Cu XXVI line (111.20 Å) emission was observed, and its intensity decreased with increasing the outer gap. The fast ion loss induced by a large toroidal ripple could be related to generation of Cu. The Cu line intensity was almost zero at $\Delta=0.4$ m and the radiation in the core plasma was much smaller than that with small outer gap ($\Delta=0.08-0.15$ m). The main plasma radiation loss was changed by scanning the outer gap for the investigation of effects of metal impurity accumulation on the confinement. With $\Delta=0.08$ m, the strong impurity accumulation was observed and radiation in the main plasma reached up to 80% of the heating power. Even with such a large radiation in the main plasma, high confinement of $HH_{y2}=1.2$ was sustained at $\bar{n}_e/n_{GW}\sim 1$. The confinement degradation with the large radiation loss in the main plasma was not observed in the RS plasmas. The ITB seems to be robust for radiative cooling in the core plasma.

For the understanding of the mechanism responsible for the sustainment of high confinement with high main plasma radiation at high density, the relationship between central density and central temperature was examined. With the small outer gap, the central density increased rather than the central temperature during the confinement improvement. The central temperature was higher with the large outer gap ($\Delta\sim 0.4$ m) than with the small outer gap ($\Delta\sim 0.15$ m) at the same central density. The reduction in the central temperature was compensated with the increase in the central density. The NB heating profile became off-axis with the small outer gap. Off-axis heating, radiative cooling in the core plasma and NB fueling could be responsible for relationship between central density and central temperature.

In order to form the dense divertor, heat flux to the divertor plasma is necessary and the radiation should be enhanced in the divertor plasma. In the RS plasma,

Ar accumulation inside the ITB has been observed [1.2-2]. Thus, the Ne seeding was applied to enhance the divertor radiation. The plasma configuration with $\Delta=0.15$ m was used to increase the heat flux to the divertor by reducing the main plasma radiation from Cu. Ne was puffed from the divertor region together with D_2 gas-puffing from the plasma top. The ratio of the divertor radiation to the total radiation increased from 20% without Ne seeding to 40% with Ne seeding. However, the radiation from the main plasma was still larger than that from the divertor plasma, although the edge density was increased with D_2 gas-puffing for suppressing the impurity penetration. The total radiation reached up to 90% of the absorbed heating power. The Ne radiation profile estimated using 1-D impurity transport code indicated the small contribution of Ne to the main plasma radiation. Metal impurity Cu could largely contribute to the radiation loss in the core plasma. However, the radiation loss from the main plasma and neutron yield rate were almost kept constant, indicating metal impurity did not lead catastrophic confinement degradation and fuel dilution.

1.2.3 Comparison of Electron Transport in Helical and Tokamak Devices [1.2-5, 1.2-6]

The plasmas with an electron internal transport barrier (ITB), which is characterized by peaked electron temperature profiles, are obtained in the JT-60U tokamak and in the Large Helical Device (LHD), when the ECH is focused on the magnetic axis. The maximum values of R/L_{Te} , where R is the major radius and L_{Te} is the scale length of the electron temperature gradient, are similar (R/L_{Te} is 3 -5 in the L-mode plasmas and 20 - 30 in the electron ITB plasmas both in LHD and JT-60U). However, there are differences in the mechanism that trigger the ITB formation between LHD and JT-60U plasmas. The transition of the radial electric field triggers the formation of an ITB in LHD, while the negative magnetic shear is an important parameter in the formation of the electron ITB in JT-60U. The difference in the trigger mechanism results in the difference in the dependence of the temperature gradient, R/L_{Te} , on the heating power as shown in Fig. I.1.2-3. There is a clear transition of the R/L_{Te} in the formation of the LHD electron ITB and the transition is associated with the transition from ion root (weak

negative radial electric field) to electron root (large positive electric field) in the collisionless regime $v_b^* < 0.3$, without a change in magnetic shear. On the other hand, the formation of the electron ITB is gradual in JT-60U, since the electron ITB needs the change in magnetic shear (positive or negative shear), which changes on the time scale of current diffusion.

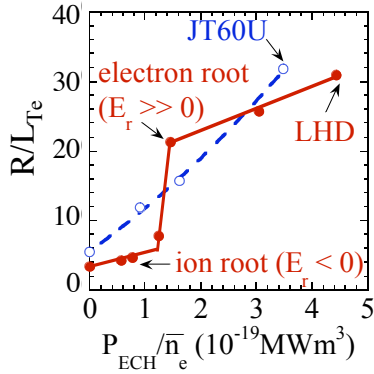


Fig. I.1.2-3 The normalized electron temperature gradient, R/L_{Te} , as a function of ECH power normalized by electron density, P_{ECH}/\bar{n}_e in LHD (closed circles and solid line) and JT-60U (open circles and dashed line).

In order to obtain a comprehensive understanding of the non-linearity of heat transport in toroidal devices, transient transport experiments (cold or heat pulse) are performed in plasmas on LHD and JT-60U without ITB. The dependence of electron heat diffusivity, χ_e , on electron temperature, T_e , and its gradient, ∇T_e , is analyzed by an empirical non-linear heat transport model ($\chi_e \propto T_e^\alpha |\nabla T_e|^\beta$). The heat diffusivity, χ_{tr} , obtained in LHD with $R_{ax}=3.5$ m from the transient analysis based on the empirical non-linear transport model is shown in Fig. I.1.2-4(a). The heat diffusivity estimated by power balance analysis, χ_{pb} , is also shown in Fig. I.1.2-4(a). The small difference between χ_{pb} and χ_{tr} indicates a weak ∇T_e dependence of χ_e ($\beta \ll 1$) in LHD. On the contrary, a gyro-Bohm like T_e dependence ($\alpha=3/2-5/2$) is obtained. In JT-60U, the short pulse ECH is injected at $\rho \sim 0.6$ for transient transport analysis. In order to compare the ∇T_e dependence of χ_e with the critical gradient length model, both χ_{tr} and χ_{pb} normalized by $T_e^{3/2}$ are plotted as a function of R/L_{Te} in Fig. I.1.2-4(b). The dependence of χ_{pb} on R/L_{Te} seems to be changed at $R/L_{Te}=6-8$ i.e. the temperature gradient-driven mode

may be switched on above this value. The value of χ_e has the ∇T_e dependence and χ_{tr} seems to be enhanced from χ_{pb} at $R/L_{Te}=6-8$. The ∇T_e dependence factor β decreases from 3 to 1.6 with the increase in R/L_{Te} , while the T_e dependence factor $\alpha=0.5-2$ is not different from that obtained in the LHD plasma. For the stabilization of microturbulence, the local shear is a critical parameter. The influence of local and global shear on turbulence might be one of the candidates to explain the difference in the non-linearity between LHD and JT-60U plasmas.

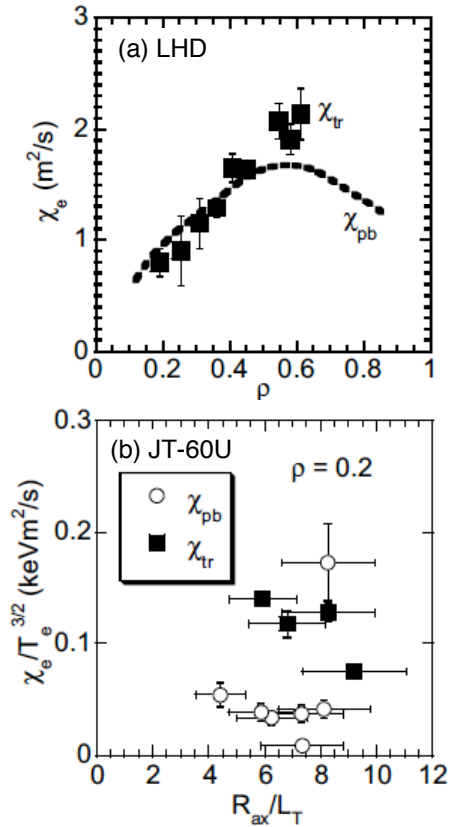


Fig. I.1.2-4 (a) Radial profiles of χ_{tr} and χ_{pb} in LHD. (b) R/L_{Te} dependence of χ_{tr} and χ_{pb} normalized by $T_e^{3/2}$ in JT-60U.

References

- 1.2-1 Sakamoto, Y. *et al.*, *Nucl. Fusion* **45**, 574 (2004).
- 1.2-2 Kamada, Y. *et al.*, *Fusion Sci. Technol.* **43**, 185 (2002).
- 1.2-3 Takenaga, H. *et al.*, in *Proc. 20th Int. Conf. on Fusion Energy 2004 (Vilamoura, 2004)*.
- 1.2-4 Takenaga, H. *et al.*, *Nucl. Fusion*, **43**, 1235 (2003).
- 1.2-5 Ida, K., *et al.*, *Plasma Phys. Control. Fusion* **46**, A45 (2004).
- 1.2-6 Inagaki, S., *et al.*, in *Proc. 20th Int. Conf. on Fusion Energy 2004 (Vilamoura, 2004)*.

1.3 MHD Instabilities and Control

1.3.1 Stabilization of the Neoclassical Tearing Mode

In obtaining a stationary high-beta plasma with positive magnetic shear, suppression of neoclassical tearing modes (NTMs), which appear below the ideal MHD limit, is the most critical issue. In JT-60U, two scenarios have been developed for NTM suppression: (a) NTM avoidance by modification of pressure and current profiles, and (b) NTM stabilization with electron cyclotron current drive (ECCD) / electron cyclotron heating (ECH). In 2004, these scenarios have been applied to a high-beta plasmas with $\beta_N=2.9-3$ [1.3-1, 2, 3].

(1) NTM avoidance with low q_{95}

Experiments in JT-60U demonstrated that NTM can be avoided by adjusting the mode rational surface (typically $q=1.5$ and 2 surfaces) at the location with low pressure gradient, that is, low local bootstrap current. It can be considered that the mode rational surfaces can be located at peripheral region with low pressure gradient if the safety factor is reduced. To demonstrate the feasibility of this scenario, operations at very low- q regime were performed.

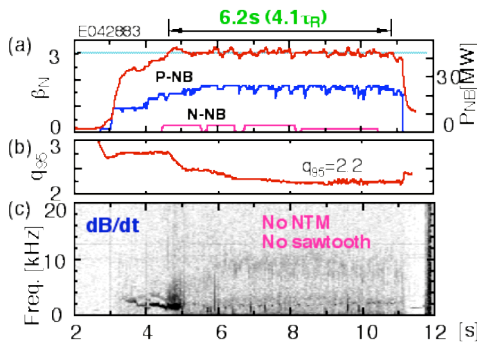


Fig. I.1.3-1 Typical discharge of a stationary high-beta plasma with NTM avoidance. (a) β_N and NB power, (b) q_{95} and (c) frequency spectrum of magnetic perturbations.

Typical discharge is shown in Fig.I.1.3-1, where $I_p=1$ MA and $B_t=1.7$ T. In this discharge, safety factor is decreased to ~ 2.2 during NB injection by lowering the plasma height and as a result decreasing plasma minor radius. The value of β_N is kept at 3 without NTMs for 6.2 s ($4.2\tau_p$). Owing to the high- β_N operation at low- q regime, high value of $\beta_t \sim 2.4\%$ is kept stationary. It is notable that no sawtooth is observed by any available diagnostics. MSE diagnostic also shows that the central

factor is not below 1, and that very flat q -profile is sustained for ~ 6 s. Although internal inductance l_i decreases to ~ 0.7 due to the flat q -profile resulting in $\beta_N/l_i \sim 4$, no major disruption is observed.

(2) NTM stabilization with ECCD in $\beta_N \sim 3$ regime

Another approach to suppress NTMs is to stabilize them by localized current drive and heating at the magnetic island with EC wave. In 2004, demonstration of NTM stabilization and improvement of plasma performance in high beta region ($\beta_N \sim 3$) has been performed using the second harmonic X-mode ECCD. Typical discharge is shown in Fig.I.1.3-2, where plasma parameters are as follows: $I_p=0.85$ MA, $B_t=1.7$ T, $q_{95}=3.5$. In this discharges, beta value is gradually increased by feedback control on NB power to avoid a 2/1 mode which degrades the plasma performance significantly. At $t=4$ s, β_N reaches 2.9, and a 3/2 mode appears. As the mode grows, NB power is increased to sustain a given beta value. At $t=5.8$ s, beta value begins to decrease due to further degradation of confinement. After the unmodulated EC wave injection of ~ 2.4 MW from $t=6$ s, beta value begins to increase until it reaches the target value of the feedback. At $t=7-8$ s, $\beta_N \sim 2.9$ is sustained with smaller amount of NB power, which shows improvement in confinement. Actually, H_{89PL} increases to 1.8 after the stabilization, resulting in successful sustainment of a high-beta and high-confinement plasma with $\beta_N H_{89PL}/q_{95}^2 \sim 0.4$ (Fig.I.1.3-2(c)).

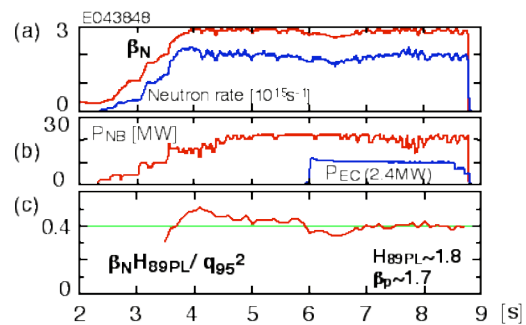


Fig. I.1.3-2 Typical discharge of a stationary high-beta plasma with NTM stabilization. (a) β_N and neutron emission rate, (b) NB and EC wave power and (c) $\beta_N H_{89PL}/q_{95}^2$.

1.3.2 MHD Activities in a Low Beta RS Discharge

A reversed shear (RS) plasma is expected as a

discharge of advanced scenario of ITER because it has good confinement and a large bootstrap current fraction. It is understood that the disruption at $q_{\min} > 2$, $\beta_N > 2$ is caused by stability limit of $n=1$ ideal kink ballooning mode. However RS plasmas with a strong ITB disrupt frequently even at lower β_N . By now, low beta disruptions are explained by double tearing mode [1.3-4] or resistive interchange mode [1.3-5], and these are MHD instabilities at the q_{\min} surface and around the ITB. However these cannot explain all of the observed low beta disruptions. To understand the cause of the low beta disruption, we investigated the MHD instabilities of RS plasmas with a strong ITB and a central flat pressure by measuring plasma current profiles and MHD fluctuations. We observed two types of disruptions. One is the disruption without precursor at $q_{\text{surf}} > \text{integer}$. The other is the disruption with $n = 1$ precursor. The poloidal mode number of the $n=1$ mode is equal to the q value of the outermost rational surface ($q=\text{integer}$). The $n=1$ modes exist continuously from the peripheral region to the ITB layer or separately at peripheral region and at ITB and the phase difference is 180 degree between them as shown in Fig. I.1.3-3.

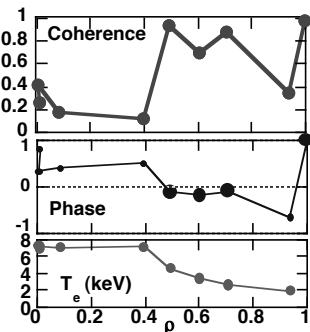


Fig. I.1.3-3 Coherence and phase difference of the $n=1$ modes.

From the MSE measurement q_{eff} is not below 4 in any case and q_{\min} scatters and is significantly below 2 at disruptions $q_{\text{eff}} \sim 4$ as shown in Fig. I.1.3-4. Moreover, disruption frequently occurs around $q_{\text{eff}} \sim 5$ and 4. These imply that disruptions depend on q_{surf} rather than q_{\min} . To explain these characteristics of disruption, we introduce a simple model that, disruption occurs when the both MHD instabilities at the plasma surface and at an inner rational surface with the safety factor being equal to the surface mode are unstable [1.3-6]. This simple model can explain almost all observed disruptions by two processes. One is that the surface

mode triggers disruption, which occurs when q_{surf} changes, and the corresponding q surface at ITB layer changes discretely. The other is that the internal mode triggered disruption, which occurs when the mode at an inner rational surface become unstable gradually. In the former case, the mode number of surface mode changes to a next integer as surface q changes and relative location of ITB and the rational surface in the RS region changes discretely. For instance, when the surface mode changes from $m=5$ to $m=4$, the corresponding internal rational surface changes discretely. Disruptions take place when the pressure gradient around $q=4$ is very large because of ITB, while instability of $q=5$ is stable due to central flat pressure profile. If the ITB is far from the internal $q=4$ surface, disruption does not occur. The $m/n=4/1$ mode changes to $3/1$ mode, when the surface q decreases below 4. The $q=3$ surface in the RS region is always in the large $-dT_i/dr$ region, therefore surface q cannot be below 4 any longer. In the latter case, disruption occurs when the pressure gradient increases or relative position of internal rational surface and ITB changes gradually. For example, the plasma with $4 < q_{\text{eff}} < 5$ is stable when the $q=4$ surface in the RS region exists in central T_i plateau region. After the $q=4$ surface moves to the large $-dT_i/dr$ region, internal mode becomes unstable and leads to disruption. This disruption triggered by the internal mode can explain disruptions observed when β_N is decreasing.

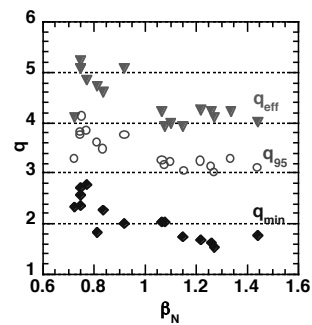


Fig. I.1.3-4 Surface safety factor (q_{95} and q_{surf}) and q_{\min} at disruption of various β_N .

1.3.3 Disruption study

(1) Fast Discharge Shutdown

It is shown that disruption deleterious effects on plasma facing components of a tokamak device can be greatly reduced or avoided by simultaneous puffing of small

amounts of high-Z noble gases, particularly, krypton and large amounts of hydrogen gas. A high electron density caused by the intense hydrogen gas puffing amplified the radiation of High-Z atoms. In turn the stored energy was radiated and plasma was terminated quickly. The high electron density and high effective charge made by high-Z species prevents runaway electron generation. [1.3-7]

(2) Mitigation of Post-Disruption Runaways

A clear deposition of impurity neon ice pellets in a post-disruption runaway plasma was observed, where most of plasma current was driven by runaway electrons. A high normalized electron density was stably obtained with $n_e^{\text{bar}}/n^{\text{GW}} \sim 2.2$. Effects of prompt exhaust of runaway electrons and reduction of runaway plasma current were found (Fig.I.1.3-5). One possible explanation for the basic behavior of runaway plasma current is that it follows the balance of avalanche generation of runaway electrons and slowing down predicted by the Andersson-Helander model, including the combined effect of collisional pitch angle scattering

and synchrotron radiation. It was suggested that the impurity pellet injection reduced the energy of runaway electrons in a step wise manner. [1.3-8]

References

- 1.3-1 Isayama, A. *et al.*, *Phys. Plasmas* **12**, 056117 (2005).
- 1.3-2 Suzuki, T. *et al.*, *Proc. 20th IAEA Fusion Energy Conf.*, EX-1/3.
- 1.3-3 Nagasaki, K. *et al.*, *Proc. 20th IAEA Fusion Energy Conf.*, EX-7/4.
- 1.3-4 Ishii, Y., *Physical Review Letters* **89**, 205002 (2002).
- 1.3-5 Takeji, S., *et al.*, *Nucl. Fusion* **42**, 5 (2002).
- 1.3-6 Takechi, M., *et al.*, *the 20th IAEA Fusion Energy Conf.*, Vilamoura 2004, EX/P2-32.
- 1.3-7 Bakhtiari, M., Kawano, Y., Tamai, H., *et al.*, "Disruption Mitigation Experiments in the JT-60U Tokamak", *IAEA FEC 2004*, EX/10-6Rb.
- 1.3-8 Kawano, Y., Nakano, N., Isayama, A., *et al.*, "Characteristics of Post-disruption Runaway Electrons with Impurity Pellet Injection", to appear in *J. Plas. Fusion Res.*

1.4 H-mode and Pedestal Research

1.4.1 Dimensionless Pedestal Identity Experiments in JT-60U and JET in ELMy H-Mode Plasmas [1.4-1]

Dimensionless identity experiments in JT-60U and JET, aimed at the comparison of the plasma pedestal characteristics and ELM behavior in the two devices, were continued in this year. The method chosen for this study is the "dimensionless identity technique", based on the invariance of plasma physics to changes of dimensional parameters, e.g. n_e , T_e at the pedestal, when the dimensionless plasma parameters are conserved (normalised plasma pressure β , safety factor q , Larmor radius ρ^* and collisionality ν^*). In contrast to other dimensionless comparison experiments, the similar size of JET and JT-60U results in dimensionless matched plasmas that are also very similar in their dimensional parameters, with the exception of the major radius.

The comparison of the pedestal profiles of dimensionless matched JET and JT-60U H-modes may help to gain further insight in the underlying physics mechanisms determining the similarities and difference in the H-mode characteristics. Figure I.1.4-1 shows a

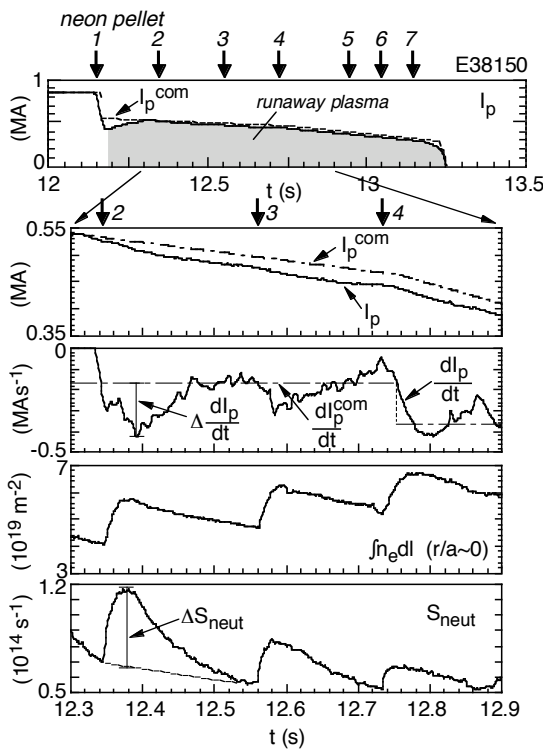


Fig. I.1.3-5 Waveforms of impurity pellet injection into a runaway plasma.

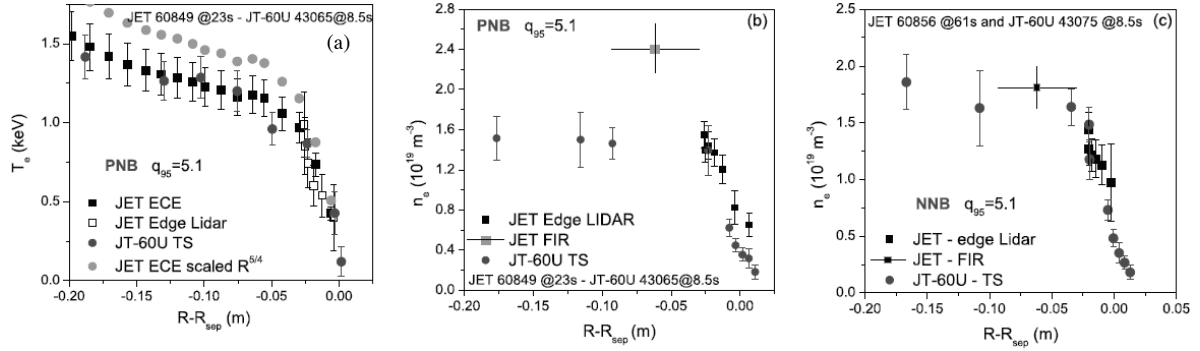


Fig. I.1.4-1. Pedestal profiles comparison for the two $q_{95}=5.1$ nearly matched JET/JT-60U discharge pairs. (a) Experimental T_e profiles for #60849 (JET) and E43065 (JT-60U, PNB) experimental values (black dots) and scaled values (grey dots). (b) Density profiles for the same pair of pulses as (a). (c) n_e profiles for #60856 (JET) and E43075 (JT-60U, NNB).

comparison of some pedestal profiles for the nearly matched discharges at $q_{95}=5.1$. Figure I.1.4-1(a) compares T_e profiles for the pair E43065 (JT-60U, PNB) and JET #60849, while Fig. I.1.4-1(b) shows the pedestal n_e profiles for the same pair in Fig. I.1.4-1(a). As for the T_e profile, a reasonable match is obtained for T_e at the pedestal top, pedestal width and gradients. The picture is quite different for the pedestal densities as shown in Fig. I.1.4-1(b). The density pedestal of JET is much higher and wider than that of JT-60U. A comparison of the edge density gradient ∇n_e is not straightforward, since $n_e(r)$ of these JET discharges is measured with good space resolution only over a part of the pedestal density gradient region.

A major difference between JET and JT-60U identity configuration is the B_T ripple, $\sim 0.1\%$ in JET compared to $\sim 1.2\%$ in JT-60U at outer midplane. The associated fast ion losses in JT-60U are substantial, of the order of several MW for the plasma investigated. The resulting edge electric field may provide a counter-rotation source at the plasma edge sufficient for JT-60U plasmas to counter-rotate even for net positive parallel momentum injection. Experiments where a large fraction of perpendicular PNB were substituted by co-NNB gave conflicting results: at low q , no significant increase of the pedestal pressure was observed, in contrast to the high q plasmas, where the use of NNB resulted in the highest pedestal pressures. In this case, the pedestal density obtained in JET and JT-60U are quite similar (within 15%) as shown in figure I.1.4-1(c). In both q cases, though, the plasma toroidal rotation changed in a similar way (V_T is less negative). The reasons for the different behavior of the pedestal pressure at low and high q , as well as that for

the improved performance at high q , are not yet understood.

As for the reason of smaller pedestal performance in JT-60U, two possible mechanisms have been considered. One is the effect of toroidal rotation on the pedestal performance. The other is that the ripple may have a direct effect on the thermal ion transport. In order to separate both effects in the experiments, further experiments are planned in both devices, an installation of ferritic steel in JT-60U to reduce the ripple and ripple enhancement experiment on JET by changing toroidal field coil currents for every other coil.

1.4.2 Impact of Toroidal Rotation on ELM Behavior [1.4-2]

The ability to actively change the plasma rotation using a combination of the tangential and perpendicular NBIs in JT-60U has aided the efforts to determine the effects of counter rotation on the ELM characteristics in grassy ELM regime ($q_{95} \sim 4.9$ and $\delta \sim 0.59$) and type I ELM regime ($q_{95} \sim 4.1$ and $\delta \sim 0.28$), in terms of accessibility and controllability of small ELM regimes.

In JT-60U, the edge plasma near the top of the temperature pedestal rotated in the counter (CTR) direction even when CO-NBIs were applied. One possible reason is that the ripple-induced fast ion loss may cause a negative E_r . Therefore, replacing perpendicular (PERP) NBIs with tangential CO-NBIs leads to less CTR toroidal rotation. Figure I.1.4-2 shows the response of the divertor D_α signal during these rotation scans with fixed plasma shape. As can be seen, the ELM type was clearly changed from type I ELMs to grassy ELMs with higher frequency up to

1500 Hz. As the CTR rotation was increased, the ELM frequency gradually increased together with a reduction in the ELM amplitude.

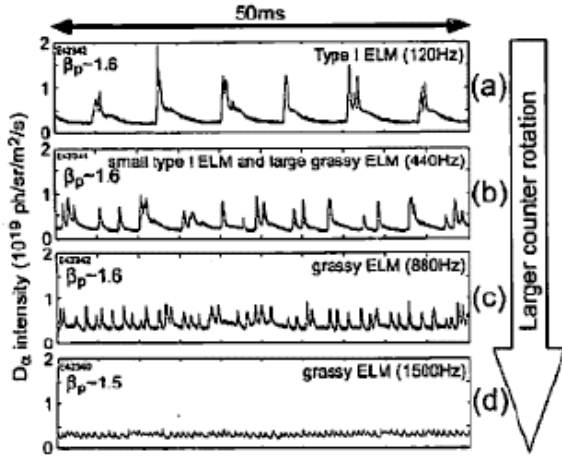


Fig. I.1.4-2 Time evolution of D_α signal during plasma toroidal rotation scan at $q_{95} \sim 4.9$ and $\delta \sim 0.59$. Plasma rotation profiles were changed by using different combinations of NBIs: (a) 2CO+2PERP +2N-NB, (b) 2CO+3PERP+1N-NB, (c) 2CO+5PERP and (d) 1CO+1CTR+5PERP.

All the plasmas shown in Fig. I.1.4-2 satisfied the typical parameters (e.g. q_{95} , d and β_p) for access to the grassy ELM regime, but the ELM characteristics were clearly different. Therefore, the toroidal rotation can be considered as an important parameter for access to the grassy ELM regime. One can question whether the most important parameter affecting the ELM type is the absolute value or the direction of the toroidal rotation. Since we cannot obtain a larger CO rotation as yet, further experiments are required to resolve this issue.

In the type I ELMy H-mode plasmas, the change of plasma rotation (or direction of the momentum input) affects the ELM frequency and amplitude, but the plasma usually remains in the type I ELMy phase. When the plasma position was carefully optimized, a steady ELM free phase (QH-mode) with stationary pedestal parameters was obtained as shown in Fig. I.1.4-3. After the LH transition at $t=3.45$ s, an intermittent ELMing phase is observed. Then, the D_α signal remains at a high level from $t=4.56$ s, which is concurrent with clear coherent temperature fluctuations (T_e fluctuation) with frequencies of ~ 9 kHz and ~ 18 kHz. The mode was localized at the edge ($R-R_{sep} \sim 2$ cm), and edge density and ion-saturation current at divertor target were also modulated with the same frequency as the edge temperature fluctuation. This edge fluctuation

may cause the reduction of pedestal pressure by $\sim 18\%$.

Basically, the QH-mode seems to be easily reproducible with CTR-NBIs. However, we have also observed partial QH phase during CO-NB injection phase with almost no net toroidal rotation at the plasma edge and during BAL-NB injection phase. The occurrence of T_e fluctuations together with enhancement of the D_α signal was also observed in all QH phases.

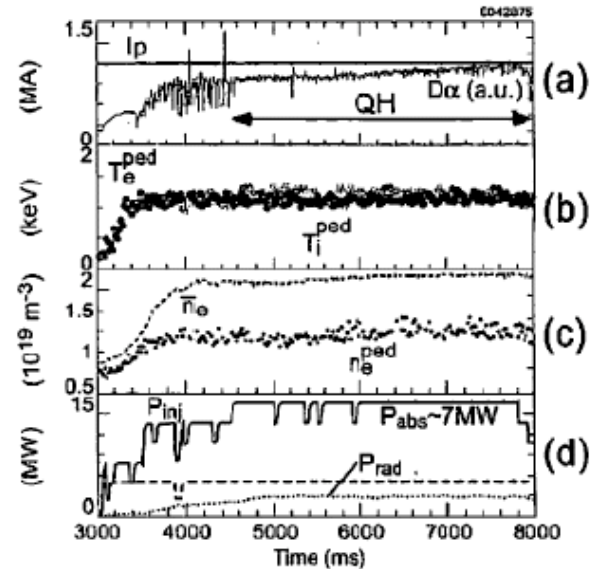


Fig. I.1.4-3 Typical waveforms of QH-mode plasma in JT-60U. (a) plasma current and divertor D_α signal. (b) pedestal T_e (black) and T_i (gray). (c) line-averaged density and pedestal density. (d) Solid (dashed) line show total (CTR) NBI power together with radiation power shown by dotted line.

1.4.3 Reduced Heat Transport during the Inter-ELM Phase [1.4-3]

For the H-mode physics, the characteristics of the heat transport in a time scale longer than ELM events has been studied to predict the performance in future reactor. In addition, the energy pulse expelled by ELMs has also been intensively studied for the interest of predicting the peak heat load onto plasma facing components. However, little is known about heat transport that occurs during the phase between ELMs (or 'inter-ELM phase'). In fact, the modelling of ELMy H-mode involving MHD stabilities and anomalous transport process cannot be developed without the transport process responsible for the inter-ELM phase. In this study, the reduction of electron heat diffusivity during the inter-ELM phase to the level of ion

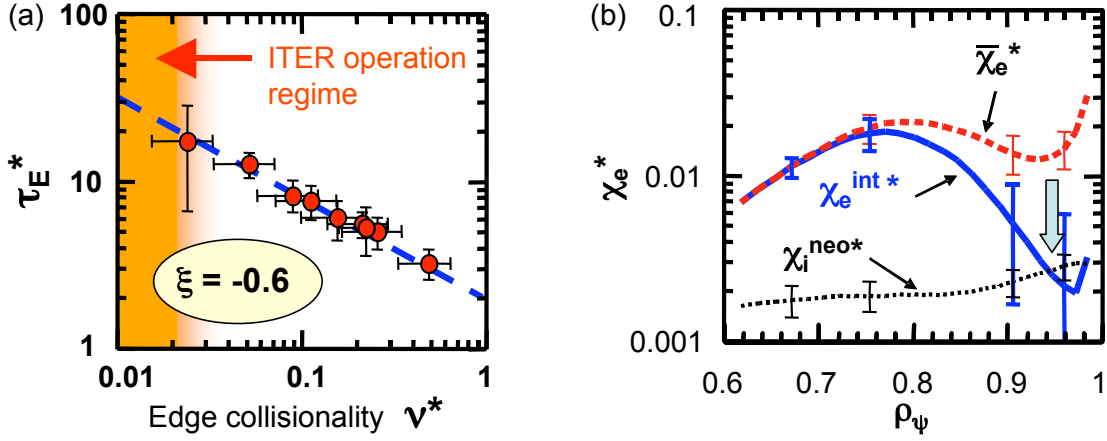


Fig. I.1.4-4 (a) Dependence of the normalized energy confinement time between ELMs τ_E^{int}/τ_B on ν^* at $\rho_{pol}^* \sim 0.05$, $\beta_{pol} \sim 0.3$, $q_{95} \sim 4.0$ and $\delta \sim 0.3$. (b) The profiles of the electron heat diffusivity during the inter-ELM phase. The electron heat diffusivity in a global time scale and the ion neoclassical heat diffusivity are also shown for reference.

neoclassical transport was found in the plasma edge region affected by an ELM burst.

Understanding the completed system of self-regulating dynamics of ELMI cycle is realized by separating the recovery phase between ELMs from the instantaneous ELM burst phase. In JT-60U, we have investigated the characteristics of the heat transport during the inter-ELM phase for the first time in the world. In a steady-state phase in a time scale much longer than an ELM event, the energy balance near the plasma boundary can be expressed as: $P_{heat} = P_{int} + P_{ELM}$ where P_{int} and P_{ELM} ($= f_{ELM} DW_{ELM}$) are the loss powers of the inter-ELM transport and ELMs, respectively. The source heating power crossing the separatrix is assigned to these two loss channels. In this study, it has been found that, as ν^* is increased, the inter-ELM transport is enhanced and the ELM heat loss is reduced. Since the reduced heat transport is always accompanied by a large ELM loss power, one can find that it is not simple to achieve the high energy confinement simultaneously with small ELM heat loss particularly at low ν^* .

In order to understand the process responsible for heat transport during the inter-ELM phase, we have examined the dependence of the inter-ELM energy confinement time τ_E^{int*} ($= \tau_E^{int}/\tau_B$) on ν^* as shown in Fig. I.1.4-4(a). It is obviously seen that τ_E^{int*} is significantly improved as ν^* is reduced, satisfying the relation of $\tau_E^{int*} \propto \nu^{*-0.6}$. Since the energy confinement in a global time scale shows weaker ν^* dependence given as $\tau_E^* \propto \langle \nu^* \rangle^{-0.35}$, this result is indicative of a

more collision-based heat transport during the inter-ELM phase. We have also examined the ρ_{pol}^* dependence. In the peripheral plasma region, it is hard to conduct the pure ρ_{pol}^* scan because of the existing edge stability boundary. Thus, by adopting the knowledge of the ν^* dependence obtained former, we have obtained the relation of $\tau_E^{int*} \propto \rho_{pol}^{*-0.7}$. During the inter-ELM phase, this collapsed profile is replenished by the heat flux from the plasma core. From this point of view, the electron heat diffusivity during the inter-ELM phase χ_e^{int*} ($= \chi_e^{int}/\chi_B$) has been calculated using the relative perturbations of T_e profiles due to an ELM. (see Fig. I.1.4-4(b)). In the plasma edge region which is affected by ELM burst, the electron heat diffusivity is reduced significantly to the level of the ion neoclassical transport.

References

- 1.4-1 Saibene, G, *et al.*, *Proc. 20th Int. Conf. on Fusion Energy 2004 (Vilamoura, 2004) IAEA-CN-116//IT/1-2*.
- 1.4-2 Oyama, N, *et al.*, *Proc. 20th Int. Conf. on Fusion Energy 2004 (Vilamoura, 2004) IAEA-CN-116/EX/2-1*.
- 1.4-3 Urano, H, *et al.*, *Phys. Rev. Lett.*, 95 035003 (2005).

1.5 Current Drive Research

1.5.1 Real-Time Control of Safety Factor Profile

[1.5-1]

Active control of safety factor profile is essential in sustaining a high performance plasma that is optimized in stability and confinement. A real-time control system of safety factor (q) profile has now been developed in

JT-60. This system, for the first time, enables 1) real time evaluation of q profile using local magnetic pitch angle measurement by motional Stark effect (MSE) diagnostic and 2) control of current drive (CD) location (ρ_{CD}) by adjusting the parallel refractive index N_{\parallel} of lower-hybrid (LH) waves through the change of phase difference ($\Delta\phi$) between multi-junction launcher modules.

A newly developed method for the q profile evaluation realized q profile calculation within every 0.01s, which is much faster than current relaxation time, typically order of 1s. Safety factor profile by the real-time calculation agreed well with that by equilibrium reconstruction with MSE. See section I.2.6.2 for comparison of $q(r)$ by the two methods. From temporal evolution of q (or current) profile, the system also evaluates ρ_{CD} in real-time. The location ρ_{CD} is where the rate of the current enclosed between two magnetic surfaces on which MSE channels are viewing are increasing. The control system changes ρ_{CD} through N_{\parallel} (or directly $\Delta\phi$) in such a way to minimize the largest residual between the real-time q profile and its reference profile. Since we had a dataset showing increase of N_{\parallel} or $\Delta\phi$ shifts ρ_{CD} outward in minor radius, we employed an algorithm to control $\Delta\phi$ as follows; $d(\Delta\phi)/dt = -\alpha(\rho_{CD} - \rho_{CDref})$; α is a positive constant. The system determines ρ_{CDref} , comparing real-time $q(r)$ and a give reference $q(r)$; ρ_{CDref} is where the system wants to drive current. Thus, when CD location ρ_{CD} is smaller than the reference CD location ρ_{CDref} , the system increase $\Delta\phi$ in order to shift CD location outward.

The real-time control system was applied to positive shear plasmas having $q(0)\sim 1$ at $I_p=0.6MA$, $B_t=2.3T$, and $n_e=0.5\times 10^{19}m^{-3}$. The reference q profile was set to $q(0)=1.3$. In order to keep good coupling of LH waves to the plasma, gap between the launcher and the plasma surface was controlled to about 0.1m. Figure I.1.5.1 (a) shows waveforms of the discharge. When the LH power was stably injected ($t>10s$), the loop voltage dropped down to 0V, $q=1$ surface vanished and $q=1.25$ surface shrank. The largest residual decreased close to its error level. The real-time q profile (Fig. I.1.5-1 (b)) approached to its reference profile after application of the real-time control; the controlled q profile was sustained for 3s ($t=13-16s$), which was limited by injected LH power.

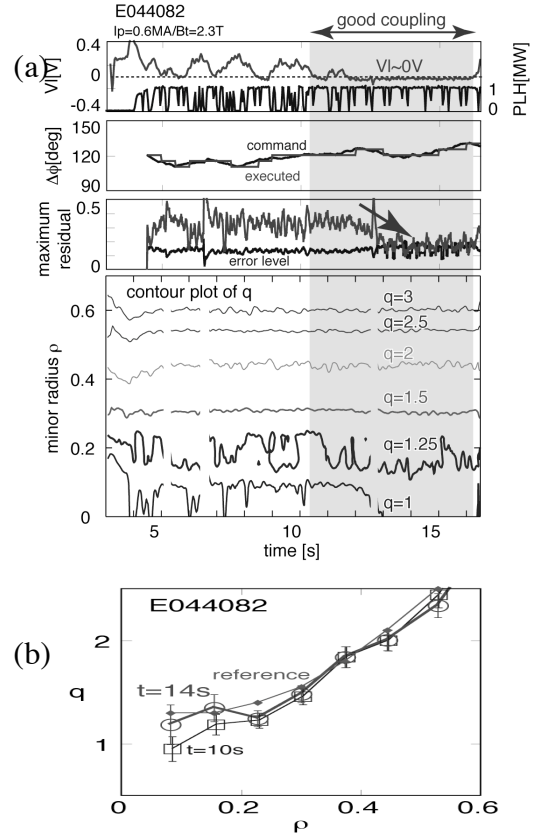


Fig. I.1.5-1 (a) Waveforms of loop voltage (V_l), LH power (P_{LH}), phase difference between launcher modules ($\Delta\phi$), the largest of residuals between q by real-time calculation and reference q , and contour plot of safety factor profile $q(\rho, t)$. (b) q profiles in (a) by real-time calculation at beginning of the control ($t=10s$; open rectangles), and during the control ($t=14s$; circles). Closed rectangles show the reference q profile.

1.5.2 Validation of Beam Particle Self Interaction

Circulating fast ions generated by NBI are predicted to affect the beam stopping cross-section of the neutral beam itself through the interaction between the neutrals and the fast ions. This "beam-particle self-interaction (BPSI)" can be notable especially for a high-energy beam injected into a low density plasma [1.5-2,3].

One of the beam lines of N-NB, N-NB (U), was used for this experiment. The beam power was 1.5 MW with an energy of 350 keV. The major plasma parameters have been maintained nearly in constant; $I_p=1MA$, $B_t=2.5T$, $\langle n_e \rangle = 0.92 \times 10^{19} m^{-3}$, $\langle T_e \rangle = 1.2 keV$. The beam pulse duration was 1.5 sec, which is much longer than the beam slowing down time. The shine-through power is evaluated using temperature increment of N-NB facing tiles measured by an infra-

red (IR) camera. Heat transport analysis of the facing tile has shown that the time evolution of the tile temperature is not reproduced by assuming the shine-through power in proportion to beam power, but it has been well reproduced assuming that the shine-through fraction decreases exponentially about by 35% within several hundred msec.

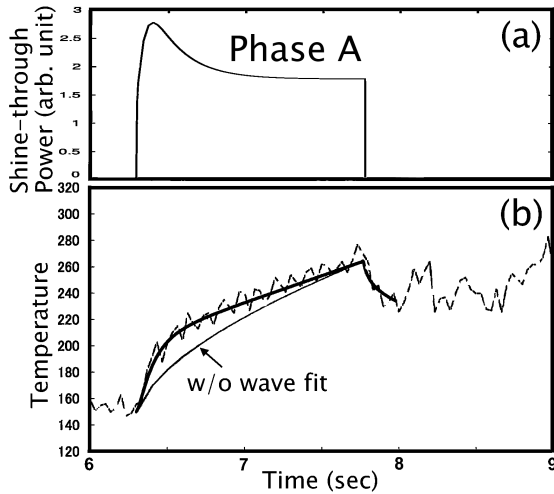


Fig.I.1.5-2 (a) An estimated waveform for shine-through and (b) temperatures of the facing tiles. The measured temperature is denoted by a dotted curve while the numerical calculation is denoted by a solid curves.

This time scale is close to the build-up time of fast ion component (~ 200 msec). The reduction of shine-through is also consistent to the estimated range by the BPSI theory[1.5-4].

1.5.3 Current Clamp in the Current Hole

A stable tokamak plasma with nearly zero toroidal current in the central region (a “current hole”) is sustained for several seconds in the JT-60U tokamak [1.5-5]. However, it has not been clear whether the current drive source such as inductive toroidal electric field E_ϕ and non-inductively driven current j_{NI} remains at zero level during the sustainment of current hole or some mechanism works to clamp the current density at zero level against the current drive source.

Two kinds of experiments were performed to investigate responses to E_ϕ and j_{NI} separately [1.5-6, 1.5-7]. In the first experiment, E_ϕ was changed transiently by variation of j_{NI} outside the current hole, keeping j_{NI} inside the current hole as small as possible. The electron cyclotron wave (ECW) power of 2.6 MW

at the frequency of 110 GHz was injected outside the current hole at $t = 5.2$ s during the current flat top in a plasma of $I_p = 1$ MA and $B_t = 3.6$ T, to increase j_{NI} (the EC-driven current and the bootstrap current) in the direction of the main plasma current. In the same discharge, at $t = 6.0$ s or 0.8 s after the start of ECW injection, ECW power and almost all NB power were turned off, to decrease j_{NI} rapidly. Radial profiles of loop voltage $V_{loop}(\rho)$ are shown in Fig. I.1.5-3(a), where ρ denotes the normalized minor radius. The $V_{loop}(\rho)$ is obtained from the time-derivative of the poloidal magnetic flux $\Psi(\rho)$ which is determined by the equilibrium reconstruction using the MSE data. The $V_{loop}(0)$ was negative (~ -0.3 V) during EC injection ($t = 5.4$ -5.6 s) while it was positive ($\sim +0.4$ V) after the stop of EC injection ($t = 5.98$ -6.4s). Note that uncertainties in $V_{loop}(\rho)$ are relatively small near the axis though they are large around $\rho = 0.5$ where $\Psi(\rho)$ has a large gradient. In Fig. I.1.5-3, the sum of calculated j_{OH} , j_{EC} , j_{BD} and j_{BS} and the measured j_{tot} are

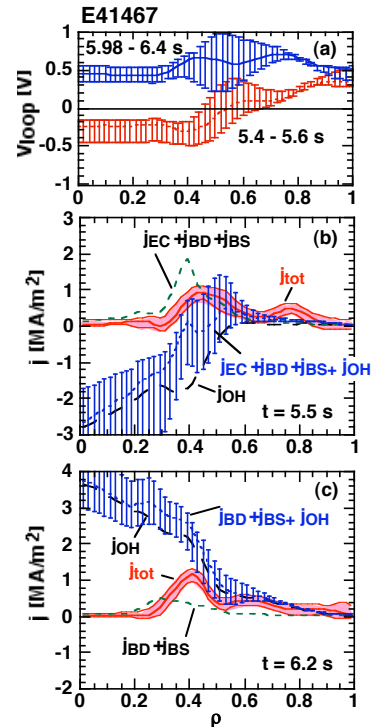


Fig. I.1.5-3. Radial profiles of loop voltage and current density in a discharge with E_ϕ changed transiently. (a) Loop voltage V_{loop} during $t = 5.4$ -5.6 s and $t = 5.98$ -6.4 s. (b), (c) Current densities at $t = 5.5$ s and $t = 6.2$ s. In (b) and (c), j_{tot} (solid line with a shaded belt) denotes the measured current density, while the summation of $j_{OH} + j_{BD} + j_{BS} + j_{EC}$ is shown by the dotted line with the error bars.

compared for (b) negative $E_\phi(0)$ and (c) positive $E_\phi(0)$ cases. Here j_{OH} , j_{EC} , j_{BD} and j_{BS} denote the calculated inductive, EC-driven, beam-driven and bootstrap current densities, respectively. In both cases, the calculated current density is dominated by the inductive current, and is largely negative in (b) and is largely positive in (c). The measured current density, however, remained nearly zero. In the second experiment, EC current drive inside the current hole was attempted in the same and opposite directions to the plasma current in a plasma of $I_p = 1$ MA and $B_t = 3.7$ T during the quasi stationary period with small $E_\phi(0)$. In neither direction did the EC current drive change the current inside the current hole, and the current hole was maintained.

From these results, it has been shown experimentally for the first time that although the current drive source exists in the current hole, some mechanism works to clamp the current density at zero level once when it becomes at zero level in the central region. Simulation results show that resistive MHD instabilities take place in the current hole, leading to the current clamp. In our experiments, however, no MHD instabilities with a high frequency (1-100 kHz range) were observed. Though small collapses with longer intervals (~ 0.1 s) were observed in some discharges, no clear change in the current density inside the current hole was observed between or at these collapses, indicating that these collapses are not the cause of the current clamp in the current hole.

References

- 1.5-1 Suzuki, T., *et al.*, *Proc. 20th Fusion Energy 2004 (2004)* IAEA-CN-116/EX/1-3, submitted to Nuclear Fusion.
- 1.5-2 Okano, K., *Nuclear Fusion* **31**, 1349 (1991).
- 1.5-3 Okano K. *et al.*, "Non-linear increment of beam stopping cross-section by circulating fast ions", *Proc. 28th EPS Conf. Control. Fusion. Plasma. Phys.* (2001).
- 1.5-4 Okano, K. *et al.*, Submitted to Journal of Plasma and Fusion Research
- 1.5-5 Fujita, T., Oikawa, T., Suzuki, T., *et al.*, *Phys. Rev. Lett.* **87**, 245001 (2001).
- 1.5-6 Fujita, T., Suzuki, T., Oikawa, T., *et al.*, *Proc. 20th Fusion Energy 2004 (2004)* IAEA-CN-116/EX/P4-3.
- 1.5-7 Fujita, T., Suzuki, T., Oikawa, T., *et al.*, "Current Clamp at Zero Level in JT-60U Current Hole Plasmas"; to be published in Phys. Rev. Lett.

1.6 Divertor/SOL Plasmas and Plasma-Wall Interaction

1.6.1 SOL Transport of ELM Plasma and Fluctuations in L- and H-Modes

Transient heat and particle loading caused by ELM is crucial for determining the lifetime of ITER divertor materials. At the same time, study of the ELM radial propagation was recently focused to evaluate the heat and particle loadings to the first wall. Determination of the perpendicular propagation during ELM deposition (such as a few 100 μ s) was improved with increasing sampling rate from 200kHz to 500kHz for the Mach probes (at outer midplane and X-point) and magnetic pick-up coils [1.6-1]. Fluctuation level was compared in L-mode and ELMy H-mode plasmas, and analysis of the fluctuation characteristics using Probability Distribution Function (PDF) was initiated [1.6-2].

(1) Characteristics of ELM propagation

During ELM deposition, large multi-peaks appeared in ion saturation current at midplane Mach probe, j_s^{mid} , during the base level of j_s^{mid} increasing, just after large magnetic turbulences due to MHD activities (Fig.I.1.6-1). Time lags of the first j_s^{mid} peak and the maximum base-level were defined as $\tau_{perp}^{mid}(\text{peak})$ and

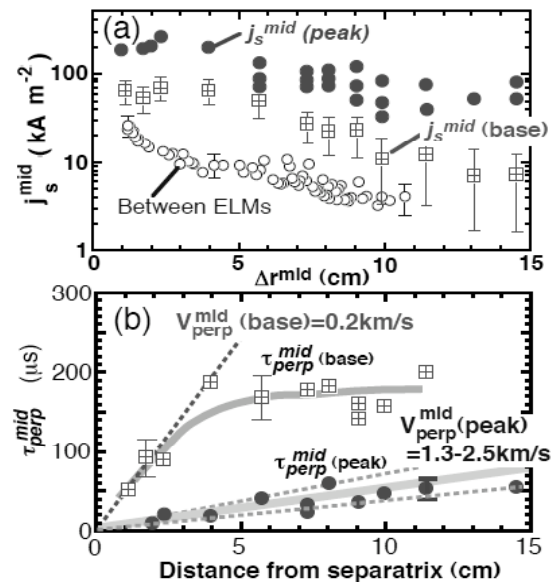


Fig.I.1.6-1 (a) Distributions of j_s^{mid} peaks, maximum base-level during ELM, and j_s^{mid} between ELMs as a function of D_r^{mid} . (b) Distributions of $\tau_{perp}^{mid}(\text{peak})$ and $\tau_{perp}^{mid}(\text{base})$

$\tau_{\text{perp}}^{\text{mid}}(\text{base})$, respectively. Here, $\tau_{\text{perp}}^{\text{mid}}(\text{peak})$ was a delay due to the SOL plasma transport across the magnetic field, and duration of large j_s^{mid} peaks, δt^{peak} , was short: 8-24 μs . For example, $\tau_{\text{perp}}^{\text{mid}}(\text{peak}) \sim 40\mu\text{s}$, and $\tau_{\text{perp}}^{\text{mid}}(\text{base}) \sim 160\mu\text{s}$ at the midplane distance from separatrix (Δr^{mid}) of 4.8 cm. On the other hand, the delay of the increase in divertor j_s^{div} , $\tau_{\text{para}}^{\text{div}}$, was 70-130 μs , and that of the maximum j_s^{div} base level, $\tau_{\text{para}}^{\text{div-peak}}$, was 130-200 μs . These time lags were consistent with parallel convective transport time along the magnetic field, $\tau_{\text{para}}^{\text{SOL-DIV}} = 140 \mu\text{s}$. As a result, the radial transport of the peak j_s^{mid} was faster than $t_{\text{para}}^{\text{div}}$, whereas parallel and radial propagation of the base-level were comparable.

The large multi-peaks in j_s^{mid} were observed over all radii ($\Delta r^{\text{mid}} < 15 \text{ cm}$) with large radial delay length. Since $\tau_{\text{perp}}^{\text{mid}}(\text{peak})$ increased with Δr^{mid} , the radial velocity, $V_{\text{perp}}^{\text{mid}}(\text{peak})$, ranged between 1.3 and 2.5 km/s. From $V_{\text{perp}}^{\text{mid}} \sim 2 \text{ km/s}$, characteristic radial scale of the j_s^{mid} peak was estimated to $\delta t^{\text{peak}} V_{\text{perp}}^{\text{mid}} = 1.5 - 4 \text{ cm}$, which may locally deposit the heat and particle loading to the first wall. Enhancement of j_s^{mid} base-level occurred globally and simultaneously in far SOL and divertor. Extension of the j_s^{mid} base-level was within smaller SOL radii ($\Delta r^{\text{mid}} < 10 \text{ cm}$), which may only influence particle and heat load to outer baffle.

(2) Characteristics of SOL Plasma Fluctuations

For ELMy H- and L-modes, fluctuation levels of the midplane SOL plasmas, $\delta j_s^{\text{mid}} / \langle j_s^{\text{mid}} \rangle$, were generally 4-5 times larger than those near X-point. At the same time, far SOL $\delta j_s^{\text{mid}} / \langle j_s^{\text{mid}} \rangle$ in H-mode was increased with Δr^{mid} , which became 5-10 times larger than L-mode. Here, e-folding lengths of j_s^{mid} profiles were comparable for H- and L-modes, thus the decay length was not influenced by the fluctuation level.

Statistical analysis of the j_s^{mid} signals using PDF showed that density bursts became remarkable around $\Delta r^{\text{mid}} = 6-7 \text{ cm}$. Since the direction of the parallel SOL flow changed from the inner divertor to the outer divertor near $\Delta r^{\text{mid}} = 7 \text{ cm}$, enhancement of the density bursts may be related to the stagnation of the SOL flow. The fast fluctuations and ELM bursts are under investigation using Wavelet analysis, which shows transient characteristics of turbulences.

1.6.2 Spectroscopic Study of H₂ Molecules in Divertor

Understanding behavior of H₂ molecules in divertor plasmas is important for control of divertor plasmas and diagnostics of neutral particles [1.6-3]. In JT-60U, H₂ molecule behavior in attached and detached divertor plasmas has been studied by observation of H₂ Fulcher line emission [1.6-4].

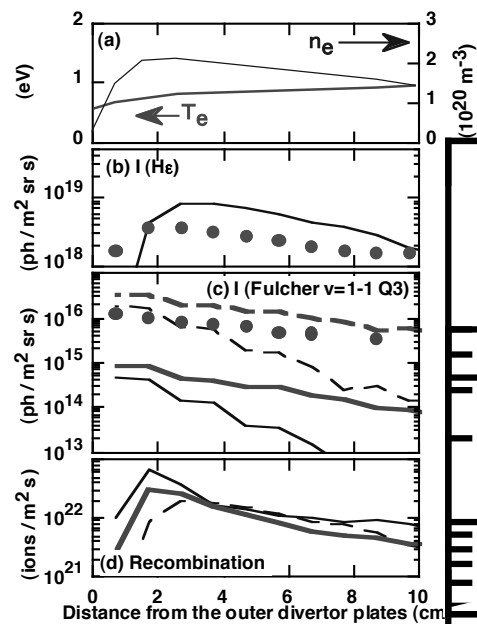


Fig. 1.1.6-2. Spatial profiles in the detached divertor plasma as functions of the distance from the outer divertor plates. (a) Calculated electron temperature and density along the separatrix, (b) observed (points) and calculated (line) He I line intensity, (c) observed (points) and calculated (continuous line: with dissociative attachment from the n=3 state, broken line: without dissociative attachment) Fulcher v=1-1 Q3 line intensity, (d) calculated MAR (continuous line) and H⁺-e recombination (broken line) rate. In both (c) - (d), the thick and thin lines indicate the results obtained by assuming that the vibrational temperatures of the ground state were 0.5 eV and 1 eV, respectively.

The decay lengths of the H₂ Fulcher line intensity in attached and detached divertor plasmas were roughly 1 cm and 4 cm, respectively. It suggested that the H₂ molecules penetrated more deeply into the detached divertor plasma than into the attached divertor plasma. The fall in intensity of the H₂ Fulcher lines with distance from the divertor plates was reproduced by calculation using a neutral transport and a collisional

radiative model code. Spatial profiles of various measured and modeled plasma parameters in the detached divertor plasma are shown as functions of the distance from the outer divertor plates in Fig. I.1.6-2. A detached divertor plasma solution was obtained from calculation using a two dimensional fluid code. The H₂ Fulcher line intensity profiles calculated with and without considering the dissociative attachment from the n=3 state are compared with the observed profile. With the ground-state vibrational temperature of 0.5 eV, the calculation reproduced the logarithmic slopes in the observed intensity profile. Molecular assisted recombination (MAR) was estimated to be as important as H⁺-e recombination in the detached divertor plasma.

1.6.3 Modelling of Impurity Transport [1.6-5]

Impurity transport has been modeled using the 2-D fluid code UEDGE [1.6-6] in the divertor plasma for the high β_p H-mode plasma with highly enhanced radiation by injecting seed impurity Ar. The impurity diffusivity was set to be 1.0 m²/s without the convection velocity. The carbon yield rate was set to be a Haasz yield [1.6-7] for both physical and chemical sputtering. The ratio of total Ar density to the electron density at the core_{edge} boundary (96% flux surface) (n_{Ar}/n_e)_{core_{edge}} was scanned in the range of 0.14-1%.

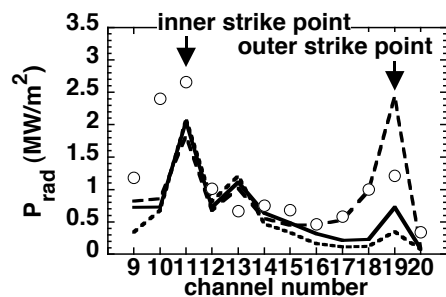


Fig. I.1.6-3. Calculated (lines) and measured (circles) radiation profiles. Dashed, solid and dotted lines show the radiation profile calculated using UEDGE results with (n_{Ar}/n_e)_{core_{edge}}=1%, 0.75% and 0.14%, respectively.

Figure I.1.6-3 shows comparison of radiation profile in the divertor plasma between measurement and calculation. The calculated divertor radiation had peaks at both strike points (ch 11 for inner and ch 19 for outer divertor) as well as the measurement. The peak at the inner strike point was almost constant even

when (n_{Ar}/n_e)_{core_{edge}} was increased. The peak at the outer strike point was largely enhanced with (n_{Ar}/n_e)_{core_{edge}}=1% and was larger than the peak at the inner strike point. The calculated radiation with (n_{Ar}/n_e)_{core_{edge}}=0.75%, which was consistent with edge Ar density estimated from the radiation in the main plasma, was consistent with the measurement at the inner strike point within the ambiguity of the measurement. At the outer strike point, the effect of misalignment of the sight lines was large due to strong localization of the radiation in front of the outer divertor plate. Therefore, when possible misalignment was considered, the radiation loss at the outer strike point increased to the same value as the measurement. On the other hand, the radiation in the divertor region (ch 9&10 for inner and ch 17&18 for outer divertor) was smaller than the measurement, indicating that the calculated radiation was localized around the strike points compared with the measurement.

1.6.4 Retention Characteristics of Hydrogen Particles

In order to study the tritium retention in different conditions (divertor geometry and operation temperature) compared with other tokamaks, we have investigated the erosion/deposition distribution and the hydrogen isotopes (H,D,T) behavior in the JT-60U plasma-facing wall (carbon-based). Fig. I.1.6-4 shows schematic views of the JT-60U W-shaped divertor with an inner pumping slot and sample locations for the analyses. The operation temperature of the JT-60U

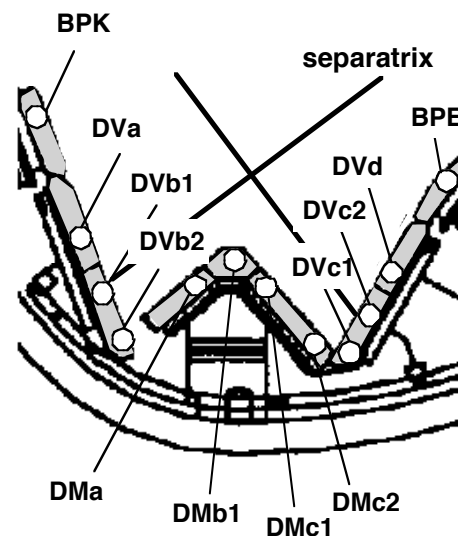


Fig. I.1.6-4 Sample locations

vacuum vessel was ~ 570 K. The base temperature of the divertor tiles were also ~ 570 K, since the divertor tiles were inertially cooled. The sample tiles were exposed to plasma from June 1997 to October 1998. The total number of deuterium discharges during this periods was ~ 3600 shots. Following the deuterium discharges, ~ 700 hydrogen shots were performed in a clean-up operation.

Deposition was found to be dominant on the inner divertor target, whereas erosion was dominant on the outer divertor target. No continuous deposition layer was obviously observed in the dome top tile [1.6-8]. Such in/out asymmetry of the erosion/deposition has been observed also in many tokamaks. In JT-60U, however, distributions of the hydrogen isotopes were not obviously correlated with the deposition distribution as described later.

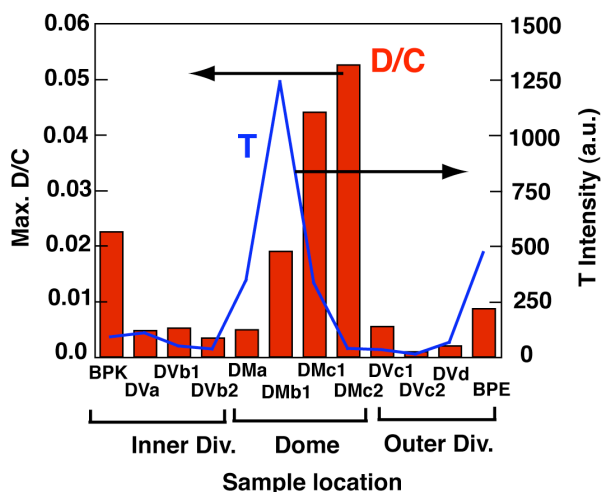


Fig. I.1.6-5 Tritium and deuterium distributions
Tritium intensity and D/C ratio were obtained by imaging plate technique and nuclear reaction analysis, respectively

Distribution of the tritium, which was produced by D-D nuclear reaction, in the plasma-facing wall reflected the distribution of high-energy tritium ion implantation due to ripple loss and a slight modification owing to high surface temperature of the divertor target tiles. According to OFMC simulation, $\sim 50\%$ of the produced tritium were lost and implanted into the wall with high energy of up to ~ 1 MeV [1.6-9].

Deuterium distribution in the JT-60U divertor region was slightly different from the tritium distribution as shown in Fig. I.1.6-5. The highest concentration of the hydrogen isotopes was estimated

to be $(H+D)/C \sim 0.07$ at the outer dome wing, which is much less than that observed in other tokamaks. Such low $(H+D)/C$ must be attributed to high surface temperature of the dome tiles (~ 800 K). For the deuterium retention, at least two retention processes (ion-implantation and co-deposition) were distinguished on the dome region. [1.6-10, 11].

From these hydrogen isotope analyses, it was found that the behavior of the hydrogen isotopes in the plasma-facing wall should be also considered with the ion implantation as well as the co-deposition for the detailed estimation of the tritium retention in ITER.

References

- 1.6-1 Asakura, N. *et al.*, *32nd European Physics Society Conference on Plasma Physics, Tarragona, (2005)* P5- 006.
- 1.6-2 Miyoshi, H. *et al.*, *32nd European Physics Society Conference on Plasma Physics, Tarragona (2005)* P1-045.
- 1.6-3 Kubo, H., in *"Nuclear Fusion Research"*, edited by R. E. H. Clark and D. Reiter, Springer-Verlag Berlin, 121 (2005).
- 1.6-4 Kubo H., *et al.*, *J. Nucl. Mater.* **337-339**, 161 (2005).
- 1.6-5 Takenaga, H., *et al.*, to be published in *Journal of Plasma and Fusion Research SERIES 7*.
- 1.6-6 Rognlien, T.D., *et al.*, *Contrib. Plasma Phys.*, **34** 362 (1994).
- 1.6-7 Davis, J.W., Haasz, A.A., *J. Nucl. Mater.* **241-243**, 37 (1997).
- 1.6-8 Gotoh, Y., *et al.*, *J. Nucl. Mater.*, **313-316**, 370 (2003).
- 1.6-9 Masaki, K., *et al.*, *J. Nucl. Mater.*, **337-339**, 553 (2005).
- 1.6-10 Hirohata, H., *et al.*, *J. Nucl. Mater.*, **329-333**, 785 (2004).
- 1.6-11 Hayashi, T. *et al.*, *J. Nucl. Mater.*, in press.

2. Operation and Machine Improvements

Two cycles of the JT-60 operation were implemented in FY 2004, which includes 902 shots of plasma pulse discharge, 43 shots of commissioning pulse sequence, 15 hours of Taylor-type discharge cleaning and 239 hours of glow discharge cleaning.

In the operation of the JT-60 facilities, the motor generator for toroidal magnetic field coil (T-MG) was used tentatively in place of the motor generator for plasma heating systems which had been out of order in FY 2003. Therefore the electric power feeder lines and control system of the T-MG were modified. On the other hand, the toroidal magnetic field was activated only by the grid power line. With careful operation of these electric power systems, JT-60 experiments were successfully implemented as planned.

2.1 Tokamak Machine

2.1.1 Operation without a Center Solenoid Coil

Innovative plasma build-up operations without a center solenoid, which would simplify the structure of future tokamak fusion reactors, were planned in this experimental campaign. Since poloidal magnetic field coils would receive different forces from usual operations in these operations, electromagnetic force analysis was done to confirm the safety of these coils. The analysis result showed that the electromagnetic forces on the coils were smaller than 20% of the allowable limits respectively, and these coils would be mechanically safe in this experiment.

2.1.2 Transportation of Solid Radioactive Wastes

Solid radioactive wastes are taken out from JT-60 facilities and stored in metal drums in the radioactive waste storage building in every maintenance period. To reduce the combustible wastes by incineration, forty metal drums were transported from Naka site to Tokai Site, in which the facility of Department of Decommissioning and Waste Management treated with them in Tokai Site. The transportation was initiated in 1999 and a total of 240 drums were removed.

2.1.3 Fabrication of Ferritic Steel Plate and Installation into the First Wall

Installation of ferritic steel tiles was proposed in JT-60U to reduce the toroidal magnetic field ripple and to improve the fast ion loss, which decreases plasma

heating efficiency and increases heat load on plasma facing components in the operations with plasmas with a large volume. Candidate materials with a high saturated magnetization, SUS430 (18Cr), STBA26 (9Cr-1Mo) and F82H (8Cr-2W-0.2V-0.04Ta), were compared. Taking into account the cost-effectiveness to obtain a saturated magnetization required for experiments and the moderate neutron generation level in JT-60U, 8Cr-2W-0.2V ferritic steel whose activation element concentrations are a little higher than those of F82H was selected. The expected saturated magnetization is 1.8 Tesla at operational temperature of around 570 K.

Fabrication procedure of the ferritic steel mostly followed that of F82H. The steel more than 20 tons was melted in a vacuum induction furnace and cast into eight ingots. Seven ingots were used to obtain steel plates through the processes of forging and hot-rolling. These plates underwent normalizing at 1273 K for 30 min, air-cooling and then tempering at 1023 K for 90 min followed by air-cooling. The fabricated ferritic steel has clear tempered martensitic microstructures, and sufficient magnetic and mechanical properties. The saturated magnetization measured was over 1.7 Tesla at 573 K. Although it was lower than the expected value, it was confirmed by a numerical calculation that the saturated magnetization of 1.7 Tesla was sufficient for the JT-60 experiment.

2.1.4 Study of the Plasma-Surface Interaction

The cooperative research program between JAERI and universities using the JT-60 first wall tile was initiated in 2001. Under the program, various studies on the plasma facing materials have progressed [2.1-1], [2.1-2], [2.1-3]. Major research activities conducted in FY 2004 are as follows:

(1) Thermal Properties of Redeposition Layers on the Inner Divertor Tile [2.1-4]

Thermal properties of the redeposition layer on the inner plate of the W-shaped divertor of JT-60U were measured with laser flash method in order to estimate transient heat load such as ELMs onto the divertor. Morphology analysis of the redeposition layer was conducted with a scanning electron microscope.

Redeposition layers of more than 200 μm thick were observed near the most frequent striking point.

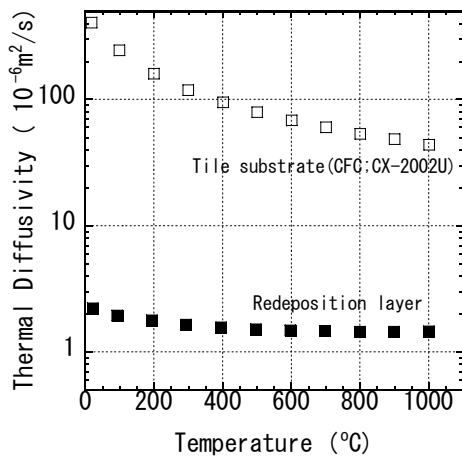


Fig. I.2.1-1 Temperature dependence of thermal diffusivity of the redeposition layer and the tile substrate (CFC).

The bulk density measured of the redeposition layer was 910 kg/m^3 . This is about half of the density of the tile substrate ($1,700 \text{ kg/m}^3$, CX-2002U). The specific heat of the redeposition layer is almost equal to that of isotropic graphite.

The thermal conductivity of the redeposition layer was calculated to be two orders of magnitude smaller than that of the tile substrate in the temperature range from room temperature to $1000 \text{ }^\circ\text{C}$ (Fig. I.2.1-1). This low thermal conductivity of the redeposition layer is considered to be caused by a high porosity and a low graphitization degree of the redeposition layer.

(2) Retention of Hydrogen Isotopes in Divertor Tiles

Retention characteristics of deuterium and hydrogen in graphite tiles placed in the inner side pumping divertor region were investigated by Secondary Ion Mass Spectrometry (SIMS) [2.1-5] and Thermal Desorption Spectroscopy (TDS) [2.1-6]. It was found that most of hydrogen and deuterium were retained in the re-deposited layers. The dominant species retained in the divertor tiles were H_2 , HD, D_2 and CH_4 . The amount of H+D retained in the inner divertor tiles covered by the re-deposited layers increased with the thickness of the re-deposited layers. Assuming that hydrogen isotopes were uniformly retained in the re-deposited layer and carbon density of re-deposited layer was 0.92 g/cm^3 , hydrogen isotope concentration (H+D)/C in the re-deposited layers were ~ 0.032 , which was much smaller than those observed in JET and other devices.

(3) Release Behavior of Hydrogen Isotopes from Graphite Tiles [2.1-7]

Hydrogen isotopes were released from the graphite tiles used in JT-60U by the thermal desorption method. When the first wall tile was left under helium atmosphere at 600°C for 8 hours, about 40 % of total amount of hydrogen and deuterium were released, while the amount of released tritium was only about 20 %. At high temperature of 1000°C , the release rate of deuterium and tritium was enhanced. It was found that the amount of hydrogen retained in the graphite tile was much larger than that of deuterium. This indicates that a large amount of deuterium trapped in the tiles during deuterium discharge experiments was replaced with hydrogen during hydrogen discharge experiments.

(4) Tritium Release Behavior During Air Exposure and Gas Purge Conditions [2.1-8]

Exhaust gas from the JT-60U tokamak was analyzed to understand the behavior of fuel and impurity elements in the vacuum vessel. The behavior of tritium release by an isotope exchange reaction during air exposure and gas purging phases has been investigated. For the air exposure with water vapor concentrations of 40ppm, 300ppm, 680ppm and 3400ppm, tritium concentration in the air was measured. It was confirmed that water vapor enhanced release of tritium from the vessel. Tritium concentration initially increased with time and then became constant finally at each concentration level. The total amount of tritium released from the vacuum vessel was 13MBq for 3400ppm, which is almost the same as that removed by 5 hours' H_2 -GDC that has been most effective detritiation method in JT-60U [2.1-9]. This suggests that tritium can be easily removed by water vapor.

Tritium release during the gas purging was measured. The various gases (H_2 , He and Ar) were introduced into the vacuum vessel at constant pressure by controlling the gas flow rate. Tritium concentration was about 0.1 Bq/cm^3 at room temperature and was independent of gas species within pressure from 0.05 to 0.3 Pa., indicating that isotope exchange of tritium with hydrogen molecules was not so active under these purge conditions.

A trace of Oxygen purge was also examined. In the tokamak discharge, various hydrocarbons such as CD_4 , C_2D_6 , C_2D_4 and C_2D_2 were detected and possible

relation with formation of codeposit is suggested because hydrocarbon could be produced by a shift reaction related with oxidized elements, such as water, carbon oxide and carbon dioxide. A gas purging and a glow discharge cleaning with 0.1% oxygen contained He showed a possibility of enhance the carbon removal. No effect of oxygen onto tokamak discharge was observed.

References

- 2.1-1 Masaki, K., *et al.*, *Proc., 16th PSI, Portland (2004)* to be published in *J. Nucl. Mater.*
- 2.1-2 Tanabe, T., *et al.*, *ibid.*
- 2.1-3 Tanabe T., *et al.*, *Proc. 20th IAEA Fusion Energy Conf., Vilamoura, EX/P5-32 (2004)*.
- 2.1-4 Ishimoto, Y., *et al.*, "Thermal properties and structure of redeposition layers in JT-60U", to be submitted in *J. Nucl. Mater.*
- 2.1-5 Oya., Y., *et al.*, 23rd Symp. on Fusion Technology, Venice, (2004), to be published in *Fusion Eng. Design.*
- 2.1-6 Hirohata, Y., *et al.*, 7th Int. Conf. Tritium Sci. and Technol., Barden-Barden, (2004), to be published in *Fusion Science and Technology.*
- 2.1-7 Katayama, K., *et al.*, *ibid.*
- 2.1-8 Isobe, K., *et al.*, *ibid.*
- 2.1-9 Nakamura, H., *et al.*, *Fusion Eng. Design*, **70**, 163 (2004).

2.2 Control System

2.2.1 Development of an Innovative Integrator Resistant to Plasma Instabilities

A new integrator for magnetic measurements aiming at long pulse operation have been developed and tested in JT-60U [2.2-1]. Although most of the technical issues have been resolved, an amplifier saturation caused by exposure of excessive voltage input from the sensor is still remaining as the major issue [2.2-2]. Therefore we had built an advanced integrator system, which is composed of the three sets of the VFC-UDC unit with different amplitude gains and a digital signal processor (DSP) to prevent at least one of the operational

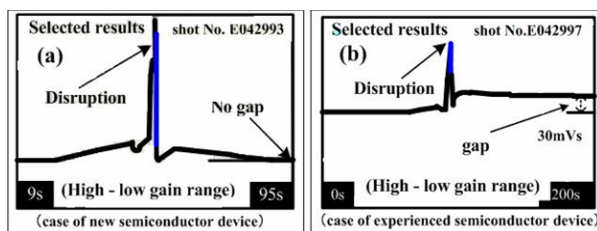


Fig. I.2.2-1 A gap of integral results occurred after several exposures to high voltage at a disruption.

amplifiers from saturating due to excessive voltage input. In addition, necessary numbers of FET-Zener diodes were added to the signal input line for protection of each operational amplifier.

The total performance test was conducted using one of the magnetic probes in JT-60. Figure I.2.2-1 (a) shows a good, accurate integration result even with a disruptive instability in tokamak discharge. In this case, no baseline change was observed before and after plasma discharge. Unexpectedly, soon after a few disruption plasma shots, clear baseline gap was again observed as shown in Fig. I.2.2-1 (b). The cause of this phenomenon has been identified to be semiconductor characteristics change of the FET-Zener diode elements equipped in the signal input circuit.

We have prepared three cases of modifications in the signal input circuit.

(1) Diode Withstanding ± 1 kV (Case I)

A gap ("stepped change") of the integrated signal came to be observed after several plasma disruptions. We considered that the exposure of continual extreme high-voltage inputs could make the FET-Zener diode characteristics degrade drastically. To prevent this, a new diode withstanding high voltage (± 1 kV) has been superseded the FET-Zener diode.

The linearity errors for three ranges (range: 10 V, 100 V, and 1000 V) exceed the specification of the employed operational amplifier ($\pm 0.001\%$). The cause of this linearity error is presumed the large leakage current of the diode with a 250 V pull-up power supply.

(2) Attenuator Insertion (Case II)

Since we are concerned about a large amount of diode leakage current at the signal front-end in the above case, the diode elements were removed from the input circuit. This improvement makes the circuit withstand ± 1.0 kV without a diode.

The linearity errors for this case are permissible (less than 0.001%) except for the 1000-V range.

(3) Power Mos FET-Zener (Case III)

Since the Case I trial board does not satisfy the accuracy requirements due to the large amount of leakage current, the Power Mos FET-FET, that does not need any high voltage power supply, has been chosen to make a short circuit in case of over-voltage

input. The test for this case is under preparation

We have built three trial boards as a measure to avoid the semiconductor characteristics change of the FET-Zener diode caused by the continual extreme high-voltage inputs in JT-60, and tested two of them. We will conclude our development result soon after the tests on the Case III including an impulse surge test.

References

2.2-1 Kurihara K., Kawamata Y., *Proc. of IEEE 17th Symposium on Fusion Engineering*, 799 (1997)
 2.2-2 Kawamata Y., *et.al.*, *IEEE 19th Symposium On Fusion Engineering*, 172 (2002)

2.3. Power Supply System

2.3.1 Tentative Power Transmission from the T-MG to the NBI and RF Heating Systems

Since a serious trouble on the H-MG happened in February 2004, a large-scale repair came to be required for the complete recovery. In order to restart the plasma heating experiments as early as possible, we decided to disconnect the T-MG from the toroidal field coil power supply and to reconnect it to the heating devices in place of H-MG as shown in Fig. I.2.3-1. Followings

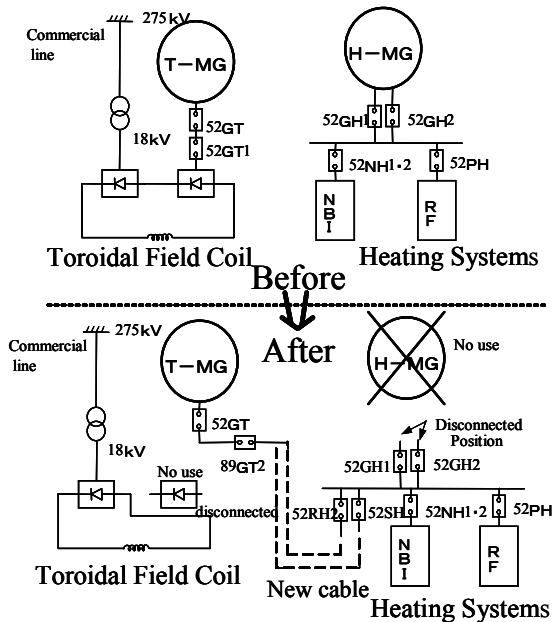


Fig. I.2.3-1 Main circuit reconfiguration.

are its details.

(1) Circuit Configuration

From the viewpoint of energy available directly from the power grid, the maximum toroidal magnetic field

coil current was considered about 70% of the rated current. This implies that large toroidal field could be produced sufficiently for the long pulse operation to study the high-beta plasmas. The actual difficulty was arisen in the coil current control capability in contrast with the output voltage control of the T-MG. Then, we modified the On/Off control scheme of the diode rectifier banks on the technical basis of discharge pulse prolongation (from 15 s to 65 s), conducted in the previous year.

The power line of H-MG was disconnected completely for safety at the point near the MG-pit by removing the bus-bars in the metal covered duct. The T-MG and the heating systems are connected by two lines of CV cables which has 22 kV rating and its cross section of 800 mm² by utilizing the unused switch gear boxes. According to the change of main circuit, the hard wired protection system was also modified to adjust the difference of ratings and the protection.

(2) T-MG Output Voltage to the Heating Devices

The major ratings of T-MG and H-MG are summarized in Table I.2.3. The voltage disturbance caused by the power fluctuation is basically anti-proportional to the capacity of generator. In this case, since the synchronous impedances for both MGs are similar in quantity, the voltage disturbance of T-MG is expected about two times of that of H-MG. To prevent the excessive over-voltage generation of T-MG that might be happened at the moment to separate the large electrical loads we reduced the T-MG output voltage to 16 kV from the rated value of 18 kV.

Table I.2.3 Specifications of T-MG and H-MG.

	T-MG	H-MG
Capacity	215 MVA	400 MVA
Voltage	18 kV	18 kV
Current	6,896 A	12,830 A
Frequency	80-56Hz	77.6-54.2Hz
Drive Type	Thyristor	Scherbius

(3) Re-Acceleration of T-MG

While the H-MG has an exclusive induction motor (IM) on the top of the generator for its acceleration, the T-MG is designed to be driven by thyristor drive device (AC-DC-AC drive) without IM. Therefore, the voltage distortion due to the commutation of thyristor drive was expected, because there is no inverter

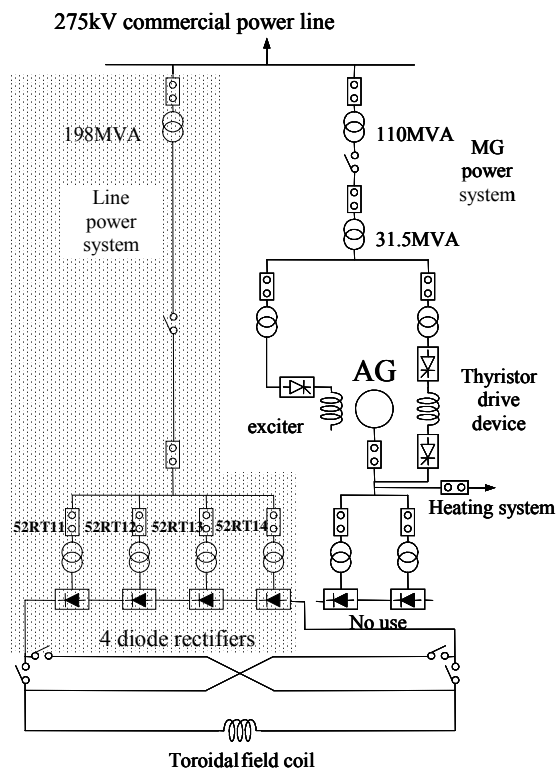


Fig. I.2.3-2 Configuration of toroidal field coil power supply. The upper hatch shows the temporary toroidal field coil power supply only powered from the commercial power line.

transformer as shown in Fig.I.2.3-2. To avoid the commutation failure in the thyristor drive device and the NBI system, we stopped the re-acceleration of T-MG during the period of plasma discharge and the NBI conditioning.

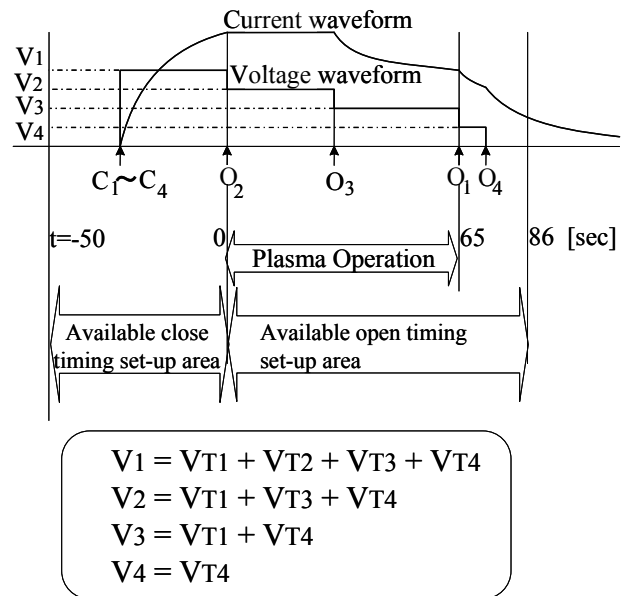
2.3.2 A Temporary Method for TF Coil Current Control

(1) Toroidal Field Coil Power Supply Configuration

The toroidal field coil power supply (TFPS) consists of the four diode rectifier banks powered directly from the commercial line of 275 kV and the two diode rectifier banks powered by the T-MG as shown in Fig.I.2.3-2. Since the T-MG was exclusively connected to the heating systems due to the H-MG trouble, the toroidal field coil current must be controlled by the four diode rectifier banks solely.

(2) On/Off Control of the Diode Rectifier Banks

Since the four diode rectifier banks are completely identical, the DC output voltages of the banks are also identical. It means that only four levels of the TF coil voltage could be selected. Then, we utilized the transformer tap changer in order to improve the flexibility in determining TF coil voltage. Here, the



Breaker	Use / No use	Secondary Voltage	Close timing	Open timing
52RT11	Use	V_{T1}	C_1	O_1
52RT12	Use	V_{T2}	C_2	O_2
52RT13	Use	V_{T3}	C_3	O_3
52RT14	Use	V_{T4}	C_4	O_4

Fig. I.2.3-3 Example of current and voltage waveform.

transformer tap can control the secondary voltage from 0.95 p.u. to 1.17 p.u. compared to the present tap position. In the actual experiments, the tap position was chosen to different position from each other to maximize the flexibility of TF strength.

Fig.I.2.3-3 is an example of the On/Off control in the diode rectifier banks. The current waveform is usually provided by the physics operator as a pre-programmed form. The turn-on/off timings, which are the close timings of $C_1 \sim C_4$ and the open timings of $O_1 \sim O_4$, of the diode rectifier banks that could realize the expected toroidal field are automatically set up by the control system prior to the start of discharge sequence.

2.4. Neutral Beam Injection System

The pulse duration of the NBI system was extended from 10 s to 30 s to study quasi-steady state plasmas on JT-60U. As for four positive-ion based (P-NBI) units with tangential beams, the electric power supplies and the beam limiters were mainly modified and the pulse duration was successfully extended up to 30 s with 2 MW at 80 keV. Other seven P-NBI units with

perpendicular beams, whose pulse durations were 10 s, were operated in series for 30 s in total instead of extending the pulse duration of each unit. The ion source of the negative-ion based (N-NBI) unit, whose target beam energy is 500 keV for 10 s, was also modified to reduce the heat load of the acceleration grids for 30 s operation at ~350 kV. The pulse duration was extended up to 25 s at ~1MW and 20 sec at 1.6MW. The total injected energy reached up to 340 MJ with 330MJ for P-NBI and 10MJ for N-NBI.

2.4.1 Modification of Control System for NBI

The NBI control system gives the commands of the outputs and timing for each power supply and the gas introduction systems, where the operations of all components are optimized to generate a high power neutral beam. For the long pulse operation, two timing sequences have been developed to achieve a high power injection for 30 s. One is to extend the acceptable sequence period of the tangential P-NBI and N-NBI units from 10 sec to 30 sec, where the NBI control system accept the commands from the JT-60 control system (ZENKE). The other is to make it possible to start the sequence of perpendicular P-NBI units (10 sec) at any time during the 30 sec period. Thus, a long pulse injection of 30 sec can be obtained by adjusting the timing of each perpendicular unit in series.

2.4.2 Modification of Beam Limiter

The beam limiters are made of molybdenum and protect the drift duct from the divergent beam. The reduction in heat load onto the beam limiters is the

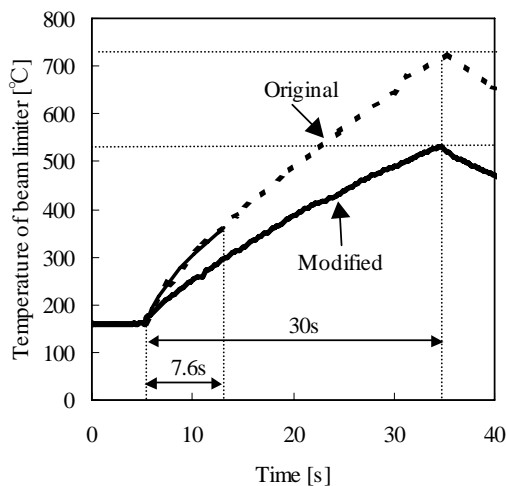


Fig. I.2.4-1 Time evolution of temperatures for original and modified beam limiters at 2MW injection power. The solid and dotted lines are measured and simulation results, respectively.

critical issue to extend the pulse duration, because the beam limiter is not actively cooled. The temperature measurement of the original beam limiter indicated that the maximum temperature would rise up to above 750 °C for 2MW injection for 30 s and molybdenum would be transformed only after several long pulse operations. Therefore, the shape of the beam limiter was modified to reduce the heat load density, and the volume was enlarged to decrease the temperature rise. Figure I.2.4-1 shows the time evolution of the maximum temperature of both the original beam limiter and improved one. The solid and dotted lines are measured and calculation results, respectively. It is found that the maximum temperature remains below 520 °C for 2MW injection for 30 s [2.4-1].

2.4.3 Reduction of Grid Heat Load of Negative Ion Source

One of main issues for extending the pulse duration of the negative NBI was to reduce the heat load to the ion source grids [2.4-2]. The large heat load to the grounded grid (GRG), in fact, limited the extension of the pulse duration. There are two causes; bombardments of accelerated negative ions and accelerated electrons stripped from negative ions. To reduce the electron stripping, it is necessary to decrease the neutral pressure in the accelerator. While the pressure in the ion source chamber is required to be more than ~0.3 Pa for negative ion production. The gas flows from the ion source chamber to the cryogenic

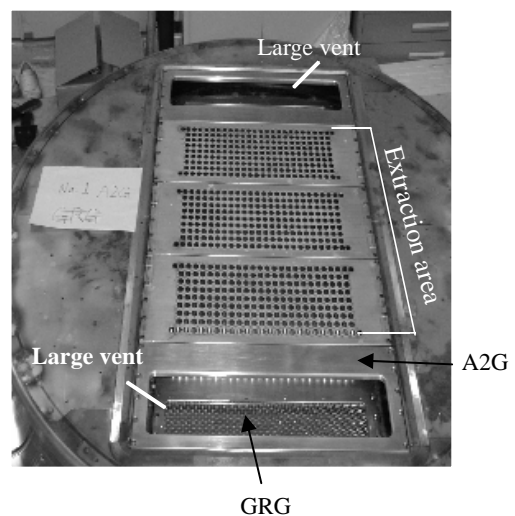


Fig. I.2.4-2 Picture of second acceleration grid of the negative ion source. Both edge segments are large vent grids and only inside three segments accelerate negative ions

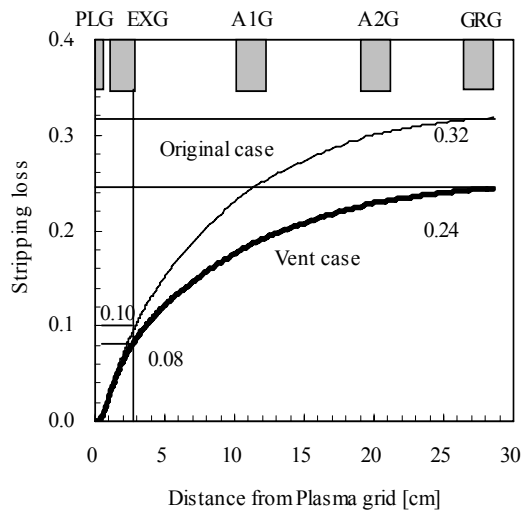


Fig. I.2.4-3 Simulated stripping loss in the ion source

pump through the grids. The negative ion source is composed of five grids; plasma grid (PLG), extraction grid (EXG), first acceleration grid (A1G), second acceleration grids (A2G) and GRG. Each grid is divided to five segments. Both sides of the acceleration grids were removed to increase the gas flow conductance in the accelerator column as shown in fig.I.2.4-2. Correspondingly, both sides of the PLG were masked entirely so as not to extract negative ion beams, which decreased the extraction surface to 73 % of the original area.

Stripping losses in the ion source were estimated from the calculated pressure profiles in the ion source, where the pressure in the extractor and accelerator were evaluated from the grids conductance and gas flow rate. Figure I.2.4-3 shows the integrated stripping loss along beam axis calculated from the cross section of neutralization on this pressure profile. The stripping loss is mainly generated in the region between the PLG and A1G where the pressure is high and the cross section of neutralization is high due to low beam energy. In the figure, the stripping loss in the ion source is reduced from 0.22 to 0.16 (a 27% improvement) by increasing the vacuum conductance. Figure I.2.4-4 shows the measured GRG heat load normalized by beam power as a function of the source pressure (P_{is}). The heat load ratio is decreased from 9.2 % to 7.0 % at 0.3 Pa after the modification. The heat load increases linearly with P_{is} , but the slope of the pressure dependence of the heat load became weaker after the modification. The pressure dependence of the

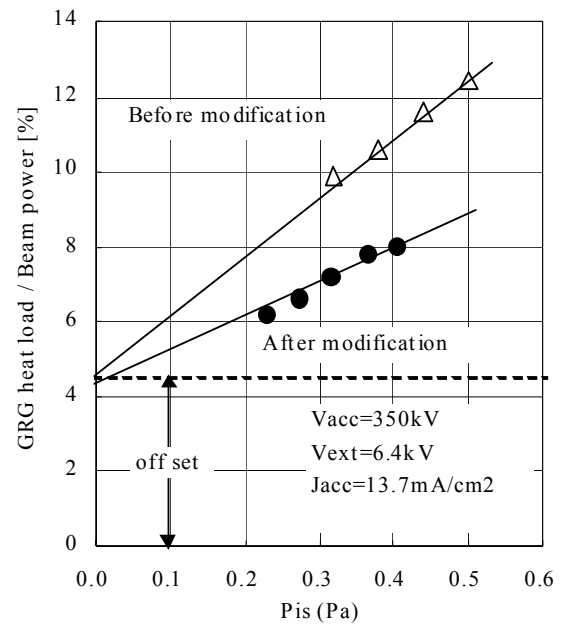


Fig. I.2.4-4 Dependence of the GRG heat load ratio on pressure before and after modification.

heat load is presumed to arise from the interception of accelerated electrons which are created by stripping being intercepted on the GRG. So the improvement of vacuum conductance was effective in reducing the stripping loss. The offset of the heat load at zero pressure is assumed to be due to direct interception of divergent negative ions, which has little pressure dependence. Therefore the direct interception of the negative ion beam on the GRG is about 4.5 % and the stripping loss is reduced from 4.6 % to 2.6 % (a 43 % improvement) at 0.3Pa after the modification. By this modification, the pulse length of negative NBI could be expanded up to ~20 s at 345keV, 1.6MW power.

Reference

- 2.4-1 Akino N., *et al*, *Fusion Sci. Technol.*, **48**, 758 (2005).
- 2.4-2 Umeda N., *et al*, *Proc. of 23rd Sym. on Fusion Technology, Venice, 2004, to be published in Fusion Eng. Des.*

2.5. Radio-Frequency Heating System

Performance of the JT-60U radio-frequency (RF) heating system has been constantly improved to extend the parameter region of experiments such as sustainment of high performance plasmas for a few tens seconds. In FY 2004, major improvements of the JT-60U RF heating system were extending the pulse duration of the electron cyclotron heating (ECH)

system and raising the performance of the lower hybrid (LH) system.

2.5.1 Long-Pulse Operation of the ECH System

Extension of the pulse duration of the ECH system was required since the maximum duration of the JT-60U discharge was extended from 15 s to 65 s in 2003 to investigate long sustained high performance plasmas. A tentative objective was set at the pulse duration of 30 s with an injected power of 0.6 MW. However, the ECH system was confronted with a difficulty in extending the pulse duration. It was a slight decay of the electron beam current of an oscillator gyrotron because of cathode cooling by electron emission. This decay caused abrupt termination of the gyrotron oscillation. Against the problem, some countermeasures were examined to compensate the beam current decay so as to keep the oscillation condition. Those were to control actively the magnetic field at the cavity, cathode temperature and electron pitch angle at the electron gun. Among those, in particular, we found that changing the electron pitch angle through controlling anode voltage of the gyrotron was most effective to keep the gyrotron oscillation, of which time response is quite faster than the others [2.5-1]. The electron pitch angle α is defined by $\alpha = v_{\perp} / v_{\parallel}$, where v_{\perp} and v_{\parallel} are the velocity of the electron perpendicular and parallel to the magnetic

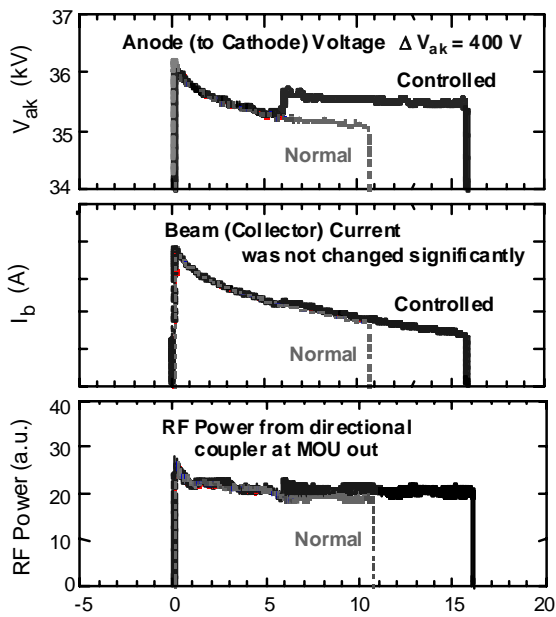


Fig. I.2.5-1 Oscillation duration was extended up to 16 s by anode voltage control indicated as "Controlled" while it was terminated at 10.5 s in normal operation.

field line, respectively. In the operation without anode voltage control, as shown in Fig. I.2.5-1, the oscillation terminated at around 10.5 s, though the immediate changes of the beam currents, pressure or temperature in the gyrotron was not observed. It seems to be out of the oscillation condition through changing the electron density or spatial distribution at the cavity due to decaying the electron beam current. In the operation with anode voltage control so as to keep the oscillation condition, the gyrotron oscillation was sustained for 16 s, which was the setting time of the pulse duration, with increasing anode voltage by 400 V at 6 s after the operation start, as shown in Fig. I.2.5-1. A pulse duration of 16 s, in this moment, is the maximum operation time due to the limitation of the temperature rise of the DC break in the gyrotron. As a result of the operation way, the injected power of 1 MW for 15 s was obtained in combined operation of three gyrotrons, and a pulse duration of 45 s with 0.35 MW was achieved in series operation of four gyrotrons, as shown in Fig. I.2.5-2.

The temperature rise of the DC break is another issue for further extension of the pulse duration, as mentioned above. The DC break, originally made of Al_2O_3 , between the body and the collector of the gyrotron is heated by scattered RF waves through diffraction loss at the outlet of the mode converter. To improve the excessive temperature rise of the DC break, Si_3N_4 which was developed for the ITER ECH (170 GHz) system in place of Al_2O_3 was tried to one of four gyrotrons. The new DC break is being tested.

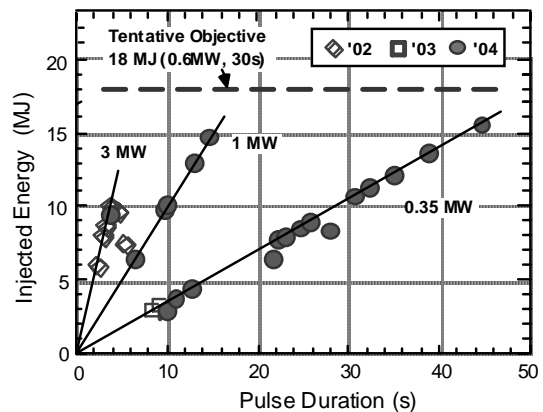


Fig. I.2.5-2 Progress in RF injection of the ECH system.

2.5.2 Performance of the LH System Having the Modified Launcher with Developed Carbon Grills

The LH system has contributed to studies of high performance plasmas such as reversed shear plasmas, adopting a multijunction-type launcher. However, the launcher [2.5-2] was damaged due to excessive heat loads around its mouth during 10-year operation. The injected power gradually decreased year by year. As a result, thin carbon grills were developed to recover the power injection capability [2.5-3], because carbon materials have high resisting capability against heat load, and further less harmful influence to plasma performances due to low ionic charge even if the sublimation of the materials occurs.

Eight carbon grills were connected with each of stainless steel (SUS) grills of the original LH launcher. Each carbon grill consists of a SUS base frame (10 mm thick), an RF conductor (~0.2 mm thick) and a carbon grill mouth (15 mm thick). The base frame was welded to the original grill. The RF conductor of a thin copper plate was used to improve electrical contact between the base frame and the carbon grill mouth. Each carbon grill mouth was held on the base frame by 22 bolts. The carbon mouth will be able to change when it is strongly damaged, even though the arc monitor system protects the LH launcher mouth from RF breakdown, which detected light emitted from the breakdown near the grill and immediately shut-off RF power.

After the modification of the LH launcher the launcher conditioning was substantially progressed both with and without plasma in 2004 operation. Injected energy, so far, has reached up to ~16 MJ into plasma, as shown in Fig. I.2.5-3, with a low reflection coefficient of 5 % by adjusting plasma position. A pulse modulation method was used to suppress RF breakdown owing to outgassing through temperature rise of the grills. Even in the conditioning phase, it was found that ~60 % of the plasma current of 1 MA was driven by LH injection by estimating the drop in one-turn loop voltage. The current drive efficiency is roughly estimated to be $\sim 1.6 \times 10^{19}$ A/W/m², which is 50 - 70 % of that with the original launcher, and seems to be improved with progressing the conditioning. Thus the performance of the modified launcher shows sufficient abilities as a high power LH launcher. The technical key issue was to keep sufficient electrical

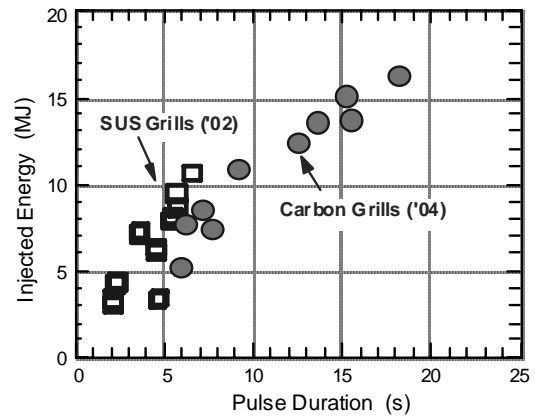


Fig. I.2.5-3 Comparison of injected energy between the stainless steel (SUS) grill and carbon grill launchers of the LH system.

contact for the LH antenna with the carbon grills, therefore a thin RF contactor made of copper was developed and inserted between the base frame and the carbon grill mouth. After the conditioning operation, severe damage by RF breakdown was observed around the base frames due to insufficient works of the arc monitor system. However, the contactor seems to trigger or to continue the RF breakdown. Therefore the contactor should be improved not to cause RF breakdown.

References

- 2.5-1 Moriyama, S., et al., "Development and Contribution of RF Heating and Current Drive Systems to Long Pulse, High Performance Experiments in JT-60U," to be published in *Fusion Engineering and Design*.
- 2.5-2 Ikeda, Y., et al., *Fusion Engineering and Design* **24**, 298 (1994).
- 2.5-3 Seki, M., et al., "Performance of the LH Antenna with Carbon Grill in JT-60U," to be published in *Fusion Engineering and Design*.

2.6 Diagnostic System

2.6.1 Infrared Imaging Video Bolometer

An infrared (IR) imaging video bolometer (IRVB) can provide a wide-angle view equivalent to hundreds of resistive bolometers. Radiation from the plasma is received with a metal foil absorber and the foil temperature is measured with an IR camera outside the vessel. Radiated power can be obtained by solving the two-dimensional heat diffusion equation numerically at each point in the foil. Recent progress in IR technology enables the sensitivity of the imaging bolometer to approach to that of the conventional resistive bolometer, as has been successfully demonstrated in the Large

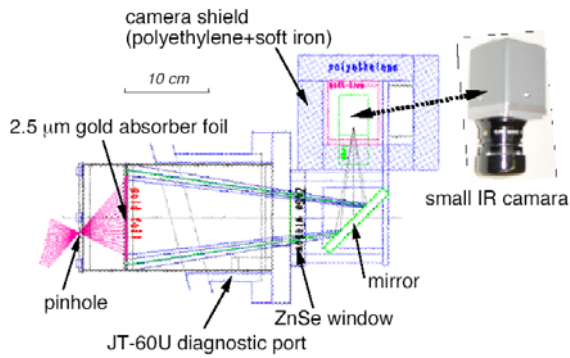


Fig. I.2.6-1 Infrared Imaging Video Bolometer

Helical Device [2.6-1]. A feasibility study of the imaging bolometer under a tokamak environment was initiated as a research collaboration with NIFS in 2003 [2.6-2].

The IRVB is illustrated schematically in Fig. I.2.6-1. A 2.5 microns gold absorber foil of 9 cm x 7 cm was shown to be durable during two years of operation with 1800 tokamak discharges including disruptions. Taking advantage of the wide-angle view of the IRVB, an adjustment for semi-tangential view of the tokamak plasma was done by shifting the pinhole 15 mm horizontally. A radiating toroidal ring has been mapped and recorded onto the foil as a clear high temperature zone at a disruption, consistent with huge core radiation measured with the resistive bolometers. Radiation from the divertor could be identified also in the foil image as a thick line having toroidal curvature. This work was partly supported by Grants-in-Aid for Scientific Research of the JSPS, Nos.16560729 /16082207.

2.6.2 Real-Time Evaluation Technique of Safety Factor Profile

In order to realize a real-time control system of the safety factor profile $q(r)$, we developed, for the first time, a method to evaluate the safety factor profile in real-time [2.6-3] using a motional Stark effect (MSE) diagnostic [2.6-4]. The MSE diagnostic measures local magnetic pitch angles inside the plasmas. The newly developed method evaluates $q(r)$ at 16 locations (maximum), within 10ms. A conventional method that solves the Grad-Shafranov equilibrium equation takes several tens of seconds to calculate $q(r)$ in, although it is accurate. Instead of solving the Grad-Shafranov equation, the method employed here assumes that the last closed magnetic surface represents internal

magnetic surfaces well. The q profile is calculated using pitch angle mapped on the internal magnetic surfaces.

Figure I.2.6-2 shows a safety factor profile evaluated with the real-time evaluation technique, in comparison to that by equilibrium reconstruction. The safety factor profile evaluated using the real-time technique agrees with the accurate profile obtained using the equilibrium reconstruction. This evaluation technique has now been built into the real-time control system of the safety factor profile.

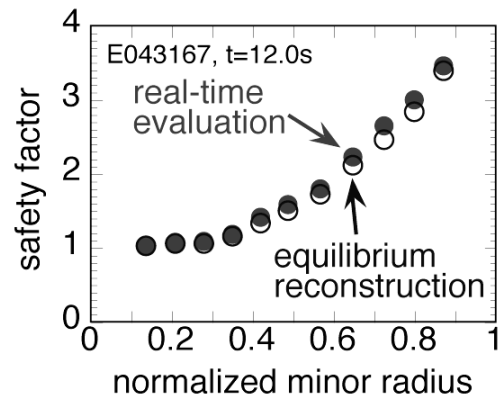


Fig. I.2.6-2. Safety factor profile by real-time evaluation (filled circles) and by equilibrium reconstruction (open circles).

2.6.3 Real-Time Processing of FIR Laser Interferometry for Long Pulse Discharges

A real-time processing (RTP) system has been newly developed for the FIR laser interferometer utilizing the compact-PCI modules and the software on the Real

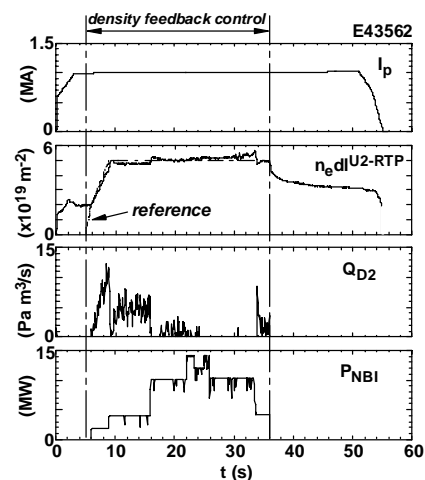


Fig. I.2.6-3. Typical waveforms of the density feedback control using the new RTP system. Here, I_p is the plasma current, $\int n_e dl^{U2-RTP}$ is the real-time line-integrated electron density measured with the new RTP system, Q_{D2} is the deuterium gas puff rate, and P_{NBI} is the neutral beam injection power.

Time LINUX OS [2.6-5]. Using this system, real-time correction of the fringe jump error, which is required for density feedback control in long pulse discharges, has become available. As a result, reliable density feedback control in the long-pulse discharges has been realized using this new RTP system (Fig. I.2.6-3).

References

- 2.6-1 Peterson B.J., *et al.*, *Rev. Sci. Instrum.* **72**, 923 (2001).
- 2.6-2 Peterson B.J., Ashikawa N., Konoshima S., Ingesson L.C. and Walker C.I., *Proc. 30th EPS Conf. on Controlled Fusion and Plasma Phys.* (St. Petersburg, 2003), **27A**, P-4.67.
- 2.6-3 Suzuki, T., and JT-60 team., "Recent RF Experiments and Application of RF Waves to Real-Time Control of Safety Factor Profile in JT-60U", *Proc. Topical Conf. on RF power in Plasmas (Park City, 2005) in print.*
- 2.6-4 Fujita, T., *et al.*, *Fusion Eng. Des.* **34-35**, 289 (1997).
- 2.6-5 Kawano, Y., *et al.*, "Real time processing of FIR laser interferometry for long pulse discharges", to appear in "Review of JT-60U experimental results in 2003-2004", *JAERI-Review* (Japan Atomic Energy Research Institute).

3. Design Progress of the National Centralized Tokamak Facility

Two designs proposed for the National Centralized Tokamak facility (NCT) is assessed with respect to the physics requirements such as break-even class plasma, heating and current drive capability, MHD stability, divertor performance, and plasma controllability. After the fruitful discussions with the scientists from universities and industries in Japan, the machine parameter with wider operational space in the plasma shape flexibility, which is regarded to be of importance for the achievement of high- β plasma, is made to be a key factor for NCT. Engineering design of the main components of superconducting TF and PF coils, vacuum vessel, in-vessel facilities, and cryostat has been performed to optimize their structure from the view points of manufacturing processes, operation and maintenance feasibility.

3.1 Physics Design

The machine parameters are assessed from the view points of the capability to break-even class plasma, high- β plasma, heat and particle controllability in divertor, flexibility of aspect ratio and plasma shaping, full current drive controllability [3.1-1].

Break-even class plasma of equivalent $Q_{DT} \sim 1$ will be achievable with $I_p = 5.5$ MA, $HH_{y2} \sim 1.4$, and the

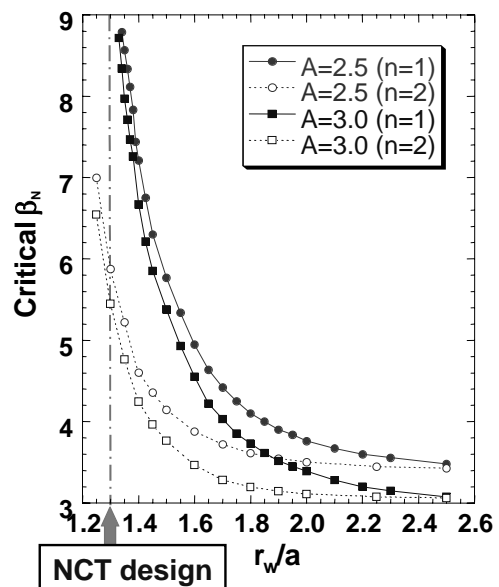


Fig. I.3.1-1 Dependence of MHD stability on a parameter of normalized wall location evaluated by ERATO-J analysis. Four cases (aspect ratio $A = 2.5$ and 3 with $n = 1$ and 2) are compared.

neutral beam power $P_{NB}=13$ MW. The consistency with a break-even class plasma and a high- β plasma is estimated, i.e., $Q_{DT}^{eq}=1$ and $\beta_N=3.5$ will be simultaneously achieved at $I_p/B_T=4.5\text{MA}/2.3\text{T}$, $q_{95}\sim 3.5$, $HH_{y2}=1.5$, $f_{GW}=0.9$, and NB power of 25MW. In such a condition, collisionless plasma with low normalized Larmor radius is satisfied in the range of $\rho^*=0.005\sim 0.008$, $v^*=0.01\sim 0.1$.

The accessibility of advanced operation of high- β with full current drive accessibility at $I_p=3$ MA and $\beta_N=4$ was estimated by the ACCOME analysis on the assumption of $HH_{y2}=2$, $q_{95}=6.1$, $q_{min}=2.0$, $f_{GW}=0.5$, with total NB power of 25MW in the case of negative NB at off-axis. Current profile control by the combination of on-axis and off-axis beams enables such an advanced operation scenario.

The advantage of low aspect ratio to the ideal MHD stability was evaluated by the ERATO-J code analysis [3.1-2]. Figure I.3.1-1 shows the dependence of the critical β_N on a parameter of the normalized wall location, r_w/a (r_w : wall location, a : plasma minor radius), by $n=1$ and $n=2$ toroidal modes in the double null reversed shear plasma with $\kappa_{95}=1.8$, $\delta_{95}=0.4$, $q_{min}=2.4$, and parabolic pressure profile. In general, critical β_N is higher in smaller r_w/a due to the wall stabilization effect. As clearly seen in the figure, the critical β_N tends to be higher in the low aspect ratio.

Preliminary analysis by ‘VALEN code’, under the collaboration with Columbia University and PPPL, was conducted to estimate the achievable β_N with the active control of RWM stabilisation in the 3-dimensional geometry of vacuum vessel and the stabilising plates. The analysis indicates that the maximum achievable β_N is about 3.8, and the limitation is brought by the weak coupling of the magnetic flux of the in-vessel coils with the plasma because of the shielding effect by the stabilising plates. The code analysis in the ITER geometry predicts that the coupling could be effectively enhanced if the in-vessel coils are located around the port duct.

Controllability of the EC resonance for the NTM suppression was estimated by modified Rutherford equation. The minimum EC power for the stabilization of $m/n=3/2$ and $2/1$ mode in the resonance of fundamental EC wave injected with 90 GHz, O-mode into the normal shear plasma with $q_0=1$ is 0.51 MW, and 1.1 MW, respectively. Those requirements meet the

present EC design.

Simulation analysis for divertor particle and heat flux controllability was performed using with SOLDOR/NEUT2D code. In the ITER-like divertor configuration with long leg length, a partial detachment is well maintained. Parameter surveys in the incline angle of the divertor plate and the distance between the pumping duct and the hit point on the plate were also made in order to optimize the divertor geometry. On the other hand, in the optimized shape configuration with a low aspect ratio and a high triangularity, the shortening of the leg length of the inner divertor and the insufficient cryopanel surface area bring the degradation of the pumping capability and of the particle controllability. Further optimization in both the aspects of the divertor pumping and of the plasma shaping is required.

3.2 Engineering Design

Based on the design with wider operational space, structures of main components and manufacturing processes were reviewed to optimize the space utility and maintenance, especially around the midplane area. Whole assemble of the NCT tokamak is illustrated in Fig. I.3.2-1.

3.2.1 TF and PF coils

In order to ensure the space margin for the extension of the flexibility in the aspect ratio and plasma shape, TF coil was been enlarged in the vertical direction. Each TF coil has 114 turns to correspond the maximum $B_T R$ of 8.11 Tm. The numbers of turns of PF coils are increased to realize the maximum plasma current of 5.5 MA for 100 s. Support structure of the CS and the divertor coil is unified with that of the TF coil in order to cancel out the mechanical stress by the electromagnetic force as an internal force.

3.2.2 Vacuum vessel

The total width of the double-wall is designed as 148 mm from the view points of the reinforcement. By the stress analysis with FEM code the interval of the ribs is determined to 300 mm with the welding depth of 24 mm.

3.2.3 Stabilizer plates

In order to compensate the thermal stress during the

baking of vacuum vessel, crank support structure is adopted. Support leg was made of SUH660 with the electrical insulation coating at the crank-pin and the joint part of crank support. Strength of such a structure was confirmed by the stress analysis with the temperature difference of 300°C between the vacuum vessel. Mechanical strength was also confirmed against the electromagnetic force during disruption event including a halo current.

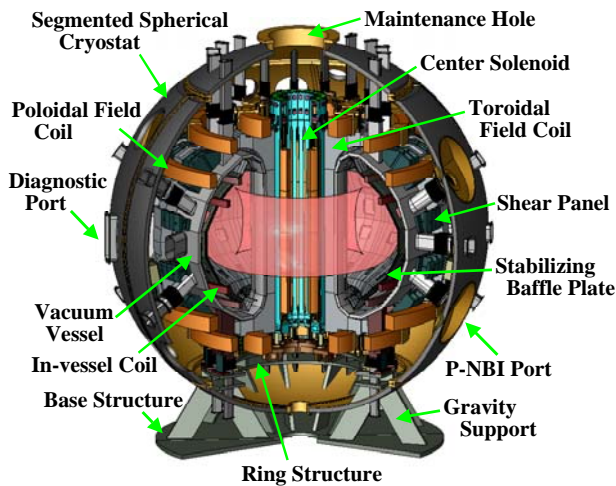


Fig. I.3.2-1 Birdseye view of the National Centralized Tokamak Facility

3.2.4 Divertor

Movable louver or sliding shutter in order to adjust the divertor pumping speed during the plasma discharge was designed. It is located in front of the cryopanel under private dome or outer baffle plates. The effective pumping speed for deuterium gas was estimated as 100% to 10% due to the change of the conductance of the adjustable louver or shutter in 100 m³/s to 1 m³/s within the duration of about 1s. Strength of the structure was confirmed by the stress analysis against the thermal stress and the electromagnetic force.

3.2.5 Cryostat

New design of the spherical cryostat is developed in order to ensure the enough space for maintenance in the joint area with NB injection port. It consists of upper pan, middle vessel, lower pan and support base. Each block is connected by the flanges with the lip seal to maintain the vacuum condition. Stress analysis performed by a 3D-model indicates that each part of the cryostat satisfies the structural strength against the complex load from electromagnetic force and seismic

force.

3.2.6 Bending strain of Nb₃Al CICC

In order to estimate the effect of bending strain on the critical current (I_c) of Nb₃Al cable in conduit coil (CICC) [3.1-3], a test facility for loading the tensile and compressive stresses was designed and manufactured. The loading test was performed on Nb₃Al strand (strand sample) wound around the spring-shape holder, and two Nb₃Al strands and one Cu wire inserted into a stainless steel conduit (triplex CICC sample). I_c of the strand was measured with the strain range from -0.86% to +0.18% at 4.2K in the external magnetic field of 6-11 T. The dependence agreed well with the theoretical prediction by Durham's equation [3.1-4]. Based on those results some relaxation mechanism of bending strain in the conduit will be investigated.

3.2.7 Shielding material

The typical performance of the heat proof boron-doped neutron shield resin, developed last year, was examined [3.1-5]. The same level of the neutron shielding characteristic as that of polyethylene was confirmed by the penetration tests of 2.45 MeV DD-neutrons and of the continuous energy neutrons from ²⁵²Cf source. The heatproof temperature determined by the deflection load was about 300°C. The tensile, bending, and compressive tests based on the JIS standard show the enough mechanical strength both at room temperature and at 250°C. The resin is suitable for NCT to set up around the port section to suppress the streaming neutron and at the neutron shielding material for diagnostics systems around the vacuum vessel.

References

- 3.1-1 Tamai, H., *et al.*, 20th IAEA Fusion Energy Conference (2004) IAEA-CN-116/FT/P7-8.
- 3.1-2 Kurita, G., *et al.*, 20th IAEA Fusion Energy Conference (2004) IAEA-CN-116/FT/P7-7.
- 3.1-3 Kizu, K., *et al.*, 20th IAEA Fusion Energy Conference (2004) IAEA-CN-116/FT/P1-6.
- 3.1-4 S. Keys, *et al.*, *Supercond. Sci. Technol.* **15**, 991 (2002).
- 3.1-5 Morioka, A., *et al.*, *submitted to Journal of Plasma & Fusion Research.*

II JFT-2M PROGRAM

A series of the experimental programs on the JFT-2M was completed in the last fiscal year. In this fiscal year, experimental data on the Advanced Material Tokamak Experiment (AMTEX) using the reduced activation ferritic steel (F82H), high performance experiment, characteristics of SOL and divertor plasma and compact toroid injection for fueling have been analyzed and evaluated. These results were presented in the 20th IAEA Fusion Energy Conference held at Vilamoura, Portugal in 2004, and submitted to journals for publication.

Concerning the AMTEX, analyses of high-beta experiments with the Ferritic Inside Wall (FIW) facing close to the plasma have apparently shown a wall stabilization effect. Moreover, by using an MHD equilibrium code in which the calculation accuracy in plasma pressure has been improved by raising the level of approximation for ferritic segments, it has been confirmed that a plasma with the normalized beta value of $\beta_N \sim 3.5$ is compatible to FIW.

As part of research program for understanding mechanism to improve plasma confinement, studies on fluctuations of electric potential in the transport-barrier region of H-mode have been made by collaboration with universities etc. Results have shown that there are two types of turbulent fluctuations, one is suppressed when the confinement is improved and the other helps to sustain the transport barrier. Moreover, the field structure has been analyzed by identifying the low frequency geodesic acoustic wave, and it has been shown for the first time that this mode influences the background turbulence and the turbulent particle flow. A comparison of experimental conditions of the new H-mode regime found in JFT-2M (HRS H-mode), which has an attractive performance for steady-state operation, with those of the EDA H-mode in Alcator C-Mod has suggested that there is a common physical process between them. On the edge plasma research, it has been found that the heat flux to the divertor plates in the ELM free HRS H-mode is reduced to about 15% of the maximum heat load due to ELMs in the ELMy H-mode.

On the research for fueling by compact toroid injection, magnetic fluctuations observed just after the CT injection have been analyzed. Results have shown that the fluctuation frequency approximately agrees

with that of Alfvén wave of theoretical prediction and that the life time of CT is well reproduced by a simulation using a slow magnetic field reconnection model. The process of fueling by compact toroid injection has been well understood by these results.

1. Advanced Material Tokamak Experiment (AMTEX) Program

The reduced activation ferritic steel is a leading candidate of structural material for the blanket of a fusion demonstration reactor (DEMO). However, it is ferromagnetic material and it easily rusts in the air. Thus the investigation of the compatibility of the ferritic steel with plasma is important and has been investigated on the JFT-2M tokamak step by step [1-1, 1-2]. Since 2002, the inside vacuum vessel wall has been fully covered with the Ferritic Inside Wall (FIW) [1-2, 1-3]. The compatibility of the ferritic wall with high normalized beta (β_N) plasma is an important issue because high normalized beta plasma of $\beta_N = 3.5 \sim 5.5$ must be realized for a commercially attractive fusion reactor by using wall stabilization effect. Thus, high beta experiments with the close wall position were carried out by changing the plasma position in the final experimental campaign of JFT-2M. The experimental data has been analyzed more quantitatively in this year.

The equilibrium calculation is a key evaluation tool for this analysis because both the normalized beta and wall position are evaluated with this code. The calculation without including the ferromagnetic effect might contain systematic error because the magnetic sensors are affected by the magnetic field from the ferritic steel. The code including the ferromagnetic effect was developed a few years ago, but it was

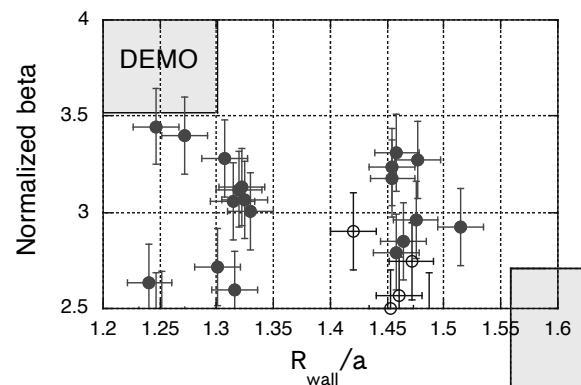


Fig. II.1-1 Normalized beta against normalized wall position for all effective shots. Open circles show data obtained in 2002.

unstable. Thus, the equilibrium code has been checked more precisely and improved [1-4]

At first, the model of the profile of plasma current and pressure was optimized. The realistic results were obtained reproducibly after this modification. The model of FIW was also improved. The ferromagnetic effect was modeled by placing the filament current on the surface of the wall. This method is suitable to represent the magnetic field structure at a relatively far region from the wall. On the other hand, the magnetic field near the wall is sensitive to the model e.g. density and position of the filaments. Since the probe position ($24 B_\theta$ probes and 8 flux loops on vacuum vessel and/or FIW) is very near to the wall, dependence of the magnetic field strength at the probe position on the model was investigated. After the optimization of the model, the obtained magnetic field profile at the probe position became more smooth and reliable. This modification caused $\sim 5\%$ increase in obtained beta value. To investigate the separatrix position more precisely, new method was developed last year to measure separatrix position using two sets of the step probe as follows [1-5, 1-6]. Two sets of double probe with different pin length (5 mm difference) are inserted into the plasma. Direction of the voltage is opposite for the probes. When the probe passes across the separatrix, the difference of the probe current becomes maximum (see 2.3.2). The obtained peak position agreed well with that obtained from the equilibrium calculation within ~ 2 mm. If the separatrix position is estimated with the code without considering FIW, the obtained position is 12.7 mm inside the peak position. These results have shown that the effect of the FIW is properly included in the equilibrium code. The beta value estimated with the code was compared with the diamagnetic signal, and a linear relation was shown between them. It should be noted that the comparison is not self-consistent because the calculation of the beta value from the diamagnetic signal also needs the shaping factor calculated in the equilibrium code. However, the reliability of the code has been demonstrated for certain degree (at least for relative value) and the improved code has been employed in following analyses and discussions.

Figure II.1-1 shows the normalized beta just before the collapse against the normalized wall position (r_{wall}/a) for all effective shots. The data obtained 2 years ago are also shown in the figure. Due to the improvement of the

Table II.1-1 Comparison of plasma parameters of three discharges for investigating the stabilization effect of FIW.

	99925	99932	99917
r_{wall}/a	1.48	1.36	1.26
R_{axis} (m)	1.35	1.38	1.39
n_e/n_{GW}	0.56	0.66	0.62
li	0.67	0.74	0.74
q_{95}	3	3	3
P_{rad} (kW)	300	260	330
H_α (a.u.)	0.9	0.75	0.88

operation scenario and the hardware, the operational region was extended to $\beta_N \sim 3.5$, $r_{\text{wall}}/a \sim 1.25$. Thus, the compatibility of the FIW with DEMO-relevant high normalized beta plasma was demonstrated [1-4]. Scattering of the data is considered to be attributed by the difference in pressure and temperature profiles, caused by the difference in the electron density, the wall condition and so on.

To investigate the wall effect, discharges with similar condition were carefully chosen. They were taken on a same day with keeping radiation level at ~ 300 kW during full power NB injection of 1.6 MW. The electron density is $n_e/n_{\text{GW}} \sim 0.5$ for co-injection phase and collapse occurs at $n_e/n_{\text{GW}} \sim 0.6$, where n_{GW} is the Greenwald density. Other parameters related to plasma stability are summarized in Table II.1-1. The parameters are almost reproducible. Another important feature is the behavior of soft X-ray profiles before the collapse. In this series of experiment, a sharp outward shift of the profile was observed, which was clearly different from the behavior of tearing mode disruption. These data suggested that the target plasmas and mechanism of the

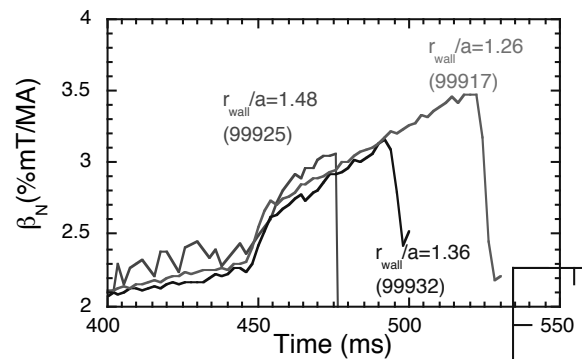


Fig. II.1-2. Time evolutions of normalized beta for similar plasma condition but different in wall position

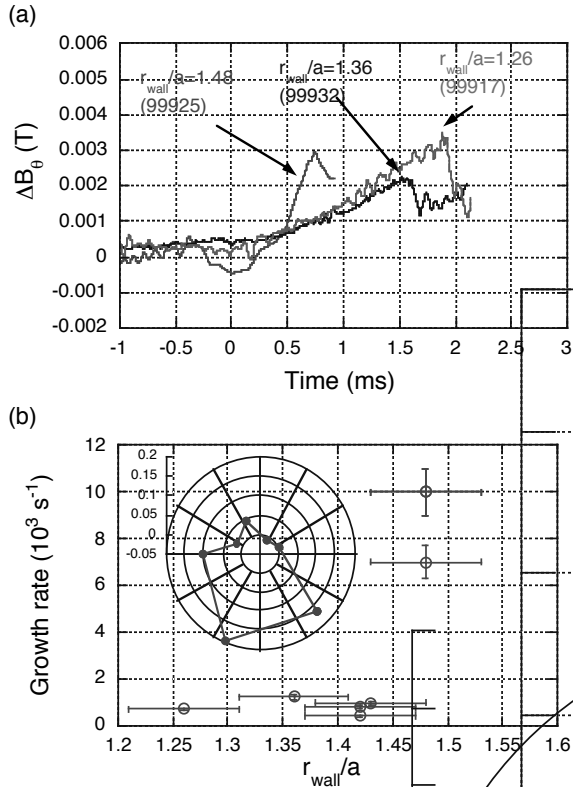


Fig. II.1-3. (a) Time evolutions of normalized beta for similar plasma condition but at different wall position. (b) Dependence of the growth rate on the plasma position and toroidal distribution of fluctuation amplitude at the mode locking.

collapse were almost reproducible and only the wall position was scanned. Figure II.1-2 shows time evolution of the normalized beta for discharges shown in Table II.1-1. The waveforms are almost identical before 480 ms. A plasma in the configuration closer to FIW survives longer, and thus, reaches the higher normalized beta. It might correspond to the wall stabilization effect. A Clear difference was observed in magnetic probe signal [1-3, 1-4]. In both cases, $n=1$ mode (n is toroidal mode number) was observed with eight B_0 probes toroidally distributed at outer mid-plane as shown in Fig. II.1-3. The position of the mode locking is reproducible, which means that the mode locking is related to the external error field. In order to compare growth rate, the difference between signal intensities of two magnetic probes located toroidally on the opposite side is plotted in Fig. II.1-3(a) for the 3 discharges. The growth rate was estimated from the gradient and summarized in Fig. II.1-3(b) as a function of r_{wall}/a . The growth rate is smaller for the closer wall

position. Similar to the resistive wall without ferromagnetism, reduction of the growth rate from the Alfvén time scale to wall time constant (a few milliseconds) was observed with ferritic wall. Thus, it has been concluded that the ferromagnetic wall shows similar behavior as normal resistive wall and the adverse effect related to ferromagnetism is not observed at least in this experimental condition. It should be noted that the thickness of the ferritic steel in this experiment (~ 10 mm) is much smaller than that of DEMO, but the normalized effect is expected to be comparable because of the larger minor radius and the strong toroidal field in DEMO. Thus, the compatibility of the ferritic wall with reactor-relevant high normalized-beta plasmas has been demonstrated.

References

- 1-1 Kawashima, H., *et al.*, *Nucl. Fusion*, **41**, 257 (2001).
- 1-2 Tsuzuki, K., *et al.*, *Nucl. Fusion*, **43**, 1288 (2003).
- 1-3 Tsuzuki, K., *et al.*, *J. Nucl. Mater.*, **329-333**, 721 (2004).
- 1-4 Tsuzuki, K., *et al.*, *Proc. 20th IAEA Fusion Energy Conference*, IAEA-CN-116/EX/P2-33 (2004), to be published on CD-ROM (IAEA, Vienna), submitted to *Nucl. Fusion*.
- 1-5 Amemiya, H., *et al.*, "Method for Detection of Separatrix Surface Using Differential Double Probe", submitted to *Jpn. J. Appl. Phys.*
- 1-6 Uehara, K., *et al.*, "Direct identification of magnetic surface by the differential double probe in JFT-2M", to be submitted to *Jpn. J. Appl. Phys.*

2. High Performance Experiments

2.1 Study of H-Mode Physics

The analysis of the experimental data of JFT-2M made a progress on the confinement physics of the tokamak plasma under the collaboration with the Univ. of Tokyo and the National Institute for Fusion Science.

On the study of the stability of the edge transport barrier (ETB) during the H-mode, some characteristic electrostatic MHD oscillations were found. The typical H-mode in JFT-2M evolves in time as the three stages as 1) ELM-free H-mode, then 2) slightly degraded H'-mode, and at last 3) EDA-like H-mode. In the third stage, the ETB seems steady for a few hundred milliseconds in a high recycle edge state. We studied the characteristic MHD instabilities at the ETB during each stage [2.1-1, 2.1-2]. In the ELM-free phase, as the ETB pressure increases, reflectometer measurement shows an

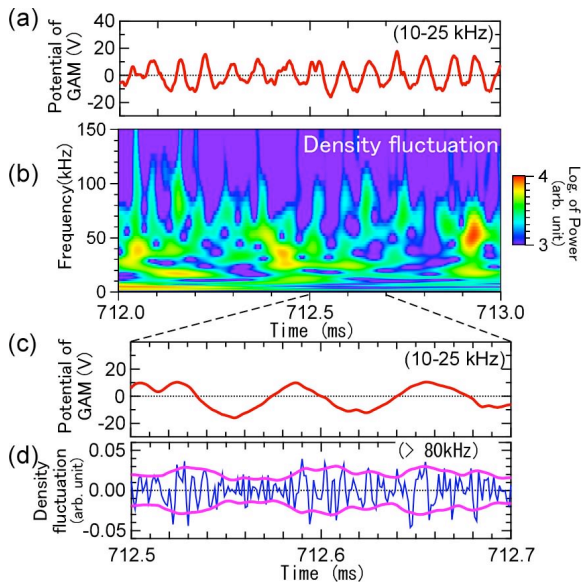


Fig.II.2.1-1 The interaction of the GAM and the background turbulent density fluctuations in the edge region of the core plasma measured by HIBP. (a) GAM potential. (b) Spectra of the density fluctuation. (c) GAM potential (time expanded) (d) density fluctuation.

appearance of characteristic electrostatic multi-modes which have frequencies around 150-200 kHz. Only the modes with high toroidal mode number around 8~11 are unstable, the feature of which is similar to that of a ballooning mode [2.1-3]. The mode frequencies decrease continuously as the mode grows and in the successive H⁻-mode phase, the modes seem to unite to a single quasi-coherent mode of frequency ~70 kHz. In the high recycle EDA-like H-mode phase during which the edge D_α level is high, the glowing electrostatic quasi-coherent mode co-exists with the higher frequency electromagnetic mode of ~300 kHz. Remarkably different part in the density fluctuation spectra between the ELM-free H-mode and the H⁻-mode is attributed to the quasi-coherent mode. By the heavy ion beam probe (HIBP) measurement the plasma potential at the ETB fluctuates with the quasi-coherent mode frequency during the H⁻-phase and the radial electric field is found to be reduced. Therefore, the quasi-coherent mode seems to decrease the radial electric field and degradation of the confinement occurs, which may contribute to the steadiness of the ETB during the H⁻-mode. Thus a control of these MHD instabilities at the ETB is found to be very important to improve the quality or steadiness of the H-mode. Also, it has been found that suppression of the turbulent

density fluctuations below ~50 kHz in the ETB is a feature of these H-modes when compared to the L-mode [2.1-1].

We found a low frequency electrostatic coherent mode of 10-15 kHz in the Ohmic heating phase [2.1-4] and in the L-mode phase [2.1-5]. The characteristic mode is identified as the geodesic acoustic mode (GAM) which has a large wave length along the poloidal direction, and is a kind of the zonal flow. The GAM and the zonal flow have grown to important topics to study the mechanism of the transport improvement (at the internal transport barrier (ITB)) or of the reduction of the anomalous transport induced by the plasma turbulence. We clarified the structure of the electric field of the GAM [2.1-5]. The GAM seemed to interact with the background turbulence in parametric/modulational nonlinear fashion [2.1-4] and the power of the density fluctuation (background turbulence) was found to fluctuate with the potential fluctuation of the GAM (Fig.II.2.1-1) [2.1-5].

References

- 2.1-1 Hoshino, K., *et al.*, *J. Plasma Fusion Research SERIES*, **Vol. 6**, 345 (2004).
- 2.1-2 Nagashima, Y., *et al.*, *Plasma Phys. Control. Fusion*, **46**, A381 (2004).
- 2.1-3 Hastie, R. J., *et al.*, *Phys. Plasmas*, **10**, 4405 (2003).
- 2.1-4 Nagashima, Y., *et al.*, "Observation of nonlinear coupling between turbulent and coherent fluctuations in the edge plasma on JFT-2M", presented in the 21st JSPF Annual Meeting, 2004, 24aA23P, submitted to *Phys. Rev. Lett.*
- 2.1-5 Ido, T., *et al.*, "Electrostatic fluctuation and fluctuation-induced particle flux during formation of the edge transport barrier in the JFT-2M tokamak", *Proc. 20th IAEA Fusion Energy Conference*, IAEA-CN-116/EX/ 4-6Rb (2004), to be published on CD-ROM (IAEA, Vienna), submitted to *Nucl. Fusion*.

2.2 High Recycling Steady H-Mode

Finding alternative scenarios to Type-I ELMy H-mode operation is a key area of research for current tokamaks. A new attractive operational regime without any large ELMs, "High Recycling Steady (HRS)" H-mode regime, was discovered in the JFT-2M tokamak that had many similarities to EDA H-mode regime on Alcator C-Mod [2.2-1~6]. To compare the properties, fluctuation behavior and access conditions of these regimes, a series of parameter scans were carried out in q₉₅-v_e*

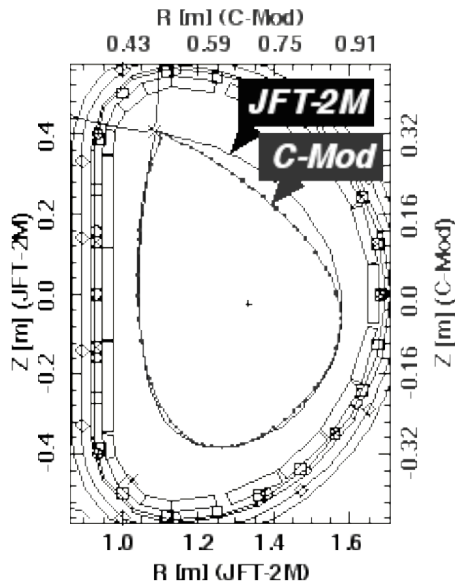


Fig. II.2.2-1. Comparison of plasma shape between JFT-2M and C-Mod

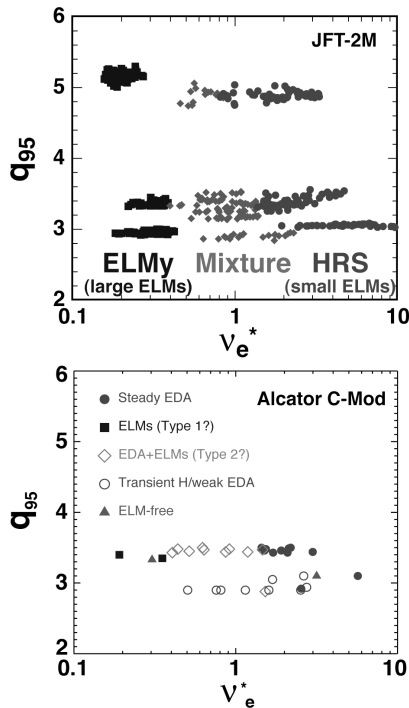


Fig. II.2.2-2. Comparison of operational regime in q_{95} - v_e^* space between JFT-2M and C-Mod.

space under the matched plasma shape condition of $\kappa \sim 1.5$ and $\delta \sim 0.5$ as shown in Fig. II.2.2-1. Here, the normalized electron collisionality v_e^* in the plasma edge region near the pedestal top is defined as the ratio of collision frequency to the bounce frequency as $v_e^* \equiv 6.9 \times 10^{-18} q_{95} R n_e \ln \Lambda / (T_e^2 \epsilon^{3/2})$, where R is major radius, n_e

is electron density, $\ln \Lambda$ is Coulomb logarithm, T_e is electron temperature, and ϵ is inverse aspect ratio. As a result, a striking similarity of access conditions was seen as shown in Fig. II.2.2-2. On both devices, most ELMy H-mode regime having large ELMs was clearly classified as the collisionless regime of $v_e^* < 1$. On the contrary, HRS/EDA regimes are found to be a high collisionality phenomena of $v_e^* \geq 1$. A ‘‘Mixture’’ regime exists near the operational boundary at around $v_e^* \sim 1$. At higher q_{95} (~ 5) on JFT-2M, it seems to be more easily to access the *pure* ‘‘HRS’’ regime at around $v_e^* \sim 1$, while the ‘‘Mixture’’ regime extends its operational regime toward a high collisionality regime of $v_e^* \geq 1$ at lower q_{95} (~ 3). These results imply the importance of both q_{95} and v_e^* to understand the access conditions for the HRS/EDA regimes. On the other hand, several differences in the edge fluctuations were found. Detail comparison will be reported in the near future.

References

- 2.2-1 Kamiya, K., *et al.*, *Nucl. Fusion*, **43**, 1214 (2003).
- 2.2-2 Kamiya, K., *et al.*, *Plasma Phys. Control. Fusion*, **46**, A157 (2004).
- 2.2-3 Kamiya, K., *et al.*, *Plasma Phys. Control. Fusion*, **46**, 1745 (2004).
- 2.2-4 Kamiya, K., *et al.*, ‘‘Studies of HRS H-mode plasma in the JFT-2M tokamak’’, *Proc. 20th IAEA Fusion Energy Conference*, IAEA-CN-116/EX/4-6Ra, to be published on CD-ROM (IAEA, Vienna), submitted to *Nucl. Fusion*.
- 2.2-5 Hubbard, A. E., *et al.*, *Physics of Plasmas*, **8** (5), 2033 (2001).
- 2.2-6 Mossessian, D., *et al.*, *Physics of Plasmas*, **10** (5), 1720 (2003).

2.3 Study on Divertor and Scrape-Off Plasma

2.3.1 Comparison between Divertor Heat Loads in ELMy H-mode and HRS H-mode

Recently, HRS H-mode [2.3-1] was shown to strongly reduce the ELM activity, and thus to have a potential for eliminating the severe ELM heat load on the divertor target. We compared the divertor heat load between the ELMy H-mode and the HRS H-mode [2.3-2].

Figures II.2.3-1(a) and (b) show time evolutions of D_{α} emission in the divertor ($D_{\alpha\text{-div}}$), electron temperature (T_e) and ion saturation current (I_s) around the strike points on the divertor targets at ELMy and HRS H-mode discharges. During the ELM event, T_e and I_s increases by 2~4 and 5~6 times, respectively

compared with that just before its generation. This result shows that large heat and particle fluxes arrive abruptly on the divertor targets. On the other hand, a transition to the HRS H-mode occurs at $t \sim 0.645$ sec after a brief ELM-free phase with enhanced D_α emission. The electron temperature remains at a low level (~ 10 eV), whereas I_s increases in a manner similar to the D_α enhancement. These findings show that the heat load in the HRS H-mode is induced dominantly by an enhancement of particle transport.

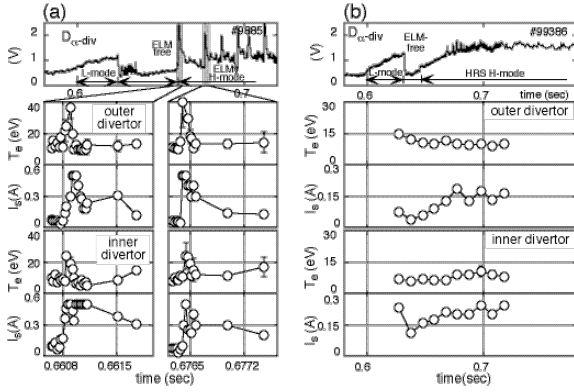


Fig. II.2.3-1 Time evolutions of the D_α emission in the divertor ($D_{\alpha\text{-div}}$), electron temperature (T_e) and ion saturation current (I_s) around the strike points on the divertor targets at ELMy and HRS H-mode discharges. Experimental conditions are $I_p=0.24\text{-}0.27$ MA, $B_r=1.6$ T, $q_{95}=2.6\text{-}2.7$, $\bar{n}_e=4\text{-}5 \times 10^{19} \text{ m}^{-3}$ and $P_{\text{NBI}} = 1.1\text{-}1.4$ MW at lower single plasmas. (From Ref. [2.3-2]).

For the ELMy H-mode and HRS H-mode, the heat load (Γ_{heat}) on the divertor target is evaluated from $\gamma J_s T_e$, where J_s is the ion saturation current density. The heat transmission coefficient γ is assumed to have a value of 7 [2.3-3]. It may change depending on the NBI power [2.3-4]. However, we consider that the change in the experiments is small because of the relatively low NBI power of 1.1-1.4 MW. As a result, the heat flux in the HRS H-mode phase becomes $\Gamma_{\text{heat}} \sim 0.3 \text{ MW/m}^2$ around the strike points. It corresponds to $\sim 15\%$ of the peak value during an ELM event. From this result, we have confirmed an attractive feature of lower heat load in the HRS H-mode than that in the ELMy H-mode.

2.3.2 Direct identification of magnetic surface by the step probe in JFT-2M

In tokamaks magnetic surfaces are estimated from the magnetic measurement by using magnetic probes equipped on the vacuum vessel with aid of the tokamak equilibrium code. However, the calculated results would

contain a systematic error when ferritic steel, which affect the magnetic measurement, is installed near the magnetic probe. The deviation of the separatrix position is estimated to be about 15 mm outer to the low field side than the calculation without considering the ferritic steel. In order to identify the deviation experimentally, we measured the absolute location of the separatrix directly by using two sets of the step probe, which is a double probe having a long and a short electrodes. The probe current of the step probe is expressed as

$$i = \frac{\alpha - 1}{2} + \frac{\alpha + 1}{2} \tanh\left(\frac{\eta_B - \Delta\eta_s - \ln(\alpha)}{2}\right) \quad (\text{II.2.3-1})$$

where $\alpha = n_c/n_s$, $\eta_B = eV_B/kT_e$, $\Delta\eta_s = \Delta V_s/kT_e$, and n_c , n_s is the density of core and the SOL plasma, respectively, V_B is the difference of the two step probe voltages, ΔV_s is the difference of the space potential between the core and SOL plasma. Negative bias voltage to the long electrode so as to $\eta_B \gg \Delta\eta_s$ and positive bias voltage to the short one so as to $\eta_B \gg \Delta\eta_s$ are applied alternately. The time evolution of two probe currents is detected with the current probes, and the difference of them is measured. The difference of the probe currents has a peak when the probe head passes across the separatrix. The separatrix position was measured by jogging the plasma so as the step probe head to cross the separatrix. The measurement has shown that the observed separatrix point is shifted 12.7 mm outward from that calculated with the equilibrium code EQFIT. On the other hand, it had been found that the correlation of the floating potential fluctuations disappears at the separatrix position when they are measured with one set of the step probe. We measured the correlation by using the two sets of the step probe mentioned here. The result has indicated that the separatrix position is shifted 12.5 mm outward from the calculation one, which supports the result using the probe current measurement [2.3-5].

References

- 2.3-1 Kamiya, K., *et al.*, *Nucl. Fusion*, **43**, 1214 (2003).
- 2.3-2 Kawashima, H., *et al.*, *J. Plasma Fusion Res.*, **80**, 907 (2004).
- 2.3-3 Stangeby, P. C., *et al.*, *Nucl. Fusion*, **30**, 12 (1990).
- 2.3-4 Asakura, N., *et al.*, *Nucl. Fusion*, **35**, 381 (1995).
- 2.3-5 Amemiya, H., *et al.*, "Method for Detection of Separatrix Surface Using Differential Double Probe", submitted to *Jpn. J. Appl. Phys.*

2.4 Compact Toroid Injection

Compact toroid (CT) injection is an advanced method of the particle fueling into the plasma, and has been investigated on JFT-2M with collaboration between JAERI and University of Hyogo (former Himeji Institute of Technology), and Hokkaido University. In 2004, we have studied the magnetic fluctuation induced just after the CT injection because the magnetic fluctuation is possibly concerned with the fueling process of CT. This fluctuation is observed after the CT injection and lasts for 30 – 40 μs corresponding to the time scale $\Delta\tau_{\text{inj}}$ of CT injection. Time-frequency analysis has shown that this magnetic fluctuation has the maximum spectral amplitude at 250 - 350 kHz. It had been found that Alfvén wave was excited by the CT injection [2.4-1]. The Alfvén frequency f_A is given by $f_A = v_A/(2\pi qR)$, where q is a safety factor and v_A is the Alfvén speed $B/(\mu_0 m)^{1/2}$. In a typical case of $v_A \sim 6 \times 10^6$ m/s, $q = 2 - 3$ and $R \sim 1.5$ m, f_A is 210 – 320 kHz,

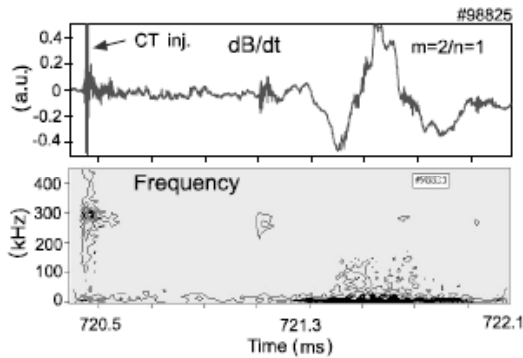


Fig. II.2.4-1 Time evolution of the edge magnetic fluctuation induced by CT injection and its time-frequency spectrum analyzed by Wavelet transform.

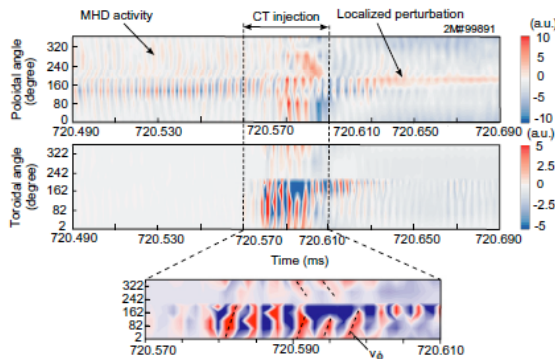


Fig. II.2.4-2 Time evolution of poloidal (top) and toroidal (second) profile contours of the edge magnetic fluctuations before and after CT injection. Time-expanded figure of the toroidal profile is also shown (bottom). A toroidal propagation velocity v_ϕ of the fluctuation is estimated to be $\sim 3 \times 10^6$ m/s.

which is well agreed with the observed frequency. Figure II.2.4-2 shows contour plots of the profile of toroidal and poloidal magnetic field measured with magnetic probes. The fluctuation excited by the injected CT propagates first in the toroidal direction (total toroidal length: $2\pi qR = 8-10$ m) within a few μs , and then its response can be also seen in the poloidal direction after ~ 10 μs . As shown by the time-expanded figure in Fig. II.2.4-2, the fluctuation propagates toroidally in both clockwise (CW) and counter-clockwise (CCW) directions at a velocity $v_\phi \sim 3-4 \times 10^6$ m/s. Such a fast propagation velocity in the toroidal direction agrees with v_A , but is two order of magnitude larger than the ion thermal speed v_{th} of CT $\sim 3 \times 10^4$ m/s, where we assume that the ion temperature is equal to the conductivity electron temperature $T_{e,\text{cond}} \sim 10$ eV as calculated from the resistive decay time τ_R of ~ 20 μs [2.4-2]. These results suggest that the CT could deposit its fuel particles along the magnetic field line at first through the resistive decay process of the magnetic field and/or the β -limit collapse possibly caused by the compression due to the tokamak field pressure [2.4-3].

References

- 2.4-1 Niimi, H., *et al.*, in *Proc. 10th Int. Congress on Plasma Phys.*, (Quebec, 2001) vol.3 768 (2001).
- 2.4-2 Fukumoto, N., *et al.*, *Fusion Eng. and Design*, **44**, 982 (2005).
- 2.4-3 Nagata, M., *et al.*, “Investigation of the Dynamics of Accelerated Compact Toroid Injection into the JFT-2M Tokamak Plasmas”, to be published in *Proc. 20th IAEA Fusion Energy Conf.*, Vilamoura, Portugal, 2004, EX/PP2-15, submitted to *Nucl. Fusion*.

III. THEORY AND ANALYSIS

The principal objective of theoretical and analytical studies is to understand the physics of tokamak plasmas. Much progress was made in transport simulation of current hole plasma, role of low order rational q -values in the ITB events, the theory of Alfvén eigenmodes in tokamaks and current spike behaviour of disruptive plasma, external MHD modes, which is the basis of resistive wall mode (RWM) and MHD ballooning mode stabilization by plasma rotation.

Progress has been made in the NEXT (Numerical EXperiment of Tokamak) project to investigate complex physical processes in transport and MHD phenomena. Formation of zonal flow and streamer in the toroidal electron temperature gradient (ETG) turbulence was examined in detail. Confinement improvement was shown by controlling the zonal flow driven by the ion temperature gradient (ITG) turbulence. The formation and sustaining process of current hole are shown by the MHD simulation.

1. Confinement and Transport

1.1 Transport Simulation of Current Hole Plasma In JT-60U

Profile formation and sustainment of the current hole (CH) plasma have been investigated by using 1.5D transport simulations. A model of the current limit inside the CH on the basis of the Axisymmetric Tri-Magnetic-Islands equilibrium is introduced into the transport simulation. We found that a transport model with the sharp reduction of anomalous transport in the reversed-shear (RS) region can reproduce the time evolution of profiles observed in JT-60U. Figure III.1.1-1(a) and (b) show profiles of T_i , T_e , n_e , j and q at 2 s after the simulation start. Each profile agrees well with the experimental one. The internal transport barrier (ITB) is formed in the RS region. Inside the CH region, profiles of T_i , T_e and n_e are nearly flat. A radius at the ITB foot position, ρ_f , is almost the same as that at the minimum q surface, ρ_{qmin} . The transport becomes neoclassical-level in the RS region, which results in the autonomous formation of profiles with ITB and CH. The ITB width and the energy confinement inside the ITB agree well with JT-60U scalings. The plasma with small bootstrap current fraction shrinks due to the penetration of inductive current. This shrink is

prevented and the CH size can be controlled by the appropriate external current drive (CD). The CH plasma is found to respond autonomically to the external CD [1.1-1].

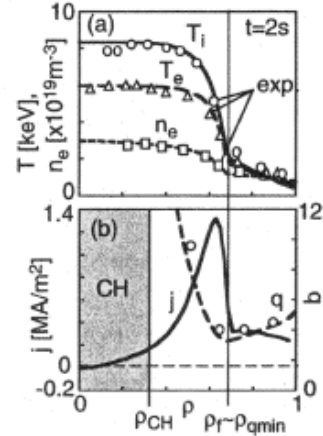


Fig. III.1.1-1 Profiles of (a) T_i , T_e , n_e , and (b) j , q at 2 s after simulation start. Symbols denote experimental data points.

Reference

1.1-1 Hayashi, N., *et al.*, "Profile Formation and Sustainment of Autonomous Tokamak Plasma with Current Hole Configuration", *Proc. 20th IAEA Fusion Energy Conference*, accepted in *Nucl. Fusion*.

1.2 Role of Rational q -values in the ITB Events in Reverse Shear Plasmas

Non-local confinement bifurcations inside and around internal transport barriers (ITBs) with a ms timescale (ITB events) have previously been found in JT-60U reverse shear (RS) and high- β_p plasmas. ITB events are observed as the simultaneous rise and decay of the electron temperature T_e in two zones. They are created by an abrupt non-local reduction (or increase) of heat flux inside 30-40% of the minor radius. Under sufficient neutral beam power P_{NB} (above ~ 8 MW for the $I_p/B_T = 1.2-1.5$ MA/3.8 T pulses described below), ITB events were previously detected at various q_{min} values (q_{min} is the minimum safety factor in the RS configuration). However, the role of q_{min} equal to 3.5, 3, 2.5, 2 is not obvious for ITB formation. We here focus on new features of ITB evolution near low-order-rational values of q_{min} . The formation of a stronger ITB and its further splitting into two radially separated ITBs is described. These ITBs are located in both positive and negative shear zones of a plasma with L-mode edge. The

similarity of space-time evolution of the electron temperature T_e and the ion temperature T_i at sufficient power is highlighted (even when the variation is significant and complicated in space and time). Within errorbars, ITB splitting occurs as q_{\min} passes through 2.5. The similarity of space-time evolution of T_e and T_i suggests a similarity in the qualitative behavior of electron and ion heat diffusivities in time and space. The temporal formation of an ITB in the zone with small positive shear, while q_{\min} passes through 3 (after periodical improvements and degradations via ITB events with 8 ms period) in H-mode, with $P_{\text{NB}} = 8\text{MW}$, is described. At lower powers, ITB events are observed only near rational values of q_{\min} . In weak RS shots with $P_{\text{NB}} = 4\text{MW}$, transport is reduced via ITB events during 0.08 s at $q_{\min} = 3.5$, and repetitive short-term phases of reduced transport are observed as q_{\min} passes through 3. The behavior of T_i looks different. The difference in T_e and T_i evolution, which was detected regularly under low power, probably indicates a decoupling of T_e and T_i transport. [1.2-1].

Reference

1.2-1 Neudatchin, S.V., Takizuka, T., Hayashi, N., et al., Nucl. Fusion **44**, 945 (2004).

2. MHD Stability

2.1 Development of the theory of Alfvén eigenmodes in tokamaks

New magnetohydrodynamic (MHD) phenomena with upward frequency-sweeping named Alfvén Cascades (ACs) were revealed recently on JT-60U and JET in discharges with non-monotonic safety factor (reversed magnetic shear, (RS)) and significant population of the hot ions. The first theoretical description of ACs was given in the paper [Berk et al., Phys. Rev. Lett. **87**, 185002 (2001)], where radial localization of Alfvén Eigenmode (AE) was provided by the non-resonant response of hot ion population. Another mode localizing toroidal MHD effect was considered by Breizman et al. [Phys. Plasmas **10**, 3649 (2003)].

We extended the theory of AE in RS tokamak plasmas (RSAE) by incorporating the effect of thermal plasma density gradient taken from theory of cylindrical Global Alfvén Eigenmodes (GAE) and kinetic (finite ion Larmor radius) effects from theory of Kinetic

Toroidicity induced Alfvén Eigenmodes (KTAE).

It was shown that the localization effect of thermal plasma density gradient on AC mode can be stronger than the toroidal MHD effect as squared aspect ratio. Thus, the Alfvén Cascade modes can be theoretically demonstrated in cylindrical geometry approximation. Then the role of thermal plasma density gradient can be dominant if the localization effect of density gradient of large orbit hot ions is sufficiently weak. This effect was found to be localizing for the mode numbers satisfying the condition $q_{\min} > m/n$ and delocalizing otherwise. The shift of the localization region of the eigenmodes and the eigenfrequency shift caused by the thermal plasma density gradient were found to be sufficiently small. [2.1-1]

Taking into account the finite ion Larmor radius (kinetic) effects in Alfvén mode equation allows us to predict a new branches of these modes called the Kinetic Reversed-Shear Alfvén Eigenmodes (KRSAs). These modes are shown to possess the features of Alfvén Cascades even for homogeneous thermal plasma density in cylindrical geometry approximation. It was found that for existence of the radially localized mode structure the requirements on the hot ion density and its gradient are less strict than those for traditional RSAE. Thus it is possible that KRSAs can be more unstable than original RSAE. [2.1-2]

We studied continuum damping of RSAE and calculated rigorously the damping rate. The damping rate depends in a complex way on the hot ion density and its gradient. Therefore the damping condition should modify RSAE onset threshold as well. [2.1-3]

In the approximation of the large orbits of hot ions the dominant hot ion contribution to the RSAE equation comes from the electrons compensating the charge of the fast ions (indirect fast ion effect on the mode). Incorporating this effect in the theoretical description of the TAE modes in discharges with monotonic (positive) shear revealed new varieties of TAEs with different energy, eigenfrequency and parity of the modes. [2.1-4, 2.1-5]

The cross field drift of the compensating electrons was shown to be of crucial importance in the theory of Energetic Particle Mode (EPM) to provide quasineutrality of perturbations. In the limiting case when compensating electron effect is dominant, the unstable EPM modes were found to be substituted by

the new kind of eigenmodes, called Compensating Electron Alfvén Eigenmodes which are heavily damped due to continuum dissipation and resonance interaction with fast ions. Therefore in general, the picture of Alfvén instabilities excited by energetic ions in discharges with monotonic safety factor is more favorable than that predicted by the EPM theory. [2.1-6]

References

- 2.2-1 Konovalov, S.V., et al., *Phys. Plasmas*, **11**, 2303 (2004).
 2.2-2 Konovalov, S.V., et al., *Phys. Plasmas*, **11**, 4531 (2004).
 2.2-3 Konovalov, S.V., et al., *Proc. 20th IAEA Fusion Energy Conference*, IAEA-CN-TH/P5-10.
 2.2-4 Mikhailovskii, A.B., et al., *Doklady Physics*, **49**, 505 (2004).
 2.2-5 Mikhailovskii, A.B., et al., *Plasma Phys. Rep.*, **31**, 93 (2005).
 2.2-6 Mikhailovskii, A.B., et al., *Doklady Physics*, **50**, 128 (2005).

2.2 TSC Simulation on Current Spike Behavior of JT-60U Disruptive Plasmas

Characteristics and underlying mechanisms for plasma current spikes, which have been frequently observed during the thermal quench of JT-60U disruptions, were investigated by simulations of Tokamak Simulation Code (TSC) including the passive shell effects of the vacuum vessel. Positive shear and reversed shear (PS and RS) plasmas were shown to have various features of the current spike in the experiments, e.g. an impulsive increase in the plasma current (positive spike) in the majority of thermal quenches, while sudden decrease (negative spike) that has been excluded from past consideration as an exception. It was clarified for the first time that the shell effects, which become significant especially at a strong pressure drop due to the thermal quench of high β_p plasmas, play an important role in the current spike in accordance with the relation of the radial location between the initial plasma equilibria and the vacuum vessel. As a consequence, a negative current spike may appear when the plasma is positioned much further out than the geometric centre of the vacuum vessel, whereas a positive current spike may appear when the plasma is positioned much more inward than the vacuum vessel centre (a broken line in Fig.III.2.2-1). It was also pointed out that a further lowering of the internal inductance, in contradiction to previous interpretation

made in the past, is a plausible candidate for the mechanism for positive current spikes observed even in the RS plasmas (arrows in Fig.III.2.2-1). The new interpretation of the shell effects and the abrupt change of the current profile enables us to reason out the whole character and the underlying mechanism for a variety of current spikes of major disruptions as well as the minor disruptions in JT-60U [2.2-1].

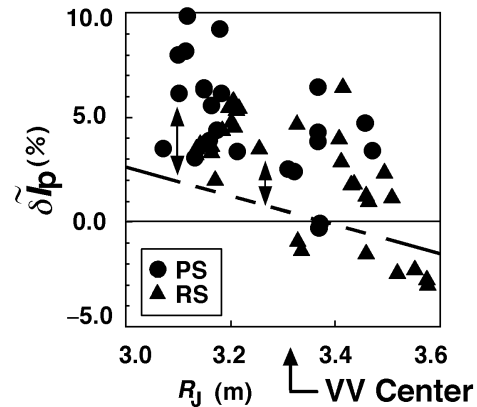


Fig. III.2.2-1 Normalized current spikes $\delta \hat{I}_p$ ($=\delta I_p/I_{p0}$) observed in JT-60U PS (●) and RS (▲) disruptive discharges versus plasma radial position R_j . The broken line indicates a TSC simulation. Notice that the abrupt change in the current profile due to the ‘magnetic braiding’ (denoted by arrows), together with the newly found shell effects due to the β_p drop (denoted by the broken line), explains the whole character of the current spikes observed in JT-60U disruption experiments.

Reference

- 2.2-1 Takei, N., et al., *Plasma Phys. Control. Fusion*, **46**, 1815 (2004).

2.3 Critical β Analyses with Ferromagnetic and Wall Geometry Effects

The critical beta, that is limited by Alfvén wave time scale external kink mode, is shown to be decreased by ferromagnetic effect by about 8 % for $m/m_0 \sim 2$, m and m_0 denote the permeability of ferromagnetic wall and vacuum, respectively, for tokamak of aspect ratio 3. The existence of the stability window for resistive wall mode opened by both effects of the toroidal plasma rotation and the plasma dissipation, which was not observed for high aspect ratio tokamak, is found for tokamak of aspect ratio 3. The effect of ferromagnetism on them is also investigated. The critical beta analyses of NCT (National Centralized Tokamak) plasma using VALEN code are started with stabilizing plate and vacuum vessel geometry with finite resistivity, and the

results for passive effect of stabilizing plate are obtained. The calculations including stabilizing effect of the vacuum-vessel and also active feedback control are also performed for present design of NCT plasma.

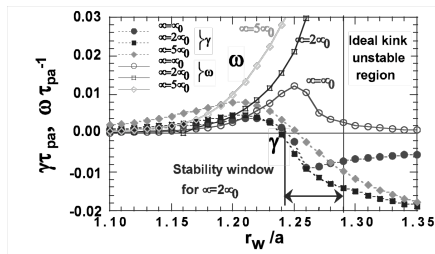


Fig. III.2.3-1 Growth rate and mode frequency as a function of the normalized wall radius for three relative permeability where the toroidal rotation velocity is 0.5 times poloidal Alfvén velocity.

Reference

2.3-1 Kurita, G., et al., *Proc. 20th IAEA Fusion Energy Conference*, CD-ROM file FTP7/7 (R).

2.4 Stability Analysis of External MHD Modes by the 2-D Newcomb Equation

The theory of the Newcomb equation has been applied to low- n external modes in a tokamak and a method has been developed for computing the stability matrix that gives the change of plasma potential energy due to external modes in terms of the surface values of the perturbations[2.4-1]. By using this method, the spectral properties of the ideal external modes have been elucidated, such as the coupling between external modes and internal modes, and the difference in the stability properties between a normal shear tokamak and a reversed shear tokamak. These results will also be useful in the stability analysis of resistive wall modes.

References

2.4-1 Aiba, N., Tokuda, S., Ishizawa, T. and Okamoto, M., *Plasma Phys. Control. Fusion* **46**, 1699 (2004).

2.5 Rotational Stabilization of High- n Ballooning Modes

A ballooning perturbation in a toroidally rotating tokamak is expanded by square-integrable eigenfunctions of an eigenvalue problem associated with ballooning modes in a static plasma[2.5-1]. A special weight function is chosen such that the eigenvalue problem has only the discrete spectrum. The eigenvalues evolve in time owing to toroidal rotation shear, resulting in a countably infinite number of

crossings among them. The crossings cause energy transfer from an unstable mode to the infinite number of stable modes; such a transfer works as the stabilization mechanism of the ballooning modes. A simple analytic formula is derived for estimating the toroidal rotation shear required to stabilize the ballooning mode.

References

2.5-1 Furukawa, M. and Tokuda, S., *Nucl. Fusion* **45**, (2004) in print.

3. Numerical Experiment of Tokamak (NEXT)

3.1 Structure Formations in Toroidal ETG Turbulence

Using a gyrokinetic toroidal particle code with global profile effects, the toroidal electron temperature gradient driven (ETG) turbulence in positive and reversed shear tokamaks is studied. In the simulation, initial saturation levels of the ETG mode are consistent with the mixing length theory, which shows a Bohm (gyro-Bohm) like ρ^* -scaling for a ballooning type (slab like) ETG mode in a positive (reversed) shear configuration, where ρ^* is the electron Larmor radius ρ_{te} divided by the minor radius a . In a realistic small ρ^* positive shear configuration, the ETG mode has a higher saturation level than the large ρ^* positive shear configuration and the reversed shear configuration. In the nonlinear turbulent state, the ETG turbulence in the

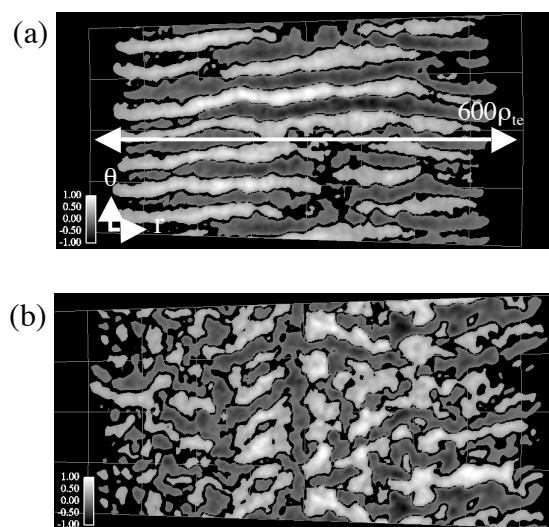


Fig. III.3.1-1 Contour plots of the electrostatic potential observed in ETG turbulence simulations in (a) positive and (b) reversed shear configurations.

positive and reversed shear configurations shows quite different structure formations. In the positive shear configuration, the ETG turbulence is dominated by streamers which have a ballooning type structure, and the electron temperature T_e profile is quickly relaxed by an enhanced heat transport in a turbulent time scale. In the reversed shear configuration, zonal flows are produced in the negative shear region, while the positive shear region is characterised by streamers. Accordingly, the electron thermal diffusivity χ_e has a gap structure across the q_{\min} surface, and the T_e gradient is sustained above the critical value reversed shear tokamaks.

References

- 3.1-1 Idomura, Y., Tokuda, S., and Kishimoto, Y., *Proc. 20th IAEA Fusion Energy Conference*, IAEA-CN-116/TH/8-1.

3.2 Confinement Improvement by Control of Zonal Flow Behavior

Based on global Landau-fluid ion temperature gradient (ITG) driven turbulence simulations, it is found that plasma confinement can be improved by control of zonal flow behavior[3.2-1,3.2-2]. Zonal flows are almost stationary in a low safety factor (q) region and suppress turbulent transport effectively. On the other hand, the zonal flows are oscillatory in a high q region. The oscillatory zonal flows cannot suppress the ITG turbulence effectively. Thus the stationary zonal flows in the low q region are favorable for plasma confinement.

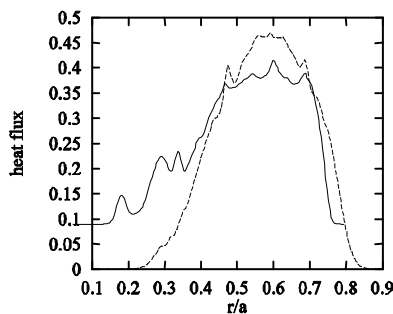


Fig. III.3.2-1 Radial profile of time averaged heat flux. The heat flux in $0.4 < r/a < 0.7$ for the q profile shown in Fig. 2(a) (solid line) is reduced compared to that for the q profile shown in Fig. 2(b) (dashed line) due to expansion of the stationary zonal flow region.

Therefore it is expected that when q profile has a broad low q region, the turbulent transport is suppressed in a broad region by the stationary zonal flows. Figure 1

shows radial profile of time averaged turbulent heat flux for the q profiles shown in Fig. 2. In the case with the q profile having a wider low q region shown in Fig. III.3.2-2(a), the heat flux is reduced in a broad region compared to that for the q profile shown in Fig. III.3.2-2(b). This result indicates that the turbulent transport can be controlled through the control of the zonal flow behavior by the q profile.

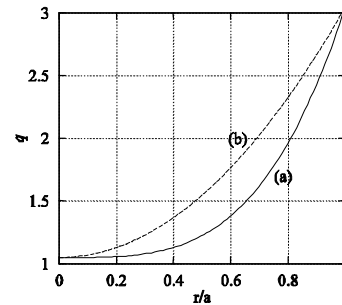


Fig. III.3.2-2 The q profiles used in the calculations: (a) $q = 1.05 + 2(r/a)^{3.5}$ and (b) $q = 1.05 + 2(r/a)^2$

References

- 3.2-1 Miyato, N., Kishimoto, Y. and Li, J., *Physics of Plasmas* **11**, 5557 (2004).
 3.2-2 Miyato, N., Li, J. and Kishimoto, Y., *Proc. 20th IAEA Fusion Energy Conf. (2004)* (Vienna: IAEA) CD-ROM file TH/8-5Rb.

3.3 Formation of Current Hole by Pair Vortex Motion

Some negative currents should be driven in the central region of the tokamak by bootstrap current and off-axis current drive when the amplitude of driven current is large enough. Once a surface with a zero poloidal magnetic field appears, however, a toroidal equilibrium is lost and any static state cannot exist. Plasma motion along the horizontal direction occurs by the force unbalance between the inside and outside of the torus. A pair of vortices with counter rotation grows in this case. Once the vortex rotation grows enough, plasma flow across a poloidal magnetic field produces an effective electric field, which almost cancel out a negative one-turn voltage. the plasma current profile is kept flat by this convective motion. We investigate the growth of this convective motion and find the appearance of the flat current profile, the formation of a current hole, by resistive MHD simulations[3.3-1]. After the current hole

is formed, additional current drive to the central becomes difficult by the plasma flow. This process is considered as an inverse process of a dynamo effect observed in RFP plasma and geophysics.

References

- 3.3-1 Tukuda, T., Kurita, G. and Fujita, T., *Proc. 20th IAEA Fusion Energy Conference*, IAEA-CN-TH/P2-10.

IV. FUSION REACTOR DESIGN STUDY

1. Reactor Design Study

1.1 Conceptual Design of Fusion DEMO Plant

Recent reactor design activity at the Japan Atomic Energy Research Institute has been mainly focused on fusion DEMO plant which is placed beyond ITER. The DEMO plant aims to demonstrate 1) an electric power generation of 1 GW level, 2) self-sufficiency of T fuel, 3) year-long continuous operation. At the same time, DEMO should present an economical prospect for commercialization. To meet the requirements, three options with different capabilities of CS are considered : 1) the "Slim CS" option, being capable of providing sufficient Ampere-turns for plasma shaping but supplying a V-sec limited to I_p ramp-up to 3.8 MA; 2) the "Full CS" option, being capable of plasma shaping and V-sec supply enough to reach the flat-top plasma current, like conventional tokamaks; 3) the "CS-less" option, having no CS functions but the most compact reactor size. The "CS-less" option corresponds to VECTOR concept [1.1-1] . The parameters comparison between those three options is shown in Table IV.-1.-1.

Table IV.-1.1 Parameter for CS-less, slim CS and full CS options

	CS-less	Slim CS	Full CS
R_p (m)	5.1	5.5	6.5
A (m)	2.1	2.1	2.1
Δ	2.5	2.6	3.1
κ	2.1	2.0	1.9
δ	0.34	0.44	0.5
$B_T/B_{max}(T)$	5.6/18.2	6.0/16.4	6.8/14.6
I_p (MA)	17.4	16.7	15.0
q_{95}	4.5	5.6	5.1
β_N	4.8	4.3	3.9
HH	1.3	1.3	1.3
n/n_{GW}	0.94	0.98	1.0
P_{fus}	3.0	3.0	3.0
$P_n(MW/m^2)$	3.7	3.5	3.0
Q	48	52	54
Weight (tons)	15,700	17,500	23,900

Among these three options, "Slim CS" is being considered to be the prime option in view of the tradeoff between required technologies especially in plasma physics and the reactor size. In this sense, "Slim CS" is a design compromise on the advanced commercial reactor VECTOR. This option shown in Fig. IV.-1-1 produces the fusion output of 3 GW with the major

radius of 5.5 m, the aspect ratio of 2.6, the normalized beta of 4.3 and the maximum field of 16.4 T. The estimated reactor weight is lighter than other conventional tokamak reactors, suggesting an economic advantage. The plant uses rather conservative technologies such as Nb₃Al superconductor, water-cooled solid breeder blanket, low activation ferritic steel as the structural material and tungsten monoblock divertor plate.

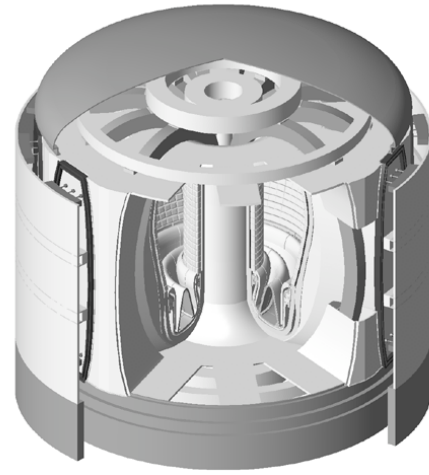


Fig. IV.1-1 Conceptual view of DEMO "slim CS" option

References

- 1.1-1 Nishio, S., *et al.*, *Proc. 20th IAEA Fusion Energy Conf. (Vilamoura)* FT/P7-35 4).

1.2 Current Ramp Simulation for CS-less Tokamak Reactor

Simulation study on internal transport barrier (ITB) of tokamak plasma has been carried out in the aspect of reactor design study.

A non-inductive current ramp-up, which is necessary to start up a CS-less tokamak like VECTOR, was investigated with the TSC code [1.2-1,1.2-2]. It was shown that a cooperative linkage between the non-inductive current and ITB-generated bootstrap (BS) current exhibited a recurrence of positive and negative shear profiles when a CDBM (current diffusive ballooning mode) model was adapted in the simulation. In addition, another cooperative linkage between BS current and the resulting modulated magnetic shear showed an oscillatory current ramp for highly BS current-driven plasmas. Figure IV.-1.2-1 shows the

consequent zero magnetic shear profile arising from the oscillation. It was shown that a profile misalignment between the BS current and the magnetic shear gave rise to these oscillatory behaviors.

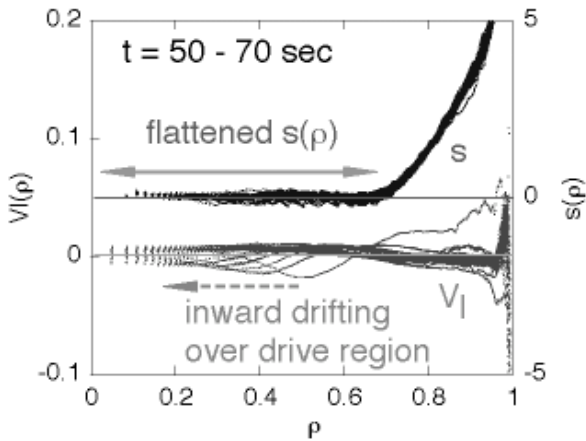


Fig. IV.1.2-1 Flattened shear profile over wide region of $0 < \rho < 0.6$ and inward drifting negative loop voltage, arising from cooperative link between BS current and BS current-modulated shear profile. Shear profile is widely suppressed to nearly "ZERO", avoiding Current Hole formation.

References

- 1.2-1 Nakamura, Y., *et al.*, 31st EPS Conference on Controlled Fusion and Plasma Physics, London, P-2.140 (2004).
- 1.2-2 Nakamura, Y., *et al.*, *J. Plasma Fusion Res. SERIES*, **6**, 196 (2004).

2. Waste Management Study

2.1 Nitrogen Concentration of F82H for Shallow Land Burial

Reduced activation ferritic steel (F82H) is considered to be the prime structural material for fusion DEMO plant. The relation between nitrogen concentration in F82H and the waste classification of the used F82H was assessed. Previously, neutronics assessment indicated that nitrogen concentration should be as low as 20 ppm to dispose of most of the used F82H by shallow land burial. This is because nitrogen can produce carbon-14 which plays a critical role in waste classification. Such a low nitrogen concentration can adversely affect toughness and creep strength of F82H. Thus, nitrogen concentration of 100-200 ppm is required on the material side. In order to find a good compromise and provide a guide line for the material development, the allowable concentration ratio of nitrogen for the shallow land burial was estimated with neutronics codes. The

result indicates that most of the used F82H can be qualified to be disposed by shallow land burial when 95%-enriched nitrogen-15 is used at 100 ppm in F82H fabrication instead of nitrogen with natural abundance.

2.2 Waste Assessment for D-³He Reactor [2.2-1]

Quantitative comparison of waste was carried out for D-T fuel and D-³He fuel fusion reactors. There is an opinion that D-³He reactors produce much smaller amount of waste than D-T reactors. However, our waste assessment indicates that the D-³He reactor will not necessarily have an advantage of reducing the radioactive waste although the reactor is widely believed to reduce the load on the environment compared with a D-T reactor because of its very low neutron yield. Our assessment indicates that the D-³He reactor with the electric output of 1 GWe will produce radioactive waste of more than 10,000 tons due to parasitic D-T reactions. The amount will be more than the radwaste of the D-T reactor with the same electric output. From the point of view of waste management, a disadvantage of the D-³He reactor is that it requires massive poloidal field coils to maintain the equilibrium of plasma with several tens of MA. If we assume an extremely advanced technology of disassembling the superconducting coils into individual homogeneous materials, the waste of the coils would qualify for clearance waste, reducing the radioactive waste to as low as 1,835 tons.

References

- 2.2-1 Tobita, K. *et al.*, *Proc. 23rd. Symp. of Fusion Technology*, Venice, Italy (2004).

Appendix A.1 Publication List (April 2004 – March 2005)

A.1.1 List of JAERI Report

- 1) Department of Materials Science, Department of Fusion Engineering Research, "Recent accomplishment for the development of reduced activation ferritic/martensitic steels – interim report for HFIR IV with results of relating activities-," JAERI-Review 2004-018 (2004).
- 2) Department of Fusion Engineering Research and Department of Material Science, "Achievement of Element Technology Development for Breeding Blanket," JAERI-Review 2005-012 (2005).
- 3) Furuya, K., "Fabrication of model for fusion nuclear first wall made from F82H steel by HIP method and the metallurgical properties," JAERI-Research 2004-013 (2004).
- 4) Fusion Neutron Laboratory, "Activity Report of the Fusion Neutronics Source from April 1, 2001 to March 31, 2004," JAERI-Review 2004-017 (2004).
- 5) Ikeshima, Y., Ishida, T., Tsuchiya, K., et al., "Examination on Detaching Method of an Irradiated Mock-up with Li₂TiO₃ Pebble Bed from the Core of JMTR," JAERI-Tech 2005-005 (2005) (in Japanese).
- 6) Inoue, T., "R&D on high power negative ion sources and accelerators for a neutral beam injector," JAERI-Research 2005-006 (2005) (in Japanese).
- 7) Kurihara, R., "Integrity of the First Wall in Fusion Reactors," JAERI-Tech 2004-052 (2004).
- 8) Maehara, S., Moriyama, S., Saigusa, M., et al., "Evaluation of RF properties by orifice design for IFMIF RFQ," JAERI-Research 2005-007 (2005).
- 9) Nakahira, M., Takeda, N., Urata, K., "Parameter Study on Dynamic Behavior of ITER Tokamak Scaled," JAERI-Tech 2004-069 (2004) (in Japanese).
- 10) Nakamura, H., Ida, M., Matsuhiro, K., et al., "Review of JAERI Activities on the IFMIF Liquid Lithium Target in FY2004," JAERI-Review 2005-005 (2005).
- 11) Nakazawa, T., Grismanovs, V., Yamaki, D., et al., "Influences of High Energy Heavy Ions on Long- and Short-Range Structures of Li₂TiO₃," JAERI-Review 2004-027 (2004).
- 12) Takahashi, K., "Research and development of high power millimeter wave injection system for fusion plasma heating and current drive," JAERI-Research 2005-11 (2005) (in Japanese).
- 13) Takeda, N., Kakudate, S., Nakahira, M., "Dynamic Analysis of ITER Tokamak Based on Results of Vibration Test Using Scaled Model," JAERI-Tech 2004-072 (2004).
- 14) Takeda, N., Kakudate, S., Nakahira, M., "Research and Development of Remote Handling System for ITER Divertor Maintenance," JAERI-Tech 2004-071 (2004).
- 15) Takeda, N., Nakahira, M., "Plan of Vibration Tests for Estimation of Seismic Performance of ITER Tokamak," JAERI-Tech 2004-073 (2004) (in Japanese).
- 16) Tsuchiya, K., Kawamura, H., Nakamichi, M., et al., "Low Temperature Tritium Release Experiment from Lithium Titanate Breeder Material," JAERI-Tech 2005-013 (2005).
- 17) Tsuru, D. et al., "Proceedings of eleventh international workshop on ceramic breeder blanket interactions, December 15-17, 2003, Tokyo Japan," JAERI-Conf 2004-012, 35 (2004).
- 18) Urano, H., "Energy Confinement and Transport of H-mode Plasmas in Tokamak," JAERI-Research, 2004-027 (2005).
- 19) Verzilov, Y.M., Sato, S., Nakao, M., et al. "Integral Experiments for Verification of Tritium Production on the Beryllium/Lithium Titanate Blanket Mock-up with a One-breeder Layer," JAERI-Research 2004-015 (2004).
- 20) Yamaki, D., Nakazawa, T., Aruga, T., et al., "Observation of Microstructural Changes in Li₂TiO₃ Caused by Ion Beam Irradiation," JAERI-Review 2004-025, 173 (2004).
- 21) Yutani, T., Sugimoto, M., Nakamura, H., et al., "Compatibility of reduced activation ferritic/martensitic steel specimens with liquid Na and NaK in irradiation rig of IFMIF," JAERI-Tech 2005-036 (2005).

A.1.2 List of papers published in journals

- 1) Adachi, T., Nagata, S., (Yamauchi, M.), et al., "Irradiation Effects on the Electrical Conductivity of Fluorine-Based Polymer Membranes," *J. Nucl. Mater.*, **329-333**, 1499 (2004).
- 2) Akino, N., Ebisawa, N., Honda, A., et al., "Long pulse operation of NBI systems for JT-60U," *J. Fusion Sci. Technol.*, **48**, 758 (2005).
- 3) Ando, M., Wakai, E., Sawai, T., et al., "Synergistic effect of displacement damage and helium atoms on radiation hardening in F82H at TIARA facility," *J. Nucl. Mater.*, **329-333**, 1137 (2004).
- 4) Asai, K., Iguchi, T., (Nishitani, T.), et al., "Detailed Design of Ex-vessel Neutron Yield Monitor for ITER," *Rev. Sci. Instrum.*, **75**, 3537 (2004).
- 5) Asakura, N., "Wall Pumping and Saturation in Divertor Tokamaks," *Plasma Phys. Control. Fusion*, **46**, B335 (2004).
- 6) Asakura, N., Takechi, M., Oyama, N., et al., "Parallel and Radial Transport of ELM Plasma in the SOL and Divertor of JT-60U," *J. Nucl. Mater.*, **337-339**, 712 (2005).
- 7) Asakura, N., Takenaga, H., Sakurai, S., et al., "Driving Mechanism of SOL Plasma Flow and Effects on the Divertor Performance in JT-60U," *Nucl. Fusion*, **44**, 503 (2004).
- 8) Brichard, B., Fernandez, A., (Nishitani, T.), et al., "Radiation-hardening Techniques of dedicated Optical Fibers used in Plasma Diagnostic Systems in ITER," *J. Nucl. Mater.*, **329-333**, 1456 (2004).
- 9) Das, M., Sawamura, T., (Nishitani, T.), et al., "Superheated Emulsion as High-energy Neutron Dosimeters," *Radiat. Prot. Dosim.*, **110**, 325 (2004).
- 10) Davies, A.R., Field, J.L., Takahashi, K., et al., "The toughness of free-standing CVD diamond," *J. Mat. Sci.*, **39**, 1571 (2005).
- 11) Enoda, M., Akiba, M., Tanaka, S., et al., "Plan and Strategy for ITER Blanket Testing in Japan," *Fusion Sci. & Technol.*, **47**, 1023 (2005).
- 12) Enoda, M., Hatano, T., Tsuchiya, K., et al., "Development of Solid Breeder Blanket at JAERI," *Fusion Sci. & Technol.*, **47**, 1060 (2005).
- 13) Ezato, K., Dairaku, M., Taniguchi, M., et al., "Development of ITER Divertor Vertical Target with Annular Flow Concept—I: Thermal-Hydraulic Characteristics of Annular Swirl Tube," *Fusion Sci. & Technol.*, **46**, 521 (2004).
- 14) Ezato, K., Dairaku, M., Taniguchi, M., et al., "Development of ITER Divertor Vertical Target with Annular Flow Concept—II: Development of Brazing Technique for CFC/CuCrZr Joint and Heating Test of Large-Scale Mock-up," *Fusion Sci. & Technol.*, **46**, 530 (2004).
- 15) Ezato, K., Suzuki, S., Sato, K., et al., "Thermal fatigue experiment of screw cooling tube under one-sided heating condition," *J. Nucl. Mater.*, **329-333**, 820 (2004).
- 16) Fujita, T., Fukuda, T., Sakamoto, Y., et al., "Formation conditions for electron internal transport barriers in JT-60U plasmas," *Plasma Phys. Control. Fusion*, **46**, A35 (2004).
- 17) Fujiwara, Y., Watanabe, K., Okumura, Y., et al., "Actively cooled plasma electrode for long pulse operations in a cesium-seeded negative ion source," *Rev. Sci. Instrum.*, **76**, 13501 (2005).
- 18) Fukumoto, N., Inoo, Y., Nomura, M., et al., "An Experimental Investigation of the Propagation of Compact Toroid along Curved Drift Tubes," *Nucl. Fusion*, **44**, 982 (2004).
- 19) Fukumoto, N., Ogawa, H., Nagata, M., et al. "Characteristics of Modified CT Injector for JFT-2M," *Fusion Eng. Des.*, **70**, 289 (2004).
- 20) Gotoh, Y., Arai, T., Yagyu, J., et al., "Transmission Electron Microscopy of Redeposition Layers on Graphite Tiles Used for Open Divertor Armor of JT-60," *J. Nucl. Mater.*, **329-333**, 840 (2004).
- 21) Hanada, M., Kashiwagi, M., Inoue, T., et al., "Experimental comparison between plasma and gas neutralization of high-energy negative ion beams," *Rev. Sci. Instrum.*, **75**, 1813 (2004).
- 22) Hayashi, N., Isayama, A., Nagasaki, K., et al., "Numerical Analysis of Neoclassical Tearing Mode Stabilization by Electron Current Drive," *J. Plasma Fusion Res.*, **80**, 605 (2004).

- 23) Hayashi, T., Nishitani, T., Ishikawa, M., "First Measurement of Time-resolved Neutron Yield on JT-60U using Micro-fission Chamber," *Rev. Sci. Instrum.*, **75**, 3575 (2004).
- 24) Heinzl, V., Bem, P., (Sugimoto, M.), et al., "Overview on the IFMIF test cell development," *J. Nucl. Mater.*, **329-333**, 223 (2004).
- 25) Hirai, T., Ezato, K., Majerus, P., "ITER Relevant High Heat Flux Testing on Plasma Facing Surfaces," *Mater. Trans.*, **46**, 412 (2005).
- 26) Hirose, T., Shiba, K., Sawai, T., "Effects of Heat Treatment Process for Blanket Fabrication on Mechanical Properties of F82H," *J. Nucl. Mater.*, **329-333**, 324 (2004).
- 27) Hoshino, K., Nagashima, Y., Ido, T., et al., "On MHD Oscillations in High Beta H-mode Tokamak Plasma in JFT-2M," *J. Plasma Fusion Res. SERIES*, **6**, 345 (2004).
- 28) Hoshino, T., Kawamura, H., Dokiya, M., et al., "Non-Stoichiometry of Li₂TiO₃ under Hydrogen Atmosphere Conditions," *J. Nucl. Mater.*, **329-333**, 1300 (2004).
- 29) Hoshino, T., Kobayashi, T., Nashimoto, M., et al., "High-Temperature Thermophysical Property Measurements on Non-Stoichiometric Composition of Li₂TiO₃," *J. Ceram. Soc. Japan, Supplement 112-1, PacRim5 Special Issue*, **112**, S354 (2004).
- 30) Ida, M., Nakamura, Hiroo, Nakamura, Hideo, et al., "Design of contraction nozzle and concave back-wall for IFMIF target," *Fusion Eng. Des.*, **70**, 95 (2004).
- 31) Inoue, T., Sakamoto, K., "Intelligible Seminar on Fusion Reactors – (3) Heating Systems to achieve Fusion Reaction in High Temperature Plasma," *J. Atomic Energy Soc. Japan*, **47**, 38 (2005).
- 32) Inoue, T., Taniguchi, T., Dairaku, T., et al., "Acceleration of 1MeV, 100mA class H- ion beams in a proof-of-principle accelerator for ITER," *Rev. Sci. Instrum.*, **75**, 1819 (2004).
- 33) Inoue, T., "Intelligible Seminar on Fusion Reactors – (1) Introduction to Fusion Reactors," *J. Atomic Energy Soc. Japan*, **46**, 27 (2004).
- 34) Inui, D., Watanabe, K., (Nishitani, T.), et al., "Development of Fusion Neutron Camera using Organic Liquid Scintillator and Wavelength Shifting Fiber," *Rev. Sci. Instrum.*, **75**, 3578 (2004).
- 35) Ioki, K., Akiba, M., Barabaschi, P., et al., "ITER Nuclear Components, Preparing for the Construction and R&D Results," *J. Nucl. Mater.*, **329-333**, 31 (2004).
- 36) Ishida, S., JT-60 team, and JFT-2M team, "High-beta steady-state research and future directions on the Japan Atomic Energy Research Institute Tokamak-60 Upgrade and the Japan Atomic Energy Research Institute Fusion Torus-2 Modified," *Physics of Plasmas*, **11**, 2532 (2004).
- 37) Ishikawa, M., Kusama, Y. et al., "Fast Neutral Particle Measurement with Natural Diamond Detector on JT-60U," *Rev. Sci. Instrum.*, **75**, 3643 (2004).
- 38) Itami, K., Sugie, T. et al., "Multiplexing Thermography for International Thermonuclear Experimental Reactor divertor targets," *Rev. Sci. Instrum.*, **75**, 4124 (2004).
- 39) Iwakiri, H., Yasunaga, K., Yoshida, N., (Uchida, M.) et al., "Thermal Desorption of Deuterium from Ion Irradiated Be₁₂Ti," *J. Nucl. Mater.*, **329-333**, 880 (2004).
- 40) Jameson, R., Ferdinand, R., (Sugimoto, M.) et al., "IFMIF accelerator facility," *J. Nucl. Mater.*, **329-333**, 193 (2004).
- 41) Kamada, Y., Saibene, G., Hatae, T., et al., "Dimensionless pedestal identity experiments in JT-60U and JET in ELMy H-mode plasmas," *Plasma Phys. Control. Fusion*, **46**, A195 (2004).
- 42) Kamiya, K., Bakhtiari, M., Kasai, S., et al., "High Recycling Steady H-mode Regime in the JFT-2M Tokamak," *Plasma Phys. Control. Fusion*, **46**, A157 (2004).
- 43) Kamiya, K., Oyama, N., Miura, Y., et al., "Pedestal Characteristics in JFT-2M HRS H-mode Plasma," *Plasma Phys. Control. Fusion*, **46**, 1745 (2004).
- 44) Kaneko, J.H., Teraji, T., (Nishitani, T.), et al., "Response Function Measurement of Layered Type CVD Single Crystal Diamond Radiation Detectors for 14 MeV Neutrons," *Rev. Sci. Instrum.*, **75**, 3581 (2004).
- 45) Kasugai, A., Sakamoto, K., Minami, R., et al., "Study of millimeter wave high-power gyrotron for long pulse operation," *Nucl. Instrum. Method Phys. Res.*, **A528**, 110 (2004).

- 46) Katayama, K., Takeishia, T., Miya, N., et al., "Tritium Release Behavior from the Graphite Tiles Used at the Dome Unit of The W-Shaped Divertor Region In JT-60U," *J. Nucl. Mater.*, **340**, 83 (2004).
- 47) Kawamura, H., Takahashi, H., Yoshida, N., et al., "Present Status of Beryllide R&D as Neutron Multiplier," *J. Nucl. Mater.*, **329-333**, 112 (2004).
- 48) Kawashima, H., Uehara, K., Nishino, N., et al., "A Comparison between Divertor Heat Loads in ELMY and HRS H-Modes on JFT-2M," *J. Plasma Fusion Res.*, **80**, 907 (2004).
- 49) Kimura, H., Sasaki, M., (Takahashi, K.), et al., "Thermal desorption behavior of deuterium implanted into polycrystalline diamond," *J. Nucl. Mater.*, **337-339**, 614 (2004).
- 50) Kitaichi, M., Sawamura, T., (Nishitani, T.), et al., "Propagation Characteristics of Neutrons Leaking from the Accelerator Facilities," *Radiat. Prot. Dosim.*, **110**, 731 (2004).
- 51) Kizu, K., Miura, Y. M., Tsuchiya, K., et al., "Application of react-and-wind method to D-shaped test coil using the 20 kA Nb3Al conductor developed for JT-60SC," *IEEE Trans. ASC*, **14**, 1535 (2004).
- 52) Klix, A., Ochiai, K., Nishitani, T., et al., "Direct Tritium Measurement in Lithium Titanate for Breeding Blanket Mock-up Experiments with D-T Neutrons," *Fusion Eng. Des*, **70**, 279 (2004).
- 53) Kondo, H., Fujisato, A., Yamaoka, N., et al., "High speed lithium flow experiments for IFMIF target," *J. Nucl. Mater.*, **329-333**, 208 (2004).
- 54) Kononov, S.V., Mikhailovskii, A.B., Shirokov, M.S., et al., "The role of thermal plasma density gradient in the problem of Alfvén cascades in tokamaks," *Physics of Plasmas*, **11**, 2303 (2004).
- 55) Kononov, S.V., Mikhailovskii, A.B., Shirokov, M.S., et al., "Kinetic reversed-shear Alfvén eigenmodes," *Physics of Plasmas*, **11**, 4531 (2004).
- 56) Kubo, H., Takenaga H., Sawada K., et al., "Spectroscopic study of hydrogen particle behavior in attached and detached divertor plasmas of JT-60U," *J. Nucl. Mater.*, **337-339**, 161(2005).
- 57) Kudo, Y., Sakasai, A., Hamada, K., et al., "Mechanical Tests on the Welding Part of SS316LN after Heat Treatment for Nb3Sn Superconducting Conductor," *J. Nucl. Mater.*, **329-333**, 634 (2004).
- 58) Luo, G.-N., Shu, W.M., Nakamura, H., "Ion species control in a high flux deuterium plasma beam produced by a linear plasma generator," *Rev. Sci. Instrum.*, **75**, 4374 (2004).
- 59) Maebara, S., Goniche, M., Kazaria, F., et al., "Development of cold isostatic pressing graphite module for a heat-resistant lower hybrid current drive antenna," *Rev. Sci. Instrum.*, **76**, 53501 (2005).
- 60) Masaki, K., Yagyū, J., Miyo, Y., et al., "In-Out Asymmetry Of Low-Z Impurity Deposition On The JT-60 Divertor Tiles," *J. Nucl. Mater.*, **329-333**, 845 (2004).
- 61) Matsukawa, M. and JT-60 team, "Design optimization study of the JT-60 superconducting coil modification," *IEEE Trans. ASC*, **14**, 1399 (2004).
- 62) Mikhailovskii, A.B., Kovalishen, E.A., Kononov, S.V., et al., "Revision of the theory of energetic-particle modes in tokamaks," *Doklady Physics*, **50**, 128 (2005).
- 63) Mikhailovskii, A.B., Kovalishen, E.A., Kononov, S.V., et al., "Toroidal Alfvén Eigenmodes in a Tokamak with a Population of High-Energy Large-Orbit Ions," *Plasma Phys. Rep.*, **31**, 93 (2005).
- 64) Mikhailovskii, S.V., Shirokov, M.S., Kononov, S.V., et al. "Suppression of toroidal Alfvén modes by gradient of the hot ion density in a tokamak," *Doklady Physics*, **49**, 505 (2004).
- 65) Miwa, Y., Jitsukawa, S., Yonekawa, M., "Fatigue properties of F82H irradiated at 523K to 3.8 dpa," *J. Nucl. Mater.*, **329-333**, 1098 (2004).
- 66) Miya, N., "Research Activities Using Plasma Facing Materials in JT-60U under a Cooperative Program between JAERI and Universities," *J. Nucl. Mater.*, **329-333**, 74 (2004).
- 67) Mizuno, T., Kitaide, Y., Hatayama, A., et al., "Numerical analysis of plasma spatial uniformity in negative ion sources by a fluid model," *Rev. Sci. Instrum.*, **75**, 1760 (2004).
- 68) Morishita, T., Inoue, T., Iga, T., et al., "High proton ratio plasma production in a small negative ion source," *Rev. Sci. Instrum.*, **75**, 1764 (2004).

- 69) Munakata, K., Kawamura, H., Uchida, M., "Stability of Titanium Beryllide under Water Vapor," *J. Nucl. Mater.*, **329-333**, 1357 (2004).
- 70) Nagashima, Y., Shinohara, K., Hoshino, K., et al., "Coherent Edge Fluctuation Measurements in H-mode Discharges on JFT-2M," *Plasma Phys. Control. Fusion*, **46**, A381 (2004).
- 71) Nakajima, H., Hamada, K., Takano, K., et al., "Development of low Carbon and Boron Added 22Mn-13Cr-9Ni-1Mo-0.24N Steel (JK2LB) for Jacket which Undergoes Nb3Sn Heat Treatment," *IEEE Trans. ASC*, **14**, 1145 (2004).
- 72) Nakamura, H., Riccardi, B., Loginov, N., et al., "Present status of the liquid lithium target facility in the international fusion materials irradiation facility (IFMIF)," *J. Nucl. Mater.*, **329-333**, 202 (2004).
- 73) Nakamura, H., and Nishi, M., "Experimental evaluation of tritium permeation through stainless steel tubes of heat exchanger from primary to secondary water in ITER," *J. Nucl. Mater.*, **329-333**, 183 (2004).
- 74) Nakamura, Y., Tsutsui, H., Takei, N., et al., "Current profile behavior during ramping-up phase in high bootstrap current tokamak plasmas," *J. Plasma Fusion Res. SERIES*, **6**, 196 (2004).
- 75) Nakano, T., Kubo, H., Asakura, N. et al., "Impurity Transport and its Application to Ion Temperature Measurement in JT-60U Divertor Plasmas," *J. Plasma Fusion Res.*, **80**, 500 (2004).
- 76) Neudatchin, S., Takizuka, T., Hayashi, N., et al., "Role of Low Order Rational q-values in the ITB Events in JT-60U Reverse Shear Plasmas," *Nucl. Fusion*, **44**, (2004).
- 77) Nishitani, T., Vayakis, G., Yamauchi, M., et al., "Radiation-induced Thermoelectric Sensitivity in the Mineral-insulated Cable of Magnetic Diagnostic Coils for ITER," *J. Nucl. Mater.*, **329-333**, 1461 (2004).
- 78) Nunoya, Y., Isono, T., Okuno, K., et al., "Experimental Investigation on the Effect of Transverse Electromagnetic Force on the V-T Curve of the CIC Conductor," *IEEE Trans. ASC*, **14**, 1468 (2004).
- 79) Ochiai, K., Hayashi, T., Kutsukake, C., et al., "Measurement of Deuterium and Tritium Retention on the Surface of JT-60 Divertor Tiles by Means of Nuclear Reaction Analysis," *J. Nucl. Mater.*, **329-333**, 836 (2004).
- 80) Ogawa, H., Yamauchi, Y., Tsuzuki, K., et al., "Impurity Release and Deuterium Retention Properties of a Ferritic Steel Wall in JFT-2M," *J. Nucl. Mater.*, **329-333**, 678 (2004).
- 81) Okubo, N., Wakai, E., Matsukawa, S., et al., "Heat Treatment on microstructures and DBTT of F82H steel doped with boron and nitrogen," *Materials Trans.*, **46**, 193 (2005).
- 82) Okuno, K., Shikov, A., Koizumi, N., "Superconducting Magnet System in a Fusion Reactor," *J. Nucl. Mater.*, **329-333**, 141 (2004).
- 83) Okuno, K., "Progress in the Superconducting Magnet Technology through the ITER CS Model Coil Programme," *IEEE Trans. ASC*, **14**, 1376 (2004).
- 84) Oya, Y., Hirohata, Y., Kizu, K., et al., "Analyses of Hydrogen Isotope Distributions in the Outer Target Tile Used in the W-shaped Divertor of JT-60U," *Physica Scripta*, **T108**, 57 (2004).
- 85) Oyama, N., Asakura, N., Chankin, A. V., et al., "Fast Dynamics of Type I ELMs and Transport of the ELM Pulse in JT-60U," *Nucl. Fusion*, **44**, 582 (2004).
- 86) Oyama, N., Bruskin, L. G., Takenaga, H., et al., "Density Fluctuation Measurement at Edge and Internal Transport Barriers in JT-60U," *Plasma Phys. Control. Fusion*, **46**, A355 (2004).
- 87) Riccardo, V., Barabaschi, P., Sugihara M., "Characterization of Plasma Current Quench at JET," *Plasma Phys. Control. Fusion*, **47**, 117 (2007).
- 88) Sakamoto, Y., Shirai, H., Fujita, T., et al., "Impact of Toroidal Rotation on ELM Behaviour in the H-mode on JT-60U," *Plasma Phys. Control. Fusion*, **46**, A299 (2004).
- 89) Sakamoto, Y., Suzuki, T., Ide, S., et al., "Properties of Internal Transport Barrier Formation in JT-60U," *Nucl. Fusion*, **44**, 876 (2004).
- 90) Sasaki, M., Morimoto, Y., (Takahashi, K.), et al., "Energetic deuterium and helium irradiation effects on chemical structure of CVD diamond," *J. Nucl. Mater.*, **329-333**, 899 (2004).
- 91) Sato, M., Isayama, A., Inagaki, S., Nagayama, Y., et al, "Feasibility of electron density measurement using relativistic downshift frequency effect of electron cyclotron emission in tokamak plasma," *Rev. Sci. Instrum.*, **75**, 3819 (2004).

- 92) Sato, S., Tanaka, T., Hori, J., et al., "Radioactivity of Vanadium-alloy induced by D-T Neutron Irradiation," *J. Nucl. Mater.*, **329-333**, 1648 (2004).
- 93) Shimada, M., Costley, A.E., Federici, G., et al., "Overview of Goals and Performance of ITER and Strategy for Plasma-wall Interaction Investigation," *J. Nucl. Mater.*, **337-339**, 808 (2005).
- 94) Shimizu, T., Sakane, H., (Nishitani, T.), et al., "Measurements of Activation Cross Sections of (n,p) and (n, α) Reactions with d-D neutrons in the Energy Range of 2.1-3.1 MeV," *Annals of Nucl. Energy*, **31**, 975 (2004).
- 95) Shinohara, K., Takechi, M., Ishikawa, M., et al., "Energetic Particle Physics in JT-60U and JFT-2M," *Plasma Phys. Control. Fusion*, **46**, S31 (2004).
- 96) Shu, W.M., Matsuyama, M., Suzuki, T., et al., "Characteristics of a promising tritium process monitor detecting bremsstrahlung X-rays," *Nucl. Instru. Meth. Phys. Res. A*, **521**, 423 (2004).
- 97) Song, Y., and Nishio, S., "Optimization study on the normal conduction center post for the low aspect ratio tokamak reactor," *Fusion Eng. Des.*, **72**, 345 (2005).
- 98) Sugie, T., Kasai, S., Taniguchi, T., et al., "Irradiation test of Mo- and W-mirrors for ITER by low energy deuterium ions," *J. Nucl. Mater.*, **329-333**, 1481 (2004).
- 99) Sugihara, M., Lukash, V., Khayrutdinov, R., et al., "Edge Safety Factor at the Onset of Plasma Disruption during VDEs in JT-60U," *Plasma Phys. Control. Fusion*, **46**, 1581 (2004).
- 100) Sugimoto, M., Takeuchi, H., "Low activation materials applicable to the IFMIF accelerator," *J. Nucl. Mater.*, **329-333**, 198 (2004).
- 101) Sugiyama, K., Tanabe, T., Masaki, K., et al., "Tritium Retention in Plasma-facing Components Following D-D Operation," *J. Nucl. Mater.*, **329-333**, 874 (2004).
- 102) Suzuki, T., Ide, S., Hamamatsu, K., et al., "Heating and Current Drive by Electron Cyclotron Waves in JT-60U," *Nucl. Fusion*, **44**, 699 (2004).
- 103) Suzuki, T., Ide, S., Hamamatsu, K., et al., "Toroidal Electric Field Effect and Non-Linear Effect on Electron Cyclotron Current Drive in the JT-60U," *J. Plasma Fusion Res.*, **80**, 51 (2004).
- 104) Suzuki, T., Oikawa, T., Isayama, A., et al., "Direct Evaluation of Spatial-Temporal Change in Current Density Profile Applied to a Discharge with Neo-Classical Tearing Mode," *J. Plasma Fusion Res.*, **80**, 362 (2004).
- 105) Takahashi, K., Imai, T., Kobayashi, N., et al., "Design performance of front steering-type electron cyclotron launcher for ITER," *Fusion Sci. Technol.*, **47**, (2005).
- 106) Takahashi, Y., Yoshida, K., Mitchell, N., et al., "Performance of Joints in the CS Model Coil and Application to the Full Size ITER Coils," *IEEE Trans. Appl. Supercond.*, **14**, 1410 (2004).
- 107) Takeda, N., Nakahira, M., Tada, E., Fujita, S., Fujita, T., "Status on Seismic Design and Verification for ITER in Japan," *J. Japan Association for Earthquake Eng.*, **4**, 298 (2004).
- 108) Takeda, N., Ohmori, J., Nakahira, M., Shibamura, K., "Design and Structural Analysis of Support Structure for ITER Vacuum Vessel," *J. Nucl. Sci. Technol.*, **41**, 1280 (2004).
- 109) Takeda, N., Shibamura, K., "Dynamic Analysis of ITER Tokamak Using Simplified Model for Support Structure," *J. Plasma Fusion Res.*, **80**, 988 (2004).
- 110) Takei, N., Nakamura, Y., Kawano, Y., et al., "Axisymmetric MHD simulation of ITB crash and following disruption dynamics of tokamak plasmas with high bootstrap current," *J. Plasma Fusion Res. SERIES*, **6**, 554-557 (2004).
- 111) Takei, N., Nakamura, Y., Tsutsui, H., et al., "Numerical simulation on current spike behavior of JT-60U disruptive plasmas," *Plasma Phys. Control. Fusion*, **46**, 1815-1830 (2004).
- 112) Tamai, H., Ishida, S., Kurita, G., et al., "Steady-state operation scenarios with a central current hole for JT-60SC," *Fusion Sci. Technol.*, **45**, 521 (2004).
- 113) Tamai, H., Kurita, G., Matsukawa, M., et al., "Advanced control scenario of high-performance steady-state operation for JT-60 superconducting tokamak," *Plasma Sci. Technol.*, **6**, 2281 (2004).
- 114) Tanaka, T., Suzuki, A., (Nishitani, T.), et al., "Radiation Induced Conductivity of Ceramic Coating Materials under 14 MeV Neutron Irradiation," *J. Nucl. Mater.*, **329-333**, 1434 (2004).

- 115) Tanifuji, T., Yamaki, D., Jitsukawa, S., "Tritium Release from Neutron-Irradiated Li₂O Sintered Pellets: Isothermal Annealing of Tritium Traps," *J. Nucl. Mater.*, **329-333**, 1266 (2004).
- 116) Tanigawa, H., Hashimoto, N., Sakasegawa, H., et al., "Microstructure property analysis of HFIR irradiated reduced-activation ferritic/martensitic steels," *J. Nucl. Mater.*, **329-333**, 283 (2004).
- 117) Tanigawa, H., Sakasegawa, H., Klueh, R., "Irradiation effects on precipitation in reduced-activation ferritic/martensitic steels," *Materials Trans.*, **46**, 469 (2005).
- 118) Toh, K., Shikama, T., (Yamauchi, M.), et al., "Optical Characteristics of Aluminum Coated Fused Silica Core Fibers under 14MeV Fusion Neutrons Irradiation," *J. Nucl. Mater.*, **329-333**, 1495 (2004).
- 119) Tsuchiya, K., Hoshino, T., Kawamura, H., et al., "Fabrication and Characterization of 6Li-enriched Li₂TiO₃ Pebbles by Wet Process," *J. Ceram. Soc. Japan, Supplement 112-1, PacRim5 Special Issue*, **112**, S183 (2004).
- 120) Tsuchiya, K., Kikukawa, A., Hoshino, T., et al., "In-Situ Tritium Recovery Behavior from Li₂TiO₃ Pebble Bed under Neutron Pulse Operation," *J. Nucl. Mater.*, **329-333**, 1248 (2004).
- 121) Tsuchiya, K., Kizu, K., Miura, Y. M., et al., "Design and stress analysis of support structure of toroidal field coil for the JT-60SC," *IEEE Trans. ASC*, **14**, 1427 (2004).
- 122) Tsuzuki, K., Shinohara, K., Kamiya, K., et al., "Investigation of Compatibility of Low Activation Ferritic Steel with High Performance Plasma by Full Covering of Inside Vacuum Vessel Wall on JFT-2M," *J. Nucl. Mater.*, **329-333**, 721 (2004).
- 123) Uchida, M., Uda, M., Iwadachi, T., et al., "Elemental Development of Beryllide Electrode for Pebble Production by Rotating Electrode Method," *J. Nucl. Mater.*, **329-333**, 1342 (2004).
- 124) Urano, H., Kamada, Y., Takizuka, et al., "Pedestal Characteristics of H-Mode Plasmas in JT-60U and ASDEX Upgrade," *J. Plasma Fusion Res.*, **81**, 280 (2005).
- 125) Vayakis, G., Sugie, T., (Nishitani, T.), et al., "Radiation-Induced Thermoelectric Sensitivity (RITES) in ITER Prototype Magnetic Sensors," *Rev. Sci. Instrum.*, **75**, 4324 (2004).
- 126) Verzilov, Y., Ochiai, K., Klix, A., et al., "Non-destructive Analysis of Impurities in Beryllium for Tritium Breeding Ratio Evaluation," *J. Nucl. Mater.*, **329-333**, 1337 (2004).
- 127) Yamada, H., Kawamura, H., Tsuchiya, K., et al., "The Neutron Irradiation Effect on Mechanical Properties of HIP Joint Material," *J. Nucl. Mater.*, **335**, 33 (2004).
- 128) Yamada, H., Uchida, M., Uda, M., et al., "Heat Load Test of Beryllium and CuCrZr Joints," *J. Nucl. Mater.*, **329-333**, 885 (2004).
- 129) Yamaki, D., Nakazawa, T., Tanifuji, T., et al., "Observation of the Microstructural Changes in Lithium Titanate by Multi-Ion Irradiation," *J. Nucl. Mater.*, **329-333**, 1279 (2004).
- 130) Yoshida, H., Nakatsuka, M., Hatae, T., et al., "Two-Beam-Combined 7.4 J, 50 Hz Q-switch Pulsed YAG Laser System Based on SBS Phase Conjugation Mirror for Plasma Diagnostics," *Jpn. J. Appl. Phys.*, **43**, L1038 (2004).
- 131) Yoshida, H., Taniguchi, M., Yokoyama, K., et al., "Deuterium retention in Carbon dust and carbon-tungsten mixed dust prepared by deuterium arc discharge," *J. Nucl. Mater.*, **329-333**, 790 (2004).
- 132) Yoshida, H., Yamauchi, Y., Hirohata, Y., et al., "Morphology and Hydrogen Retention of Carbon Dust Produced by Hydrogen Discharge in JT-60," *J. Vac. Soc. Japan*, **47**, 239 (2004).
- 133) Yoshida, H., Taniguchi, M., Yokoyama, et al., "Hydrogen retention of carbon dust prepared by arc discharge and electron beam irradiation," *Fusion Eng. Des.*, **70**, 201 (2004).

A.1.3 List of papers published in conference proceedings

- 1) Alvani, C., Tsuchiya, K., Contini, V., et al., "Kinetics of Li Depleted Li_2TiO_3 Reaction with H_2 Added to Ar Purge Gas," 23rd Symposium on Fusion Technology (2004), to be published in Fusion Eng. Des.
- 2) Bakhtiari, M., Kawano, Y., Tamai, H., et al., "Disruption Mitigation Experiments in the JT-60U Tokamak," Proc. 20th. IAEA Fusion Energy Conference 2004, EX/10-6Rb (2004).
- 3) Bakhtiari, M., Kramer, G. J., Tamai, H., et al. "Bremsstrahlung Radiation as a New Energy Limit for Runaway Electrons in Tokamaks," Proc. 46th Annual Meeting of the Division of Plasma Physics of APS (2004).
- 4) Belo, P., Buratti, P., (Isayama, A.) , et al., "Observation and Implication of MHD Modes for the Hybrid Scenario in JET," 31st European Physical Society Conference on Plasma Physics, 28th June to 2nd July 2004, Imperial College London, P1-170 (2004).
- 5) Cristescu I.R., Travis J., Kobayashi, K., et al., "Simulation of tritium spreading in controlled areas after a tritium release," Proc. 7th Int. Conf. on Tritium Science and Technology (2004), to be published in Fusion Science Technology.
- 6) Fischer, U., Batistoni, P., (Nishitani, T.), et al., "Nuclear Data for Fusion Energy Technologies: Requests Status and Development Needs," Proc. Int. Conf. Nuclear Data for Science and Technology 2004, 1478 (AIP, New York, 2005).
- 7) Fujita, T., Suzuki, T., Oikawa, T., et al., "Stiffness of Central Current and Temperature Profiles in JT-60U Current Hole Plasmas," Proc. 20th IAEA Fusion Energy Conf., EX/P4-3 (CD-ROM) (2004).
- 8) Fujita, T., and JT-60 team, "Steady state operation research in JT-60U with extended pulse length," Proc. 4th IAEA Technical Meeting on Steady State Operation on Magnetic Fusion Devices and MHD of Advanced Scenarios (Ahmadabad, India, 2004).
- 9) Furuya, K., Wakai, E., Ando, M., et al., "Effects of irradiation on mechanical properties of HIP-bonded F82H steel," Proc. 23rd Symp. on Fusion Technology (2004), to be published in Fusion Eng. Des.
- 10) Hanada, M., Seki, T., Takado, N., et al., "Experimental study on spatial uniformity of H^- ion beam in a large negative ion source," Proc. 23rd Symp. on Fusion Technology (2004).
- 11) Hanada, M., Watanabe, K., Inoue, T., et al., "Energy spectrum of atoms from negative ions in a multi-ampere negative ion accelerator," Proc 10th International Symposium on Production and Neutralization of Negative Ions and Beams (2004).
- 12) Hayashi, H., Takizuka, T., Ozeki, T., "Profile Formation and Sustainment of Autonomous Tokamak Plasma with Current Hole Configuration," 20th IAEA FEC 2004 (Vilamoura, Portugal), accepted in Nucl. Fusion.
- 13) Hayashi, T., Suzuki, T., Yamada, M., et al., "Tritium Accounting Stability of ZrCo Bed with "In-bed" Gas Flowing Calorimetry," Proc. 7th Int. Conf. on Tritium Science and Technology (2004), to be published in Fusion Science Technology.
- 14) Hegeman, J.B.J., van der Laan, J.G., Kawamura, H., et al, "Status of the HFT Petten High Dose Irradiation of Beryllium for Blanket Application," 23rd Symposium on Fusion Technology (2004), to be published in Fusion Eng. Des..
- 15) Hirohata, Y., Shibahara, T., Gotoh, Y., et al., "Hydrogen Retention in Divertor Tiles Used in JT-60 ior H Discharge Period, " The 16th Int. Conf. on Plasma-Surface Interactions in Controlled Fusion Devices (PSI-16), Portland Maine, US, May 24-28, (2004).
- 16) Hirohata, Y., Tanabe, T., Arai, T., et al., "Retention And Depth Profile of Hydrogen Isotopes in Divertor Tiles Used in JT-60U," 7th Int. Conf. Tritium Science and Technology (Tritium Conf. 2004) Sept.,12-17, Barden-Barden, Germany , (2004).
- 17) Hoshino, T., Tsuchiya, K., Hayashi, K., et al., "Crystal Structure of Li_2TiO_3 with Some Different Oxide Additives," 23rd Symposium on Fusion Technology (2004), to be published in Fusion Eng. Des..
- 18) Ichimasa, M., Awagakubo, S., Takahashi, M., et al., "Tritium elimination system using tritium gas oxidizing bacteria," Proc. 7th Int. Conf. on Tritium Science and Technology (2004), to be published in Fusion Science Technology.
- 19) Ida, M., Nakamura, H., Matsuhira, K., et al., "Thermal and Thermal-stress Analyses of IFMIF Liquid Lithium Target Assembly," Proc. 23rd Symp. on Fusion Technology (2004), to be published in Fusion Eng. Des.

- 20) Ide, S., and the JT-60 team, "Overview of JT-60U Progress towards Steady-state Advanced Tokamak," Proc. 20th. IAEA Fusion Energy Conference 2004, OV-1/1 (2004).
- 21) Ido, T., Miura, Y., Hoshino, K., et al., "Electrostatic Fluctuation and Fluctuation-Induced Particle Flux during Formation of the Edge Transport Barrier in the JFT-2M Tokamak," Proc. 20th IAEA Fusion Energy Conference, IAEA-CN-116/EX/4-6Rb (2004), to be published on CD-ROM (IAEA, Vienna).
- 22) Inoue, T., Taniguchi, M., Morishita, T., et al., "R&D on a high energy accelerator and a large negative ion source for ITER," Proc. 20th IAEA Fusion Energy Conference, IAEA-FT/1-2Ra (2004), to appear in Nucl. Fusion, **45**, (2005).
- 23) Ishikawa M., Shinohara, K., et al., "Energetic Ion Transport Induced by Alfvén Eigenmodes by Negative-Ion Based Neutral Beam in the JT-60U Weak Shear and Reversed Shear Plasmas", Proc. 20th. IAEA Fusion Energy Conference 2004, EX/5-2Rb (2004).
- 24) Isobe, K., Nakamura, H., Kaminaga, A., et al., "Tritium release behavior from JT-60U vacuum vessel during air purge phase and wall conditioning phase," Proc. 7th Int. Conf. on Tritium Science and Technology (2004), to be published in Fusion Science Technology.
- 25) Itami, K., Sugie and T., Vayakis, G., "Study of Multiplexing Thermography for ITER Divertor Targets," Proc. 30th EPS Conf. on Contr. Fusion and Plasma Phys., 27A, P-4.62 (CD-ROM) (2003).
- 26) Iwai, Y., Hayashi, T., Kobayashi, K., et al., "Case study on unexpected tritium release happened in a ventilated room of fusion reactor," Proc. 7th Int. Conf. on Tritium Science and Technology (2004), to be published in Fusion Science Technology.
- 27) Iwai, Y., Yamanishi, T., Hayashi, T., et al., "Study on tritium removal performance by gas separation membrane with reflux flow for tritium removal system of fusion reactor," Proc. 7th Int. Conf. on Tritium Science and Technology (2004), to be published in Fusion Science Technology.
- 28) Joffrin, E., Becoulet, A., (Isayama, A.) , et al., "The "Hybrid" Scenario in JET: Towards its Validation for ITER," Proc. 20th. IAEA Fusion Energy Conference 2004, EX/4-2 (2004).
- 29) Kamiya, K., Kawashima, H., Ido, T., et al., "Studies of HRS H-mode Plasma in the JFT-2M Tokamak," Proc. 20th IAEA Fusion Energy Conference, IAEA-CN-116/EX/4-6Ra (2004), to be published on CD-ROM (IAEA, Vienna).
- 30) Kashiwa, K., Saigusa, M., Takahashi, K., et al., "Study of ohmic loss of high power polarizer at 170GHz for ITER," Proc. 2004 Int. symp. Microwave Sci. (2004) 527.
- 31) Kasugai, A., Sakamoto, K., Minami, R., al., "Performance of 170GHz high-power gyrotron for CW operation," 20th IAEA Fusion Energy Conf., Vilamoura, FT 1-1Rb, (2004).
- 32) Katayama, K., Takeishia, T., Miya, N., et al., "Release Behavior of Hydrogen Isotopes from JT-60U Graphite Tiles, " 7th Int. Conf. Tritium Science and Technology (Tritium Conf. 2004) Sept.,12-17, Barden-Barden, Germany , 2004.
- 33) Kawamura, Y., Iwai, Y., Nakamura, H., et al., "Tritium recovery from solid breeder blanket by water vapor addition to helium sweep gas", Proc. 7th Int. Conf. on Tritium Science and Technology (2004), to be published in Fusion Science Technology.
- 34) Kawano, Y., Kondoh, T., and Hatae, T., "Generation and Diagnostics of Relativistic Electron Beam in a Torus Plasma," Proc. Plasma Science Symposium 2005 / The 22nd Symposium on Plasma Processing, January 26th-28th, Will Aichi, Nagoya Japan, 93 (2005).
- 35) Kizu, K., Miura, Y.M., Sakasai, A., "Development of Advanced Superconducting Coil Technologies for the National Centralized Tokamak," Proc. 20th IAEA Fusion Energy Conf., FT/P1-6 (CD-ROM)(2004)
- 36) Klix, A., Verzilov, Y., Nishitani, T., et al., "Tritium Breeding Experiments with Blanket Mock-ups Containing ⁶Li-enriched Lithium Titanate and Beryllium Irradiated with DT Neutrons," 23rd Symposium on Fusion Technology (2004), to be published in Fusion Eng. Des.
- 37) Kobayashi, K., Terada, O., Hayashi, T., et al., "The oxidation performance test of detritiation system under existence of CO and CO₂," Proc. 7th Int. Conf. on Tritium Science and Technology (2004), to be published in Fusion Science Technology.
- 38) Koizumi, N., Ando, T., Matsui, K., et al., "Development of a Nb₃Al Conductor for Toroidal Field Coil," Proc. 20th IEEE/NPSS SOFE, 419 (2004).

- 39) Koizumi, N., Takeuchi, T., Okuno, K., "Development of Advanced Nb₃Al Superconductors for a Fusion Demo Plant," Proc. 20th IAEA Fusion Energy Conference (2004).
- 40) Kokubo, S., Okamoto, M., Kikuchi, et al., "Evaluation of Current Quench Decay Time in Tokamaks and Investigation of Its Behaviours," 31st EPS Conference on Plasma Phys., London, 28 June - 2 July 2004 ECA Vol.28G, P-2.137 (2004).
- 41) Kondo, H., Fujisato, A., N. Yamaoka, et al., "Surface Wave on High Speed Liquid Lithium Flow for IFMIF," 23rd Symp. on Fusion Technology (2004), to be published in Fusion Eng. Des.
- 42) Konovalov, S. V., Mikhailovskii, A., B., Ozeki, T., et al. "Influence of Anomalous Transport Phenomena on Onset of Neoclassical Tearing Modes in Tokamaks," 20th IAEA FEC 2004 (Vilamoura, Portugal), accepted in Nucl. Fusion.
- 43) Krasilnikov, A.V., Sasao, M., (Nishitani, T.), et al., Integral Benchmark Experiments of the Japanese Evaluated Nuclear Data Library(JENDL)-3.3 for the Fusion Reactor Design," 20th IAEA Fusion Energy Conf. IT/P3-23 (2004), to be published on CD-ROM (Vienna).
- 44) Kubo, H. and the JT-60 Team, "Study of particle behavior in JT-60U," 2nd International Symposium on Sustainable Energy System, (Kyoto, 2004), Organized by Executive Committee of Kyoto University 21COE Program "Establishment of COE on Sustainable Energy System," Kyoto Univ., p34 (2004).
- 45) Kubo, H., "Production and Transport of Carbon Impurities in Fusion Plasma Devices," Proc. Plasma Science Symposium 2005 / The 22nd Symposium on Plasma Processing, January 26th-28th, Will Aichi, Nagoya Japan, p209 (2005).
- 46) Kurihara, K., Kawamata, Y., Sueoka, M., et al., "The basic methods for understanding of plasma equilibrium toward advance control," Proceedings of symposium on Fusion Technology (SOFT), (2004), to be published in Fusion Eng. Des.
- 47) Kurita, G., Bialek, J., Tsuda, T., et al., "Critical beta analyses with ferromagnetic and plasma rotation effects and wall geometry for a high beta steady state tokamak," Proc. 20th IAEA Fusion Energy Conf. (Vilamoura, Portugal, 2004).
- 48) Loring, M., Moriyama, S., Kasugai, A., et al., "Protection and Control of Accelerator Microwave Sources using a High Power IGBT Switch," Conf. Record of 26th Inter. Power Modulator Symp. & High-Voltage WorkShop, 271 (2004)
- 49) Maebara, S., Moriyama, S., Saigusa, M., et al., "Development of RF-input coupler with a multi-loop antenna for RFQ linac in IFMIF project," 23rd Symp. on Fusion Technology (2004), to be published in Fusion Eng. Des.
- 50) Maebara, S., Moriyama, S., Saigusa, M., et al., "Power-balance control by slug tuner for the 175MHz RFQ linac in IFMIF project," 16th ANS Topical Meeting on Technology of Fusion Energy (2004).
- 51) Mancini, M. R., Contini, V., Tsuchiya, K. et al., "Thermochemistry of Li-Tatanates Ceramics in Reducing Environments," 23rd Symposium on Fusion Technology (2004), to be published in Fusion Eng. Des..
- 52) Masaki, K., Sugiyama, K., Hayashi, T., et al., "Retention Characteristics of Hydrogen Isotopes in JT-60U, " The 16th Int. Conf. on Plasma-Surface Interactions in Controlled Fusion Devices (PSI-16), Portland Maine, US, May 24-28, 2004.
- 53) Matsuhiro, K., Nakamura, H., Hayashi, T., et al., "Evaluation of Tritium Permeation from Lithium Loop of IFMIF Target System," 7th Int. Conf. on Tritium Science and Technology (2004), to be published in Fusion Sci. Technol.
- 54) Murata, T., Kondo, K., S. Takagi, et al., "Development of Charged-Particle Emission DDX Spectrometer with SSD Telescope and Pencil-Beam DT Neutron Source," Proc. Int. Conf. Nuclear Data for Science and Technology 2004, 769 (AIP, New York, 2005).
- 55) Nagasaki, K., Isayama, A., Hayashi, N. et al., "Stabilization of Neoclassical Tearing Mode by Electron Cyclotron Current Drive and Its Evolution Simulation on JT-60U Tokamak," Proc. 20th. IAEA Fusion Energy Conference 2004, EX/7-4 (2004).
- 56) Nagata, M., Ogawa, H., Yatsu, S., et al., "Investigation of the Dynamics of Accelerated Compact Toroid Injected into the JFT-2M Tokamak Plasmas," Proc. 20th IAEA Fusion Energy Conference, IAEA-CN-116/EX/P2-15 (2004), to be published in Nucl. Fusion.
- 57) Nakamura, H., Hayashi, T., Kobayashi, K., et al., "Evaluation of tritium behavior in the epoxy painted concrete wall of ITER hot cell," Proc. 7th Int. Conf. on Tritium Science and Technology (2004), to be published in Fusion Science Technology.

- 58) Nakamura, H., Takemura, M., Yamauchi, M., et al., "Accessibility Evaluation of the IFMIF Liquid Lithium Loop Considering Activated Erosion / Corrosion Materials Deposition," 23rd Symp. on Fusion Technology (2004), to be published in Fusion Eng. Des.
- 59) Nakamura, Y., Tobita, K., Jardin, S.C., et al., "Bootstrap Current Effects on Stable Non-Inductive Current Buildup in Low Aspect Ratio Tokamaks," P-2.140, 31st EPS Conference on Controlled Fusion and Plasma Physics, London, UK, June 28-July 2, 2004
- 60) Nakano, T., Asakura, N., Takenaga, H., et al., "Impact of Nearly-Saturated Divertor Plates on Particle Control in Long and High-Power-Heated Discharges in JT-60U," Proc. 20th. IAEA Fusion Energy Conference 2004, EX/10-3 (2004).
- 61) Nakao, M., Hori, J., Ochiai, K., et al., "Measurement of Deuteron-Induced Activation Cross Sections for IFMIF Accelerator Structural Materials," Proc. Int. Conf. Nuclear Data for Science and Technology 2004, 1489 (AIP, New York, 2005).
- 62) Nishio, S., Tobita, K., Tokimatsu, et al., "Technological and Environmental Prospects of Low Aspect Ratio Tokamak Reactor VECTOR," Proc. 20th IAEA Fusion Energy Conf. (Vilamoura) FT/P7-35 4).
- 63) Nishitani, T., Ochiai, K., Maekawa, F., et al., "Integral Benchmark Experiments of the Japanese Evaluated Nuclear Data Library(JENDL)-3.3 for the Fusion Reactor Design," 20th IAEA Fusion Energy Conf. FT/P1-13 (2004), to be published in Nucl. Fusion.
- 64) Nishitani, T., Sugie, T., Morishita, N., et al., "Temperature Dependence of the Transmission Loss in KU-1 and KS-4V Quartz Glasses for the ITER Diagnostic Window," Proc. 23rd Symp. on Fusion Technology (2004), to be published in Fusion Eng. Des.
- 65) O'hira, S., Luo, G., Nakamura, H., et al., "New conceptual design of a test module assembly for tritium permeation experiments," Proc. 7th Int. Conf. on Tritium Science and Technology, G27-P1, 161 (2004).
- 66) Ochiai, K., Kondo, K., Murata, I., et al., "Measurement of Energetic Charged Particles Produced in Fusion Materials with 14MeV Neutron Irradiation," 23rd Symposium on Fusion Technology (2004), to be published in Fusion Eng. Des.
- 67) Ochiai, K., Verzilov, Y., Nishitani, T., et al., "International Benchmark Activity of Tritium Production Measurement for Blanket Neutronics," 7th Int. Conf. Tritium Science & Technology (2004), to be published in Fusion Sci. Technol.
- 68) Oda, Y., Komurasaki, K., Takahashi, K., et al., "Plasma generation using high power microwave and application of space propulsion," Proc. Technical meeting on Nucl. Energy IEE Japan (2004) 19, (in Japanese).
- 69) Oda, Y., Nakagawa, T., (Takahashi, K.), et al., "Plasma expansion and shock wave propagation in a microwave beaming thruster," Proc. 24th Int. Symp. Space Tech. and Sci. 228 (2004).
- 70) Oda, Y., Ushio, M., Komurasaki, K., Takahashi, K., et al., "A multi pulse flight experiment of a microwave beaming thruster," Proc. 3rd Int. Symp. Beamed Energy Propulsion (2004).
- 71) Oikawa, T., Suzuki, T., Isayama, A., et al., "Observation of Current Profile Evolution Associated with Magnetic Island Formation in Tearing Mode Discharges on JT-60U," Proc. 20th IAEA Fusion Energy Conf., EX/P5-15 (CD-ROM) (2004).
- 72) Olivers, R., Oda, T., Oya, Y., (Tsuchiya, K.) et al., "Hydrogen Isotopes Behavior on Li_2TiO_3 under Varied Surface Condition," 23rd Symposium on Fusion Technology (2004), to be published in Fusion Eng. Des..
- 73) Oya, Y., Hirohata, Y., Arai, T., et al., "Hydrogen Isotope Distribution And Retention in The Inner Divertor Tile of JT-60U," Proc. 23rd Symp. on Fusion Technology (SOFT 2004) Venice, Italy, Sept. 20-24, 2004.
- 74) Oyama, N., Sakamoto, Y., Oikawa, T., et al., "Energy loss for grassy ELMs and effects of plasma rotation on the ELM characteristics in JT-60U," Proc. 20th IAEA Fusion Energy Conf., EX/2-1 (CD-ROM) (2004).
- 75) Oyama, N., Sakamoto, Y., Takechi, M., et al., "Energy Loss for Grassy ELMs and Effects of Plasma Rotation on the ELM Characteristics in JT-60U," Proc. 20th. IAEA Fusion Energy Conference 2004, EX/2-1 (2004).
- 76) Polevoi, A.R., Shimada, M., Sugihara, M., et al., "Requirements for Pellet Injection in ITER Scenarios with Enhanced Particle Confinement," Proc. 20th IAEA Fusion Energy Conf., IT/P3-28 (CD-ROM) (2004).
- 77) Saibene, G., Oyama, N., Andrew, A., et al., "Dimensionless Identity Experiments in JT-60U and JET," Proc. 20th. IAEA Fusion Energy Conference 2004, IT/1-2 (2004).

- 78) Sakamoto, K., Kasugai, A., Minami, R., et al., "Development of High Power 170GHz Gyrotron for ITER," Proc. 29th Int. conf. IR & MM Waves (2004).
- 79) Sato, M., Isayama, A., Inagaki, S., Nagayama, Y., et al., "Relativistic downshift frequency effects on electron cyclotron emission measurements of electron density in tokamak and electron temperature in LHD," 13th Joint Workshop on ECE and ECRH, Nizhny Novgorod, Russia, (2004).
- 80) Sato, S., Iida, H., Yamauchi, et al., "Shielding Design of the ITER NBI Duct for Nuclear and Bremsstrahlung Radiation," 10th Int. Conf. on Radiation Shielding (2004), to be published in Radiat. Prot. Dosim.
- 81) Sato, S., Nakao, M., Verzilov, Y., et al., "Experimental Studies on Tungsten-armor Impact on Nuclear Responses of Solid Breeding Blanket," 20th IAEA Fusion Energy Conf. FT/P1-22 (2004), to be published on CD-ROM (Vienna).
- 82) Sato, S., Verzilov, Y., Nakao, M., et al., "Neutronics Experiments using Small Partial Mockup of the ITER Test Blanket Module with Solid Breeder," 16th ANS Topical Meeting on the Technology of Fusion Energy (2004), to be published in Fusion Sci. Technol.
- 83) Sharpe, J.P., Humrickhouse, P.W., Masaki, K., et al., "Characterization of Dust Collected from NSTX and JT-60U," The 16th Int. Conf. on Plasma-Surface Interactions in Controlled Fusion Devices (PSI-16), Portland Maine, US, May 24-28, 2004.
- 84) Shibahara, T., Hirohata, Y., Arai, T., et al., "Hydrogen Isotopes Retentions in Divertor Tiles Used in JT-60," 16th International Vacuum Congress (IVC-16), Venice, Italy, June 28- July 2, 2004.
- 85) Shikama, T., Toh, K., (Nishitani, T.), et al., "14MeV Neutron and Ionizing Radiation Detection System utilizing Radioluminescence and Optical Fiber," 23rd Symposium on Fusion Technology (2004), to be published in Fusion Eng. Des.
- 86) Shikama, T., Toh, K., (Nishitani, T.), et al., "Development of Optical Diagnostics System for Burning Plasma Machine," 20th IAEA Fusion Energy Conf. FT/P1-24 (2004), to be published on CD-ROM (Vienna).
- 87) Shimada, K., Ohmori, Y., Furukawa, H., et al., "A new intelligent coil current control system combined with a synchronous generator and a diode rectifier," Proceedings of International Conference on Electrical Engineering (ICEE), Vol.2, 777 (2004)
- 88) Shimada, M., Campbell, D., Stambaugh, R., et al., "Progress in Physics Basis and its Impact on ITER," Proc. 20th IAEA Fusion Energy Conf., IT/1-1 (2004).
- 89) Shimizu, K., Arakita, I., (Nishitani, T.), et al., "Measurement of Activation Cross Sections Producing Short-Lived Nuclei with Pulsed Neutron Beam," Proc. Int. Conf. Nuclear Data for Science and Technology 2004, 992 (AIP, New York, 2005).
- 90) Shimomura, Y., "ITER towards the Construction," Proc. 20th IAEA Fusion Energy Conf., FPM/3 (CD-ROM) (2004).
- 91) Shu, W.M., O'hira, S., Suzuki, T., et al., "Radiochemical reactions between tritium molecule and carbon dioxide," Proc. 7th Int. Conf. on Tritium Science and Technology (2004), to be published in Fusion Science Technology.
- 92) Sugihara, M., Lukash, V., Kawano, Y., et al., "Analysis of Disruption Scenarios and Their Possible Mitigation in ITER," Proc. 20th IAEA Fusion Energy Conf., IT/P3-29 (CD-ROM) (2004).
- 93) Sugimoto, M., and IFMIF International Team, "Recent Progress of Design & Development in IFMIF Activities," 16th ANS Topical Meeting on Technology of Fusion Energy (2004).
- 94) Suzuki, T., Ide, S., Hamamatsu, K., et al., "Investigation of EC Current Drive in a High Electron Temperature Plasma in JT-60U," Proc. 13th Joint Workshop on Electron Cyclotron Emission and Electron Cyclotron Heating (2004).
- 95) Suzuki, T., Isayama, A., Oikawa, T., et al., "Steady State High beta-N Discharges and Real-Time Control of Current Profile in JT-60U," Proc. 20th IAEA Fusion Energy Conf., EX/1-3 (CD-ROM) (2004).
- 96) Tajima Y., et al., "PFCs Recycling System by the Continuous Gas Chromatography," Proc. 2004 IEEE Int. Symp. on Semiconductor Manufacturing, Tokyo, 401 (2004).
- 97) Takahashi, K., Illy, S., Heidinger, R., et al., "Recent results of ECH diamond window development at JAERI," Proc. 29th Int. conf. IR & MM Waves (2004).
- 98) Takahashi, K., Moeller, C.P., Sakamoto, K., et al., "High power transmission performance of millimeter wave remote steering launcher," Proc. 29th Int. conf. IR & MM Waves (2004).

- 99) Takechi, M., Fujita, T., Ishii, Y., et al., "MHD Instabilities Leading to Disruption in JT-60U Reversed Shear Plasmas," Proc. 20th. IAEA Fusion Energy Conference 2004, EX/P2-32 (2004).
- 100) Takeishi, T., Katayama, K., Miya, N., et al., "Recovery of Retained Tritium From Graphite Tile of JT-60U, " 7th Int. Conf. Tritium Science and Technology (Tritium Conf. 2004) Sept., 12-17, Barden-Barden, Germany , 2004.
- 101) Takenaga, H., Asakura, N., Kubo, H., et al., "Compatibility of Advanced Tokamak Plasma with High Density and High Radiation Loss Operation in JT-60U," 20th IAEA Fusion Energy Conference 2004.
- 102) Takenaga, H., Miura, Y., Kubo, H., et al., "Burn Control Study Using Burning Plasma Simulation Experiments in JT-60U," Proc. plasma science symp. 2005/the 22nd symp. on plasma processing (2005).
- 103) Takenaga, H., Nakano, T., Asakura, N., et al., "Effects of Long Time Scale Variation of Plasma Wall Interactions on Particle Control in JT-60U," 4th IAEA Technical Meeting on Steady State Operation of Magnetic Fusion Devices and MHD of Advanced Scenarios, (2005).
- 104) Tanabe, T., Gotoh, Y., Masaki, K., et al., "Retention of Hydrogen Isotopes (H, D, T) and Carbon Erosion/Deposition in JT-60U, "Proc. 20th IAEA Fusion Energy Conf., Vilamoura, Portugal, 2004, to be published on CD-ROM(IAEA Vienna).
- 105) Tanabe, T., Sugiyama, K., Miya, N., et al., "Tritium Retention And Carbon Deposition On Plasma Facing Materials, " The 16th Int. Conf. on Plasma-Surface Interactions in Controlled Fusion Devices (PSI-16), Portland Maine, US, May 24-28, 2004.
- 106) Taniguchi, M., Inoue, T., Kashiwagi, M., et al., "Acceleration of 100A/m² negative hydrogen ion beams in a 1 MeV vacuum insulated beam source," Proc. 10th Int. Symp. on Production and Neutralization of Negative Ions and Beams, Kiev, AIP conference proceedings, **763**, 168 (2005).
- 107) Tobita, K., Konishi, S., Nishio, S., "Radioactive Waste from a D-3He Fusion Reactor", in Proc. 24th Sym. of Fusion Technology, Venice, Italy (2004).
- 108) Tsuchiya, K., Kawamura, H., Casadio, S., et al., "Effects of Gelation and Sintering Conditions on Granulation of Li₂TiO₃ Pebbles from Li-Ti Complex Solution," 23rd Symposium on Fusion Technology (2004), to be published in Fusion Eng. Des..
- 109) Tsuzuki, K., Kamiya, K., Shinohara, K., et al., "Compatibility of Reduced Activation Ferritic Steel Wall with High Performance Plasma on JFT-2M," Proc. 20th IAEA Fusion Energy Conf. IAEA-CN-116/EX/P2-33 (2004), to be published on CD-ROM (IAEA, Vienna).
- 110) Umeda, N., Yamamoto, T., Hanada, M., et al., "Recent progress of negative ion based neutral beam injector for JT-60U," 23rd Symp. on Fusion Technology (2004).
- 111) Umeda, N., Yamamoto, T., Inoue, T., et al., "Recent progress of negative ion based neutral beam injector for JT-60U," Proc. 23rd Symp. on Fusion Technology, (2004), to be published in Fusion Eng. Des.
- 112) Verzilov, Y., Ochiai, K., Nishitani, T., et al., "Methods for the Tritium Production Rate Measurement in Design-Oriented Blanket Experiments," 7th Int. Conf. Tritium Science & Technology (2004), to be published in Fusion Sci. Technol..
- 113) Wakai, E., Ando, M., Matsukawa, S., "Effect of initial heat treatment on DBTT of F82H steel irradiated by neutrons," 16th ANS Topical Meeting on Technology of Fusion Energy (2004).
- 114) Yamada, H., Kawamura, H., Kohno, W., et al., "Mechanical Properties of Weld Joints Using Irradiated Stainless Steel for Blanket," Proc. 23rd Symp. on Fusion Technology (2004), to be published in Fusion Eng. Des..
- 115) Yamanishi, T., Hayashi, T., Kawamura, Y., et al., "Interlinked test results for fusion fuel processing and blanket tritium recovery systems using cryogenic molecular sieve bed," Proc. 7th Int. Conf. on Tritium Science and Technology (2004), to be published in Fusion Science Technology.
- 116) Yamauchi, M., Ochiai, K., Morimoto, Y., et al., "Experiment and Analyses for 14 MeV Neutron Streaming through Dogleg Duct," 10th Int. Conf. on Radiation Shielding (2004), to be published in Radiat. Prot. Dosim.
- 117) Yamauchi, M., Takemura, M., Nakamura, H., et al., "Estimation of radioactivities in the IFMIF liquid lithium loop due to the erosion and corrosion of target back-wall," 16th ANS Topical Meeting on Technology of Fusion Energy (2004).
- 118) Yoshida, H., Yamauchi, M., Miya, N., et al., "Hydrogen Retention of Carbon Dust produced in JT-60, " The 16th Int. Conf. on Plasma-Surface Interactions in Controlled Fusion Devices (PSI-16), Portland Maine, US, May 24-28, 2004.

- 119) Van der Laan, J.G., Hegeman, J.B.J., Knitter, R., (Tsuchiya, K.) et al., "A High Fluence Irradiation of Ceramic Breeder Materials in HFR Petten, Materials Characterisation and Test Matrix," 23rd Symposium on Fusion Technology (2004), to be published in Fusion Eng. Des..

A.1.4 List of other papers

- 1) Akasaka, H., Takano, S., Kawamata, Y., et al., "Reconfiguration study of the JT-60 timing system based on a fast memory network," Proceedings of the topical meeting on engineering and technology (CD-ROM), P3-04 (2005) (in Japanese).
- 2) Ezato, K., "Development of ITER Divertor," J. High Temperature Soc., **30**, 248(2004) (in Japanese)
- 3) Felde, D., Thoms, K., Heatherly, D., et al, "Assembly of the US-Japan JP-27 experiment and start of irradiation in the HFIR," DOE/ER-0313/36, 124 (2004).
- 4) Futamura, Y., Kawamura, H., Tsuchiya, H., "Data Base for Tritium Solid Breeding Materials (Li₂O, Li₂TiO₃, Li₂ZrO₃ and Li₄SiO₄) of Fusion Reactor Blankets," Annual Report of Hydrogen Isotope Research Center, Toyama University, Japan, 24 (2004), Special Issue.
- 5) Hatae, T., Nakatsuka, M., Yoshida, H., "Improvement of Thomson scattering diagnostics using stimulated-B Brillouin-scattering-based phase conjugate mirrors," J. Plasma Fusion Res., **80**, 870 (2004).
- 6) Ide, S., "Current Profile Control and Application to Advanced Tokamak/Steady State Plasma Operations by Lower Hybrid Waves," J. Plasma Fusion Res. **81**, 167 (2005) (in Japanese).
- 7) Kasugai, A., Minami, R., Takahashi, K., et al., "Long pulse operation of high power gyrotron with mm-wave range for fusion reactor," Technical Report of IEICE., ED2004-200(2004) (in Japanese).
- 8) Kawamata, Y., Kurihara, K., Yonekawa, I., "A new development trend of magnetic measurements toward ITER," Proceedings of the Joint Conference on Fusion Research, 57 (2004) (in Japanese).
- 9) Kawamata, Y., Yonekawa, I., Kurihara, K., "Development of an innovative integrator being resistant to an excessive high voltage input at plasma instabilities," Proceedings of the topical meeting on engineering and technology (CD-ROM), P3-05 (2005) (in Japanese).
- 10) Kubo, H., Takenaga, H., Nakano, T., et al., "Divertor spectroscopy with molecular transport", in Nuclear Fusion Research, Clark, R. E. H. and Reiter, D. (Eds.), Springer Berlin, p.121-134 (2005).
- 11) Konishi, S., Kimura, A., Akiba, M., et al., "Fusion Blanket Construction," J. At. Energy Soc. Japan, **46**, 311(2004) (in Japanese).
- 12) Kurihara, K., "Intelligible seminar on fusion reactors, 4; Plasma control and diagnostics system," J. Nucl. Sci. Tech., **47**, 200 (2005) (in Japanese).
- 13) Kurihara, K., Kasugai, A., et al., "Present status and prospect of diagnostics and control technologies for fusion plasmas," Annual meeting record for the Institute of Electrical Engineers of Japan: 7, (Booklet & CD-ROM), S17, 32 (2005) (in Japanese).
- 14) Kusama, Y., Ishikawa, M., Takechi, M., "Energetic Neutral Particle Measurement with Natural Diamond Detector in JT-60U," Proc. Plasma Science Symposium 2005 / The 22nd Symposium on Plasma Processing, P2-091 (2005).
- 15) Matukawa, M., "Summary: Power supply system as one of the main components," J. Plasma Fusion Res., **80**, 586 (2004) (in Japanese).
- 16) Matukawa, M., Tobita, K., Rikiishi, H., et al., "Electric power flow in a nuclear fusion power plant," J. Plasma Fusion Res., **80**, 559 (2004) (in Japanese).
- 17) Miura, Y., Hoshino, K., and Kusama, Y., "Review of the History of Experiments in the JFT-2M Tokamak for 21 Years," J. Plasma Fusion Res., **80**, 653 (2004) (in Japanese).
- 18) Mori, M., "An Outline of the ITER Project," J. High Temperature Soc., **30**, 236 (2004) (in Japanese).
- 19) Mori, M., "The Trend of the ITER Project," Electrical Review., **89**, 7 (2004) (in Japanese).
- 20) Nishitani, T., Osakabe, M., Shinohara, T., et al, "Neutron Diagnostics for the Energetic Ion Transport Analysis," J. Plasma and Fusion Res., **80**, 860 (2004) (in Japanese).
- 21) Ohmori, S., "An essay to the award memory of the Shibusawa Prize," Electricity and Industry, **629**, 1 (2005) (in Japanese).
- 22) Osakabe, M., Kusama, Y., Okamoto, S., "Neutral Particle Diagnostics for the Energetic Particle Transport Analysis," J. Plasma Fusion Res., **80**, 971 (2004).

- 23) Osakabe, M., Kusama, Y., "Energetic Particle Diagnostics for Transport Analysis," J. Plasma Fusion Res., **80**, 857 (2004).
- 24) Sakakibara, S., Kurihara, K., "Recent progress in magnetic measurements," J. Plasma Fusion Res., **80**, 364 (2004) (in Japanese).
- 25) Sakurai, S., Tobita, K., Nishio, S., "Spherical tokamak concept, Its future prospect toward power reactor, section 5 ST tokamaks toward power reactor, 5.4 Divertor power handling in a low aspect ratio tokamak reactor," J. Plasma Fusion Res., **80**, 955 (2004) (in Japanese).
- 26) Sengoku, S., "Steady-State Operation of Tokamak with Bootstrap Current," J. Plasma Fusion Res., **80**, 940 (2004) (in Japanese).
- 27) Shimomura, Y., "Toward Construction of ITER", J. Plasma Fusion Res., **81**, 143 (2005) (in Japanese).
- 28) Sueoka, M., Hosoyama, H., Suzuki, T., et al., "A new GUI system for profile control of plasma internal quantities in JT-60," Proceedings of the topical meeting on engineering and technology (CD-ROM), P3-03 (2005) (in Japanese).
- 29) Suzuki, S., "First Wall and Divertor Materials as Plasma Facing Components," J. High Temperature Soc, **30**, 243-247 (2004) (in Japanese).
- 30) Takenaga, H., Oyama, N., Fujita, T., et al., "Comparison of Confinement Degradation in High Density and Particle Transport between Tokamak and Helical", Annual report of national institute for Fusion Science April 2003-March 2004 (2004).
- 31) Yamauchi, M., Nishitani, T., Nishio, S., "5. Can We Obtain the Realistic Power Reactor in the ST Approach?, 5.3 Neutron Shielding and Blanket Neutronics Design," J. Plasma and Fusion Res., **80**, 952 (2004) (in Japanese).
- 32) Yamawaki, M., Kawamura, H., Tsuchiya, K., "Tritium Breeders and Tritium Permeation Barrier Coatings for Fusion Reactor," Bulletin of the Ceramic Soc. of Japan, **39**, 843 (2004) (in Japanese).
- 33) Yoshida, H., Yamauchi, N., Miya, N., et al., "Morphology and Hydrogen Retention of Carbon Dust Produced by Hydrogen Discharges in JT-60," J. Vacuum Soc. of Japan, **47**, No.3(2004). (in Japanese).

A.2 Scientific Staff in the Naka Fusion Research Establishment (April 2004- March 2005)

Naka Fusion Research Establishment

SEKI Masahiro	(Director General)
FUJIWARA Masami	(Scientific Consultant)
INOUE Nobuyuki	(Scientific Consultant)
SHIMOMURA Yasuo	(Scientific Consultant)
MATSUI Hideki	(Invited Researcher)
KOHYAMA Akira	(Invited Researcher)
YAMADA Hiroshi	(Invited Researcher)
KISHIMOTO Yasuaki	(Invited Researcher)
AZUMI Masafumi	(Prime Scientist)
USHIGUSA Kenkichi	(Staff for Director General)
ISEI Nobuaki	(Staff for Director General)
OOHARA Hiroshi	(Staff for Director General)

Department of Administrative Services

KIKUCHI Isao	(Director)
KOBAYASHI Haruo	(Deputy Director)

Department of Fusion Plasma Research

NINOMIYA Hiromasa	(Director)
KIKUCHI Mitsuru	(Deputy Director)
NAGAMI Masayuki	(Prime Scientist)
TERAKADO Yuichi	(Administrative Manager)

Tokamak Program Division

MIURA Yukitoshi	(General Manager)	
FUJITA Takaaki	HATAE Takaki	KAWASHIMA Hisato
KURITA Gen-ichi	MORIOKA Atsuhiko	OIKAWA Akira
SAKURAI Shinji	TAKAHASHI Hiroyuki (*3)	TAMAI Hiroshi
TSUCHIYA Katsuhiko		

Plasma Analysis Division

OZEKI Takahisi	(General Manager)	
HAMAMATSU Kiyotaka	HAYASHI Nobuhiko	IBA Katsuyuki (*24)
KIYONO Kimihiro	KONOVALOV Sergei (*6)	NAITO Osamu
OHASA Kazumi	OHSHIMA Takayuki	SAKATA Shinya
SATO Minoru	SUZUKI Masaei (*24)	SUZUKI Mitsuhiro (*31)
TAKEI Nahoko (*28)	TAKIZUKA Tomonori	

Large Tokamak Experiment and Diagnostics Division

KAMADA Yutaka	(General Manager)	
KUBO Hirotaka	(Deputy General Manager)	
ASAKURA Nobuyuki	CHIBA Shinichi	HAMANO Takashi (*20)
HOSHINO Katsumichi	IDE Shunsuke	INOUE Akira (*20)
ISAYAMA Akihiko	ISHIKAWA Masao (*22)	KAMIYA Kensaku
KASHIWA Yoshitoshi	KAWANO Yasunori	KITAMURA Shigeru
KOIDE Yoshihiko	KOKUSEN Shigeharu (*19)	KONDOH Takashi
KONOSHIMA Shigeru	MATSUNAGA Go (*22)	MIYAMOTO Atsushi (*19)

NAKANO Tomohide	OYAMA Naoyuki	SAKAMOTO Yoshiteru
SAKUMA Takeshi (*20)	SHINOHARA Kouji	SUNAOSHI Hidenori
SUZUKI Takahiro	TAKECHI Manabu	TAKENAGA Hidenobu
TSUBOTA Naoaki (*19)	TSUKAHARA Yoshimitsu	TSUZUKI Kazuhiro
UEHARA Kazuya	URANO Hajime	YOSHIDA Maiko (*22)

Plasma Theory Laboratory

KISHIMOTO Yasuaki (Head)		
AIBA Nobuyuki (*1)	IDOMURA Yasuhiro	ISHII Yasutomo
KAGEI Yasuhiro (*22)	MATSUMOTO Taro	MIYATO Naoaki (*22)
SUGAHARA Akihiro (*24)	TOKUDA Shinji	TUDA Takashi

Experimental Plasma Physics Laboratory

KUSAMA Yoshinori (Head)		
KASAI Satoshi	OGAWA Hiroaki	SHIINA Tomio

Reactor System Laboratory

TOBITA Kenji (Head)		
KURIHARA Ryoichi	NAKAMURA Yukiharu	NISHIO Satoshi
SATO Masayasu		

Department of Fusion Facilities

KURIYAMA Masaaki	(Director)
HOSOGANE Nobuyuki	(Deputy Director)
YAMAMOTO Takumi	

JT-60 Administration Division

TERAKADO yuuichi	(General Manager)
------------------	-------------------

JT-60 Facilities Division I

KURIHARA Kenichi (Head)		
AKASAKA Hiromi	FURUKAWA Hiroshi (*20)	HOSOYAMA Hiromi (*9)
KAWAMATA Youichi	MATSUKAWA Makoto	OHMORI Shunzo
OHMORI Yoshikazu	OKANO Jun	SEIMIYA Munetaka
SHIMADA Katsuhiko	SUEOKA Michiharu	TAKANO Shoji (*31)
TERAKADO Hiroyuki (*7)	TERAKADO Tsunehisa	TOTSUKA Toshiyuki
YAMASHITA Yoshiki (*7)	YONEKAWA Izuru	

JT-60 Facilities Division II

MIYA Naoyuki (Head)		
ARAI Takashi	HAGA Saburo (*19)	HAYASHI Takao
HIRATSUKA Hajime	HONDA Masao	ICHIGE Hisashi
ISHIMOTO Yuki (*22)	KAMINAGA Atsushi	KIZU Kaname
KUDO Yusuke	MASAKI Kei	MATSUZAWA Yukihiko (*19)
MIYO Yasuhiko	NISHIYAMA Tomokazu	SASAJIMA Tadayuki
SUZUKI yutaka (*18)	TAKAHASHI Tatsukichi (*3)	YAGISAWA Hiroshi (*3)
YAGYU Jun-ichi		

RF Facilities Division

FUJII Tsuneyuki (Head)		
HIRANAI Shinichi	HASEGAWA Koichi	IGARASHI Koichi (*19)

ISHII Kazuhiro (*20)	KIKUCHI Kazuo	MORIYAMA Shinichi
SATO Fumiaki (*19)	SAWAHATA masayuki	SEKI Masami
SHIMONO Mitsugu	SHINOZAKI Shin-ichi	SUZUKI Sadaaki
TAKAHASHI Masami (*26)	TANI Takashi	TERAKADO Masayuki
YOKOKURA Kenji		

NBI Facilities Division

IKEDA Yoshitaka (Head)		
OHGA Tokumichi (Deputy General Manager)		
AKINO Noboru	EBISAWA Noboru	GRISHAM Larry (*23)
HONDA Atsushi	KAWAI Mikito	KAZAWA Minoru
KIKUCHI Katsumi (*20)	KOMATA Masao	MOGAKI Kazuhiko
NOTO Katsuya (*19)	OKANO Fuminori	OSHIMA Katsumi (*19)
TAKENOUCHI Tadashi (*29)	TANAI Yutaka (*20)	UMEDA Naotaka
USUI Katsutomi	YAMAZAKI Haruyuki (*3)	

JFT-2M Facilities Division

YAMAMOTO Masahiro (Head)	
SHIBATA Takatoshi (Deputy General Manager)	
SAITO Hideo (*20)	

Department of Fusion Engineering Research

SEKI Shogo (Director)	
TAKATSU Hideyuki (Prime Scientist and Deputy Director)	
KATOJI Takeshi (Administrative Manager)	
SHIHO Makoto	
(TSUJI Hiroshi passed away on December 18, 2004)	

Blanket Engineering Laboratory

AKIBA Masato (Head)		
ABE Tetsuya	ENOEDA Mikio	EZATO Koichiro
HIROSE Takanori	HOMMA Takashi	NOMOTO Yasunobu (*12)
SUZUKI Satoshi	TANIGAWA Hisashi (*22)	TANZAWA Sadamitsu
YOKOYAMA Kenji	YOSHIDA Hajime (*22)	

Superconducting Magnet Laboratory

OKUNO Kiyoshi (Head)		
ABE Kanako (*5)	HAMADA Kazuya	ISONO Takaaki
KAWANO Katsumi	KOIZUMI Norikiyo	NABARA Yoshihiro
NAKAJIMA Hideo	NUNOYA Yoshihiko	OSHIKIRI Masayuki (*20)
SUGIMOTO Makoto	TAKANO Katsutoshi (*20)	TSUTSUMI Fumiaki (*31)

Plasma Heating Laboratory

SAKAMOTO Keishi (Head)		
DAIRAKU Masayuki	HANADA Masaya	IKEDA Yukiharu
INOUE Takashi	KASHIWA Yoshitada (*4)	KASHIWAGI Mieko
KASUGAI Atsushi	KOBAYASHI Noriyuki (*30)	KOMORI Shinji (*20)
MINAMI Ryutaroh (*22)	ODA Yasuhisa (*32)	SEKI Takayoshi (*3)
TAKADO Naoyuki (*13)	TAKAHASHI Koji	TANIGUCHI Masaki
WATANABE Kazuhiro		

Tritium Engineering Laboratory

NISHI Masataka (Head)		
HAYASHI Takumi	ISOBE Kanetsugu	KAWAMURA Yoshinori
KOBAYASHI Kazuhiro	LUO Guang-Nan (*6)	NAKAMURA Hirofumi
SHU Wataru	SUZUKI Takumi	MIURA Hidenori (*12)
UZAWA Masayuki (*18)	YAMADA Masayuki	YAMANISHI Toshihiko

Office of Fusion Materials Research Promotion

SUGIMOTO Masayoshi (Head)		
ANDO Masami	FURUYA Kazuyuki	IDA Mizuho (*5)
MATSUKAWA Shingo (*14)	MATSUHIRO Kenjiro (*22)	NAKAMURA Hiroo
NAKAMURA Kazuyuki	TANIGAWA Hiroyasu	YUTANI Toshiaki (*30)
UMETSU Tomotake (*16)		

Fusion Neutron Laboratory

NISHITANI Takeo (Head)		
ABE Yuichi	KONDO Keitaro (*21)	KUBOTA Naoyoshi (*22)
KUTSUKAKE Chuzo	NAKAO Makoto (*12)	OCHIAI Kentaro
OGINUMA Yoshikazu (*20)	SATO Satoshi	SEKI Masakazu
TANAKA Shigeru	YAMAUCHI Michinori (*30)	VERZILOV Yury (*6)

Blanket Irradiation and Analysis Laboratory

HAYASHI Kimio (Head)		
HOSHINO Tsuyoshi (*22)	ISHIDA Takuya (*20)	TSUCHIYA Kunihiko
YAMADA Hirokazu (*12)		

Department of ITER Project

TUNEMATSU Toshihide	(Director)	
YOSHINO Ryuji	(Deputy Director)	
MATSUMOTO Hiroyuki	(Administrative Manager)	
KOIZUMI Koichi		
ODAJIMA Kazuo		

Project Management Division

MORI Masahiro (General Manager)		
ITAMI Kiyoshi	SENGOKU Seio	SHIMIZU Katsuhiko
SUGIE Tatsuo	YOSHIDA Hidetoshi	

International Coordination Division

ANDO Toshiro (Head)		
HONDA Tsutomu (*30)	IIDA Hiromasa	IOKI Kimihiro (*18)
KATAOKA Yoshiyuki (*3)	MARUYAMA So	MIZOGUCHI Tadanori (*3)
MORIMOTO Masaaki (*18)	OIKAWA Toshihiro	OKADA Hidetoshi (*3)
SAKASAI Akira	SATO Kouichi (*31)	SHIMADA Michiya
SUGIHARA Masayoshi	TAKAHASHI Yoshikazu	NAGAHAMA Tetsushi (*25)
YOSHIDA Kiyoshi	TERASAWA Atsumi (*17)	

Plant System Division

NEYATANI Yuzuru (Head)		
KATAOKA Takahiro (*17)	NAGAMATSU Nobuhide (*10)	OHMORI Junji (*30)
OOHASHI Hironori (*11)	SATO Kazuyoshi	SEKIYA Shigeki (*16)

TAKAHASHI Hideo (*27) TAMURA Kousaku (*15) YAGENJI Akira (*2)
YAMAMOTO Shin

Safety Design Division

OHIRA Shigeru (Head)
HADA Kazuhiko HIGUCHI Masahisa (*8) MARUO Takeshi
TADO Shigeru (*17) TAKERMURA Morio(*12) TSURU Daigo

Tokamak Device Division

SHIBANUMA Kiyoshi (Head)
KAKUDATE Satoshi KITAMURA Kazunori (*30) MOHRI Kensuke (*12)
NAKAHIRA Masataka OBARA Kenjiro TAKEDA Nobukazu

Collaborating Laboratories

Tokai Research Establishment

Department of Material Science

Research Group for Radiation Effects and Analysis

JITSUKAWA Shiro (Group Leader)
FUJII Kimio NAITO Akira NAKAZAWA Tetsutya
OKUBO Nariaki SAWAI Tomotsugu SHIBA Kiyoyuki
TANIFUJI Takaaki YAMADA Reiji YAMAKI Daiju
WAKAI Eiichi

Department of Nuclear Energy System

Research Group for Reactor Structural Materials

MIWA Yukio

Neutron Science Research Center

Research Group for Neutron Scattering from Functional Materials

IGAWA Naoki

Research Group for Nanostructure

TAGUCHI Tomitsugu

- *1 Graduate University for Advanced Studies
- *2 Hazama Corporation.
- *3 Hitachi, Ltd.
- *4 Ibaraki University
- *5 Ishikawajima-Harima Heavy Industries Co., Ltd.

- *6 JAERI Fellowship
- *7 JP HYTEC Co., Ltd.
- *8 Japan Atomic Power Company Co., Ltd.
- *9 Japan EXpert Clone Corp. (JEX)
- *10 Kajima Corporation

- *11 Kandenko Co., Ltd.
- *12 Kawasaki Heavy Industries, Ltd.

- *13 Keio University
- *14 Kokan-Keisoku Corporation
- *15 Kounoike Construction Co., Ltd.

- *16 Kumagai Gumi Co., Ltd.
- *17 Mitsubishi Electric Corporation
- *18 Mitsubishi Heavy Industries, Ltd.
- *19 Nippon Advanced Technology Co., Ltd.
- *20 Nuclear Engineering Co., Ltd.

- *21 Osaka University
- *22 Post-Doctoral Fellow
- *23 Princeton Plasma Physics Laboratory (USA)
- *24 Research Organization for Information Science & Technology
- *25 Shimizu Corporation

- *26 Sumitomo Heavy Industries, Ltd.
- *27 Taisei Corporation
- *28 Tokyo Institute of Technology
- *29 Tomoe Shokai Co., Ltd.
- *30 Toshiba Corporation

- *31 Total Support Systems
- *32 University of Tokyo